Advances in sheet metal forming research

Asim Tewari
Department of Mechanical Engineering
Indian Institute of Technology Bombay, Mumbai


IIT Bombay
Search
More Options
हिन्दी संस्करण (Hindi Version)
About IIT Bombay
IIT Indore
Entrance Exams
Academics
R&D
Academic Services
Entrepreneurship
Students
Alumni
Old Guest House overlooking Pond
In a gentle way, you can shake the world - Mahatma Gandhi

IIT BOMBAY AT A GLANCE

Engages in research, education, training, technology development and related activities in most areas of technology, science & management

- 530 acres (5.3 sq. km) of campus area
- 15 Departments, 1 School, 4 IDPs & 9 Centers
- ~600 fulltime faculty & 90 adjunct faculty
- ~1300 support staff
- ~9600 students (P.G ~ 6000; PhD~2000)
- ~750 project research staff

Patents (India and Foreign) 2012-2013	>100
Number of industries which come to us for projects	>2000
Research funding in INR (Governmental & Industrial, 2012-13)	~300 Cr
Number of technology spinoffs from IITB technologies	>50

Overview of NCAIR

Vision

- Create a World Class Aerospace Ecosystem in India

Mission

- To be a catalyst for collaboration between industry, Academia, R&D Organizations and Government
- To provide economically viable and sustainable solutions
- To promote Innovation, Knowledge Creation and Entrepreneurship
- To disseminate knowhow and develop human resources

Inception

19th November 2010

Stake-holders

DST, Sandvik, IIT-B, Delcam, BOEING, DMG-Mori Seiki, NAL, HAL → NCAIR

Key Strategic Technologies

Machining | Forming | Casting

Scope of Materials

Titanium | Super Alloys | Composites

Aluminum, Magnesium, AHSS

Services of NCAIR

Core Services

- ✓R&D Projects
- ✓Technology Transfer

Enabling Services

- ✓ Specialized Training Programs
- ✓ Adv Aero Mfg and testing facilities for R&T Activities
- ✓ Mentoring and business Services

Content

- Macro modeling
  - Constitutive property (anisotropy and evolution) based
- Micro Modeling
  - Second-phase particle based large scale modeling
- Nano Modeling
  - Nano structure modification using pre-form annealing

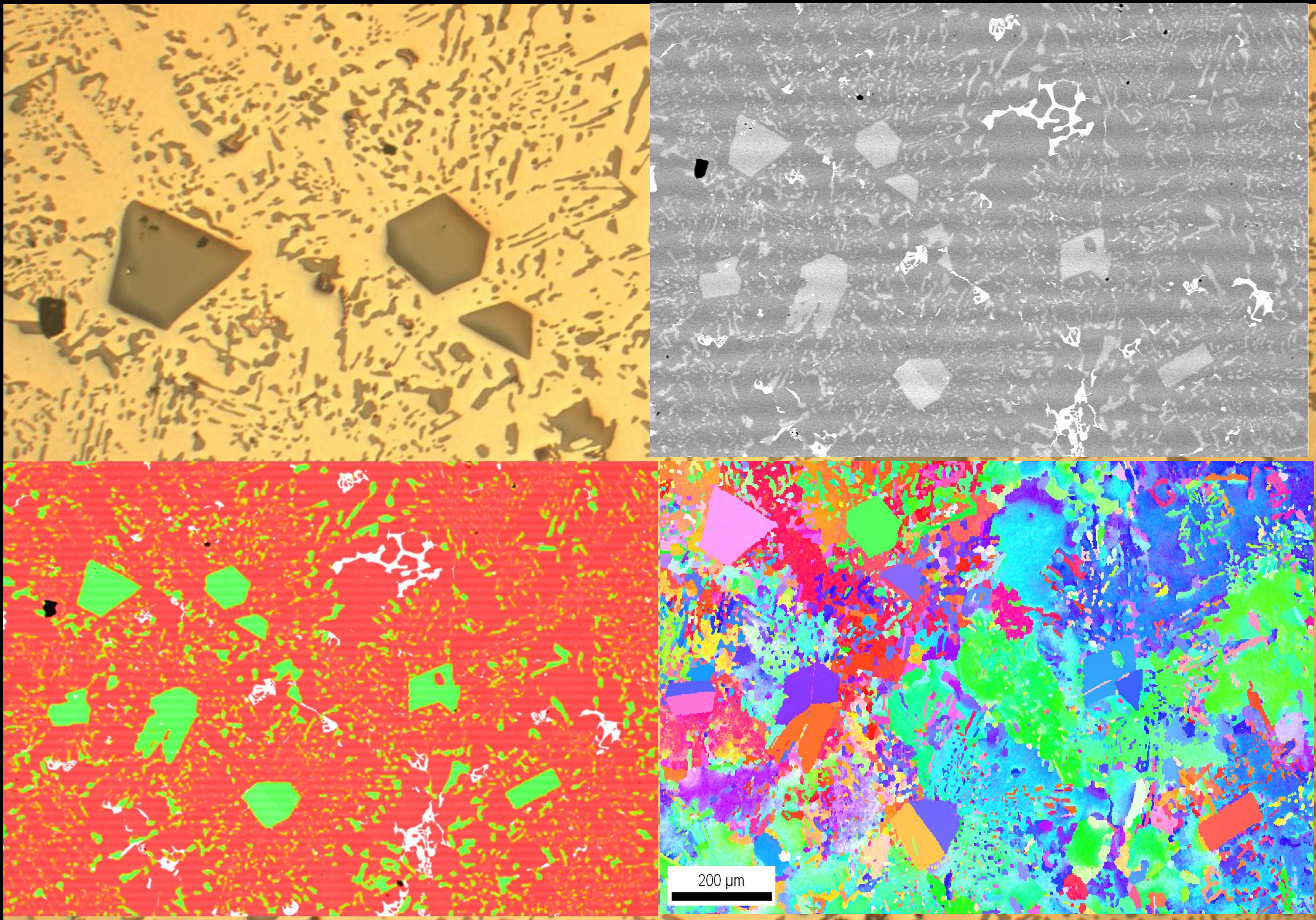
200 µm

Modalities of acquisition

- Optical
- SEM
- EBSD
- FIB
- TEM
- AFM
- SPM
- X-ray CT
- PET, MRI, SIMS, etc.

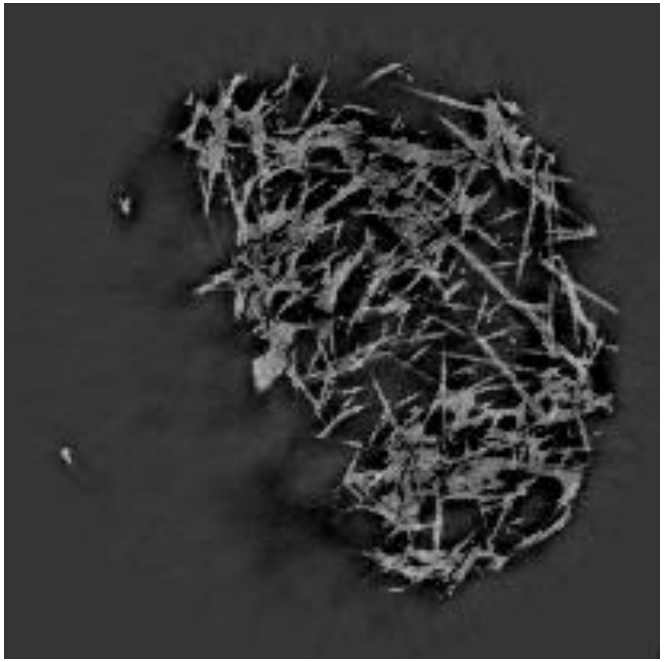

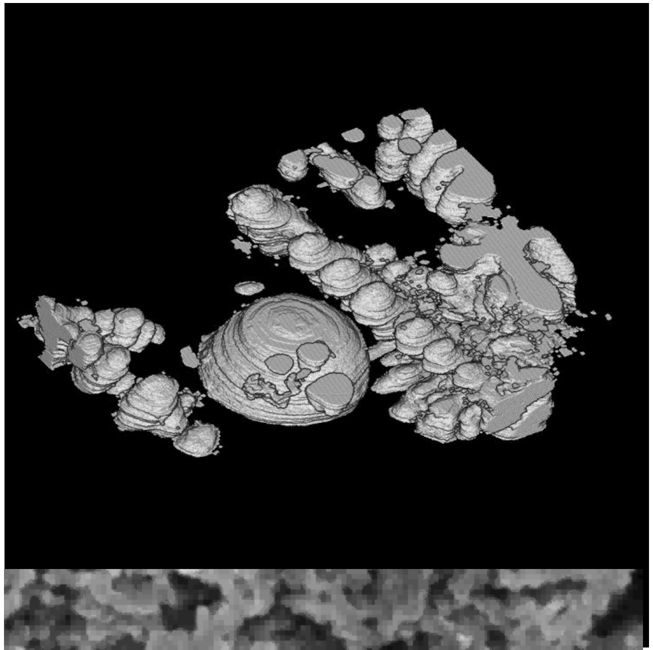

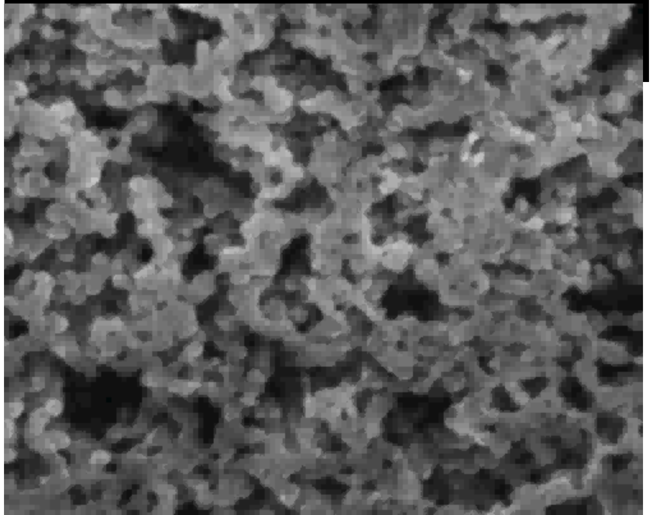

Larger to smaller

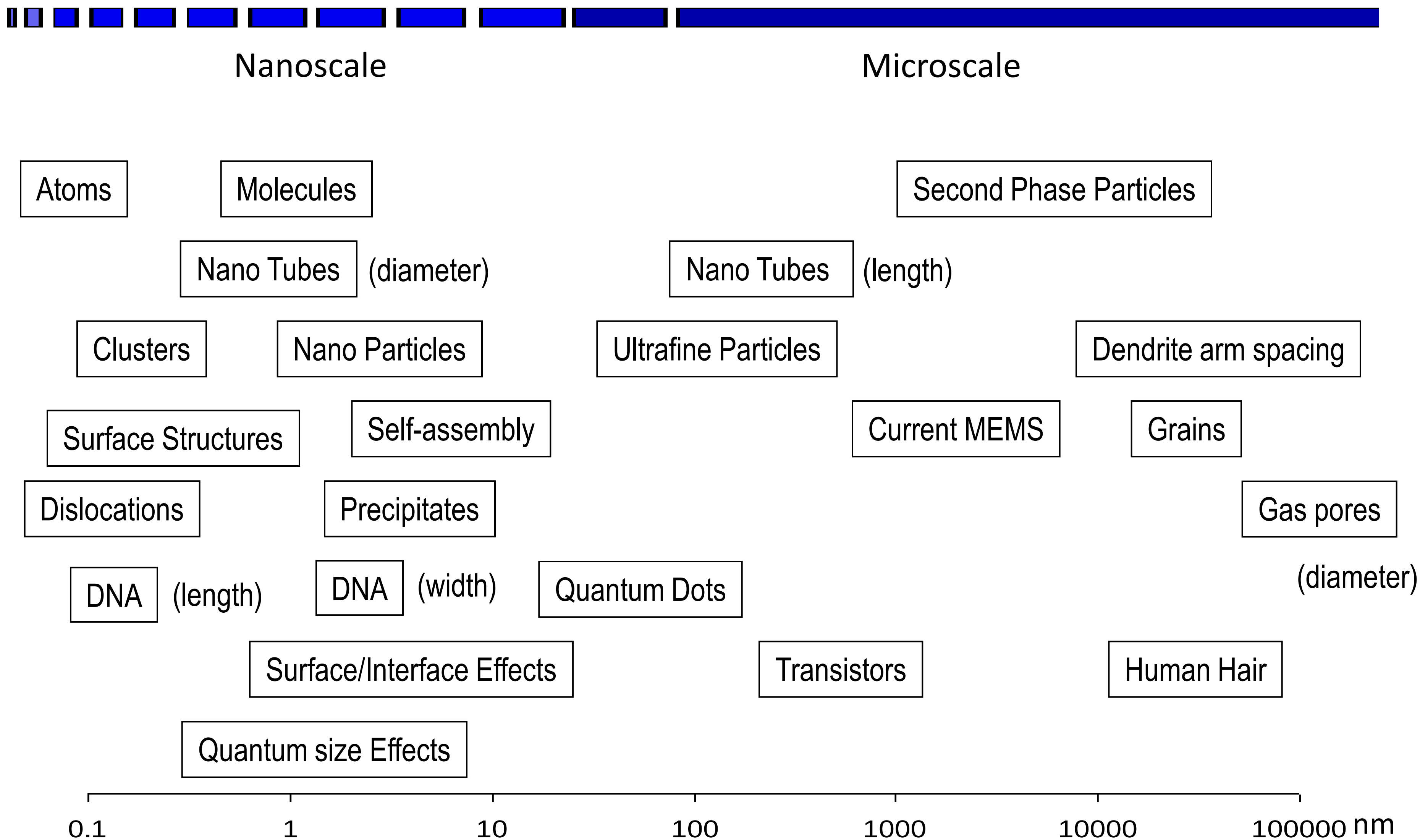

Larger to smaller

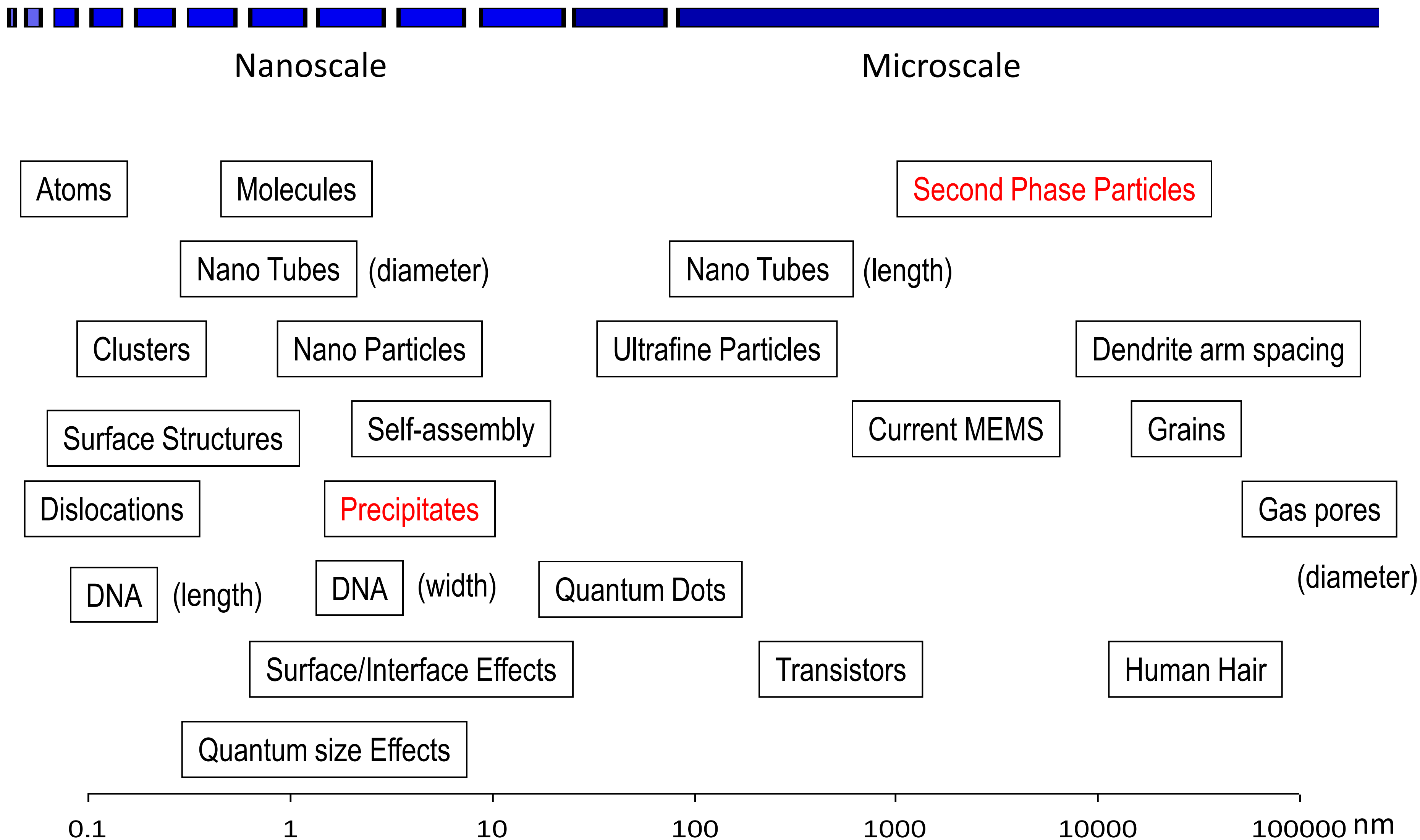

Case Study 1

Macro modeling of Ti64 sheet deformation

Technological challenges

- Formability
- A-class surface finish
- Dent resistant after paint-bake
- Cost

Forming Limit Diagram(FLD)

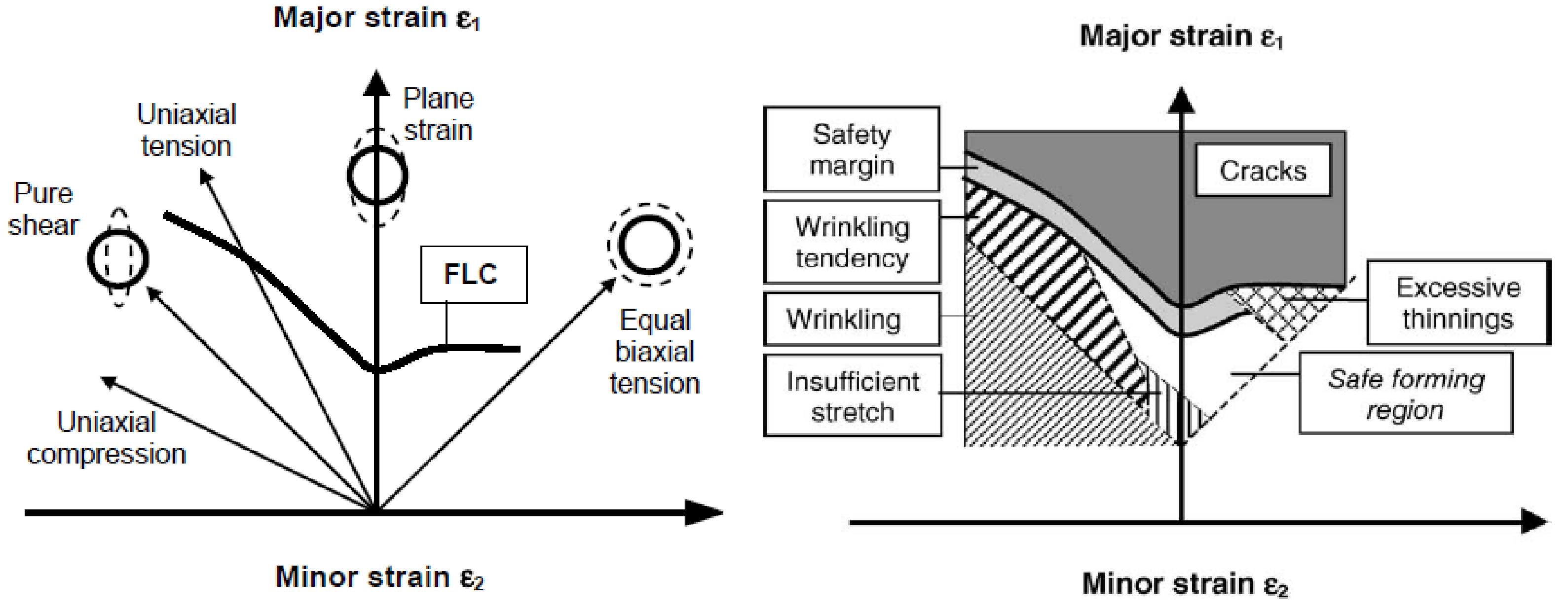

- FLD indicates different modes of deformation
- FLD indicates different forming regions

Specimens geometry for Forming Limit Diagram

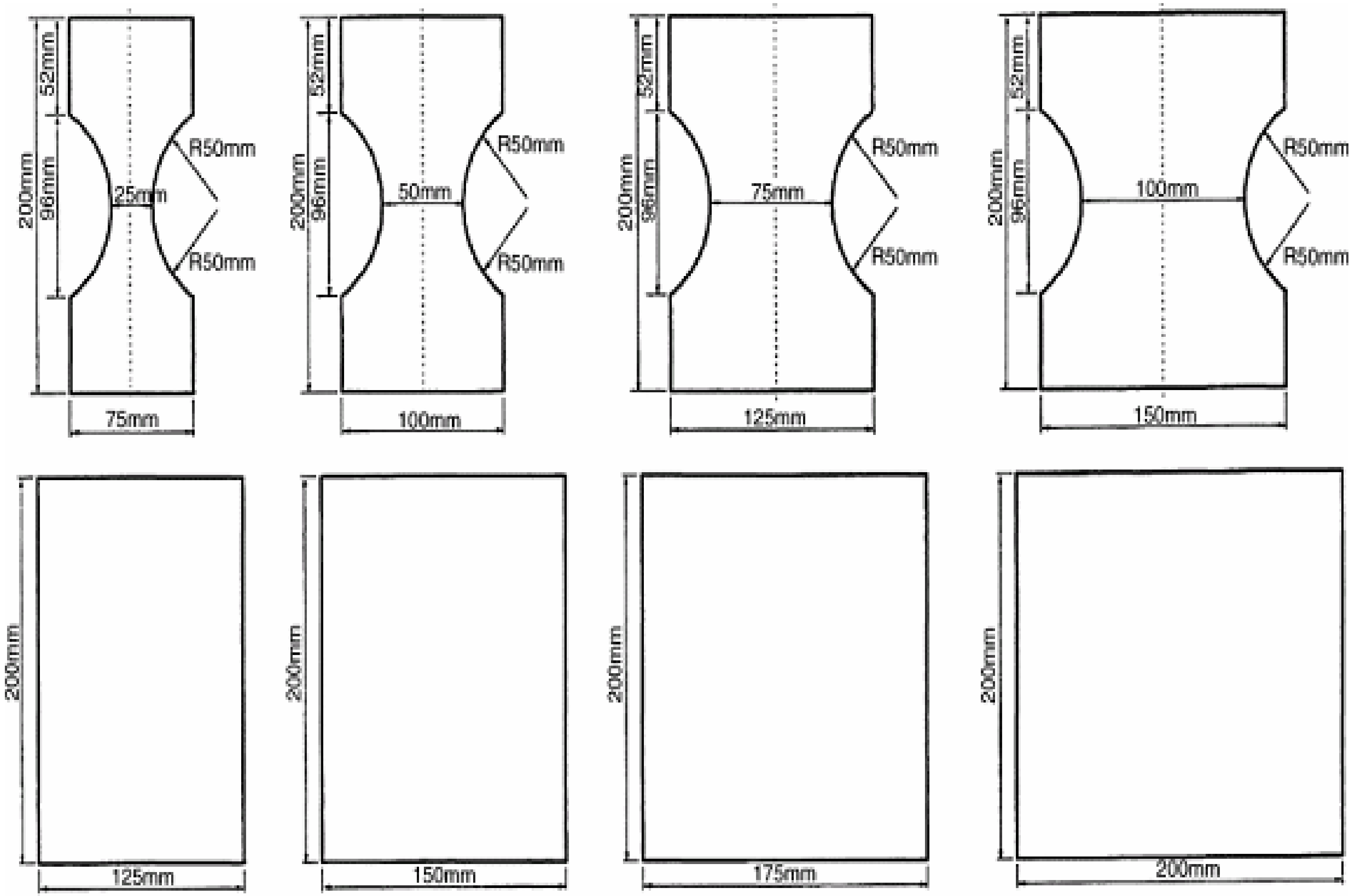

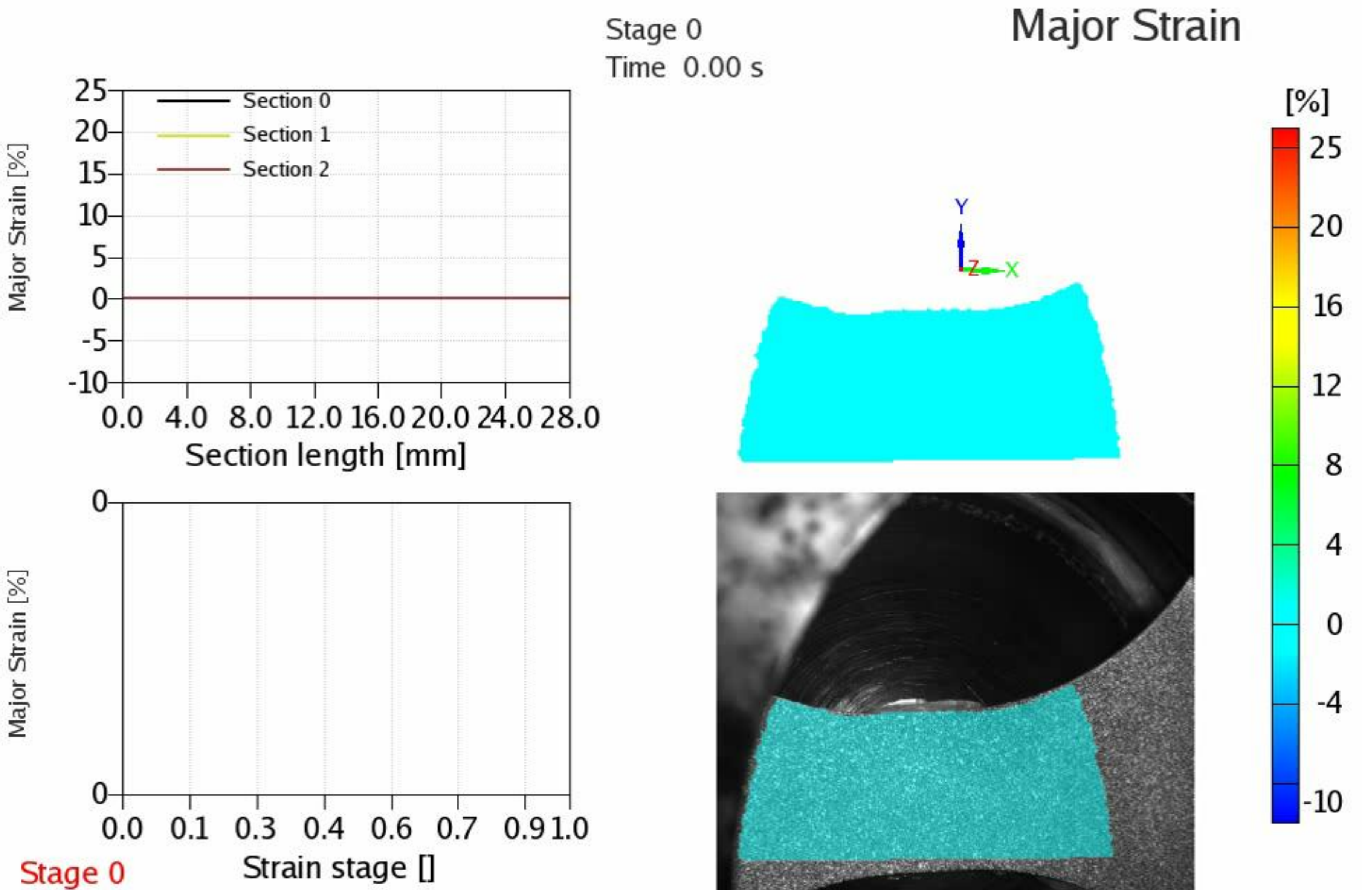
Stage 0
Time 0.00 s
Major Strain
Section 0
Section 1
Section 2
Major Strain [%]
25
20
15
10
5
0
-5
-10
0.0 4.0 8.0 12.0 16.0 20.0 24.0 28.0
Section length [mm]
Major Strain [%]
0
0
0.0 0.1 0.3 0.4 0.6 0.7 0.9 1.0
Strain stage []
Stage 0
Y
Z
X
[%]
25
20
16
12
8
4
0
-4
-10

Strain diagram

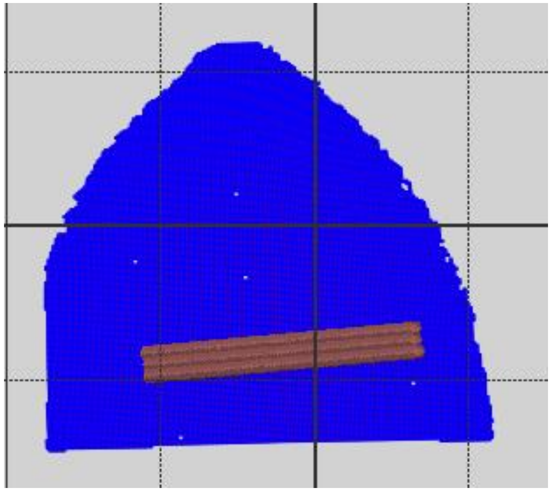

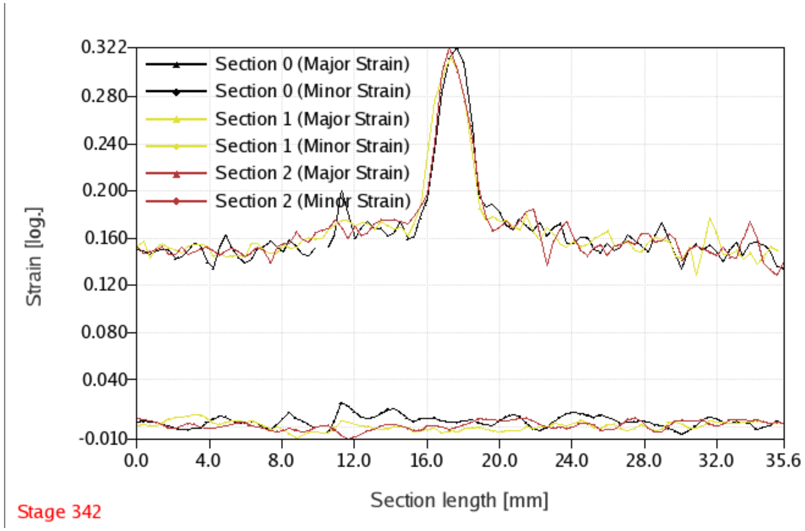

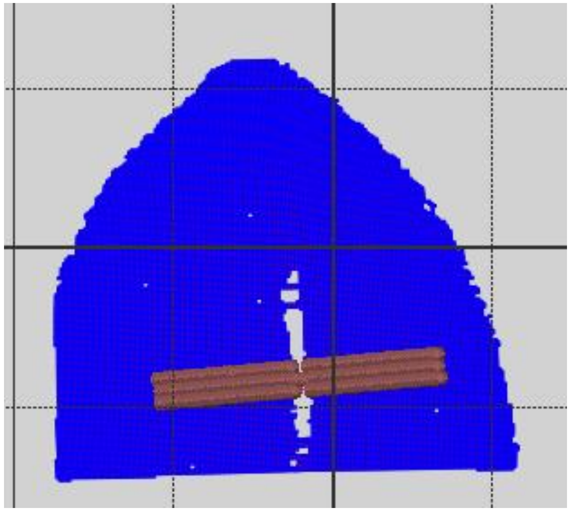

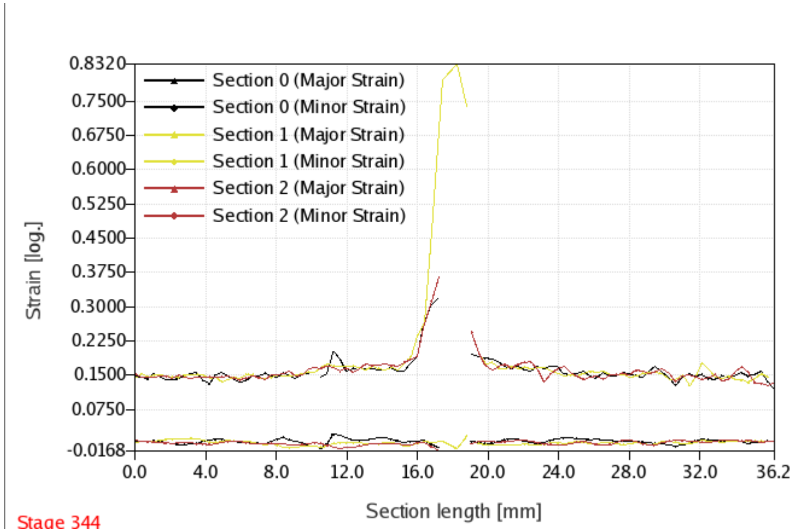

FLD with major stress along TD

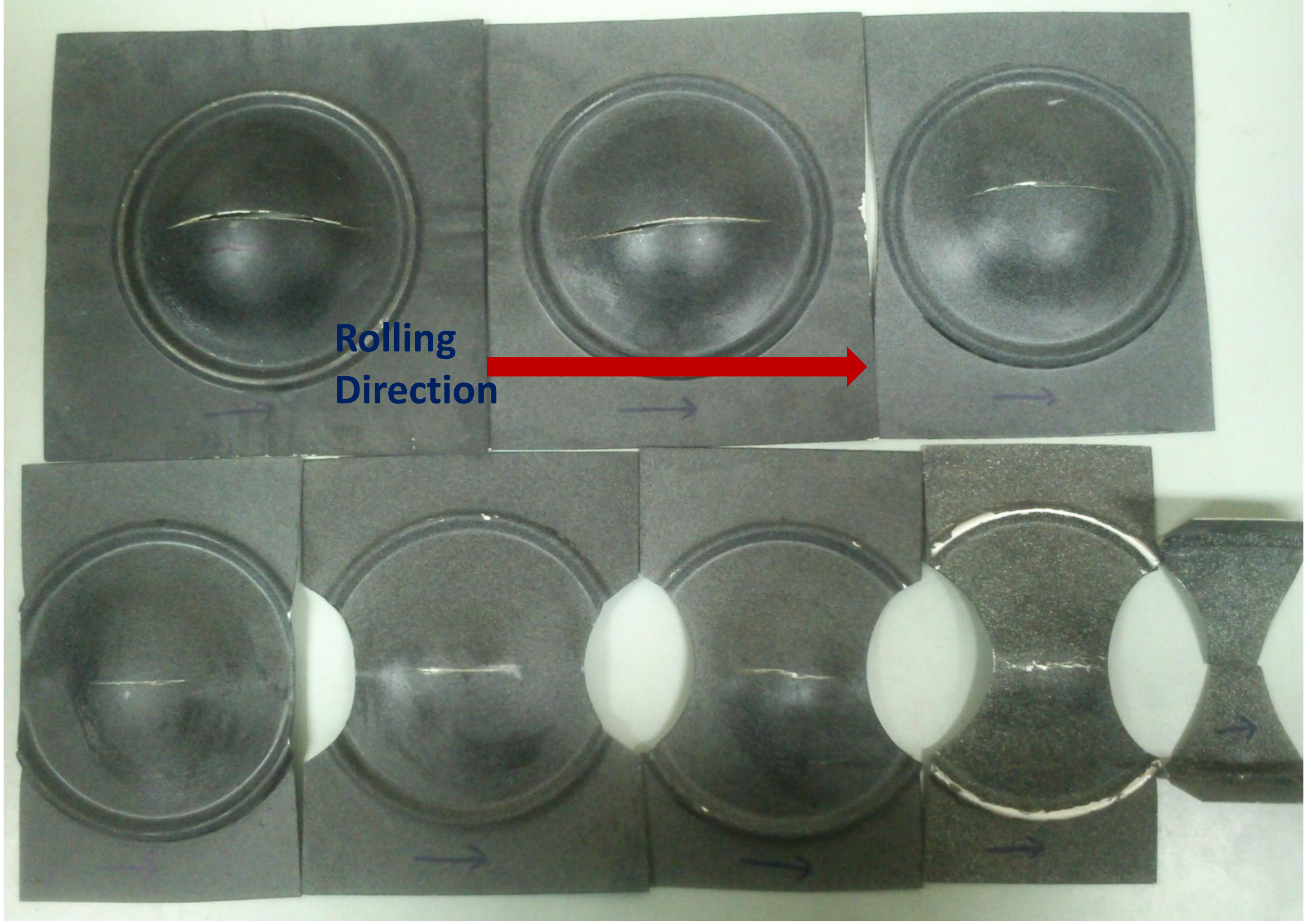

FLD with major stress along RD

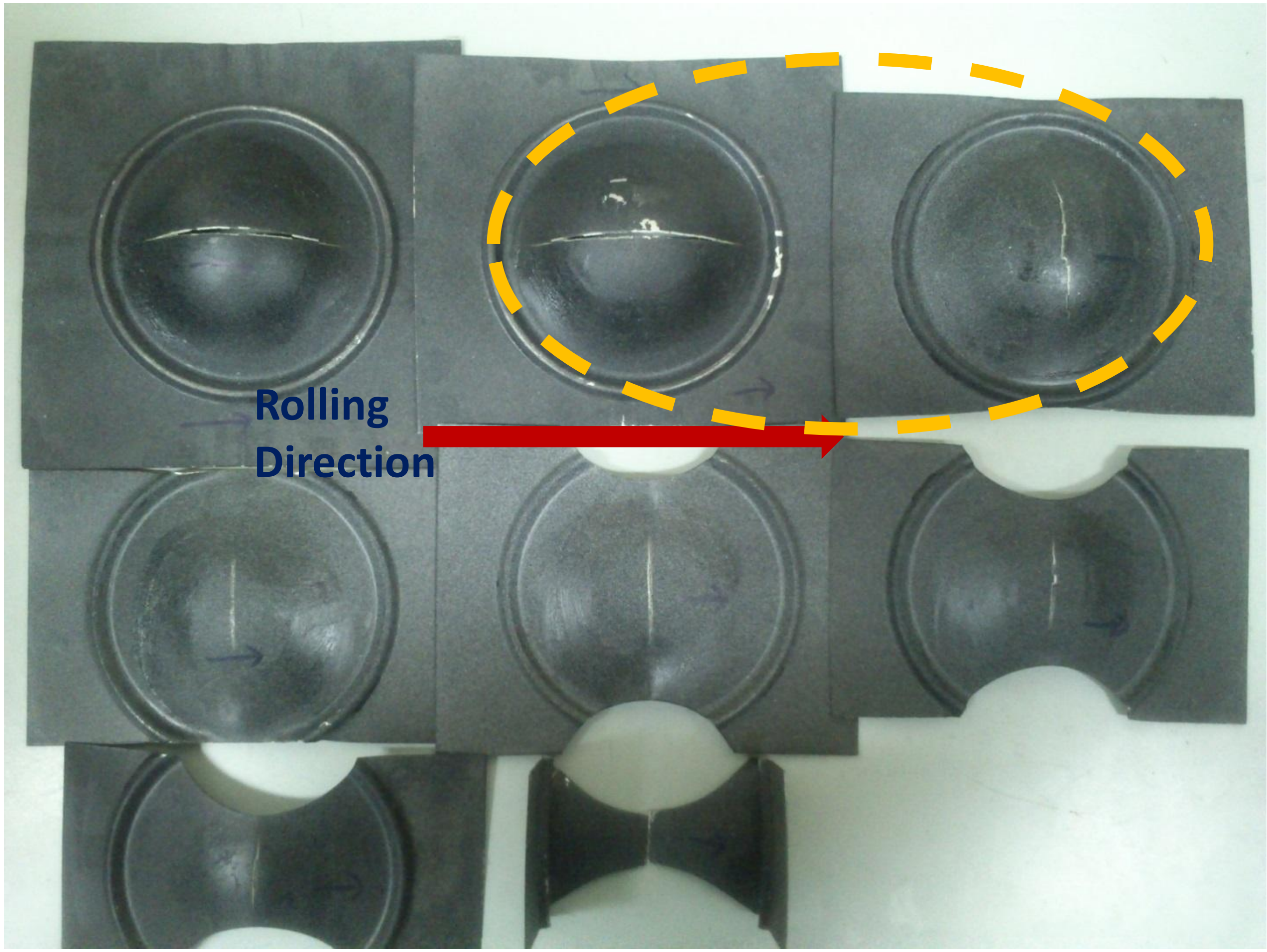

FLD with major stress along ID

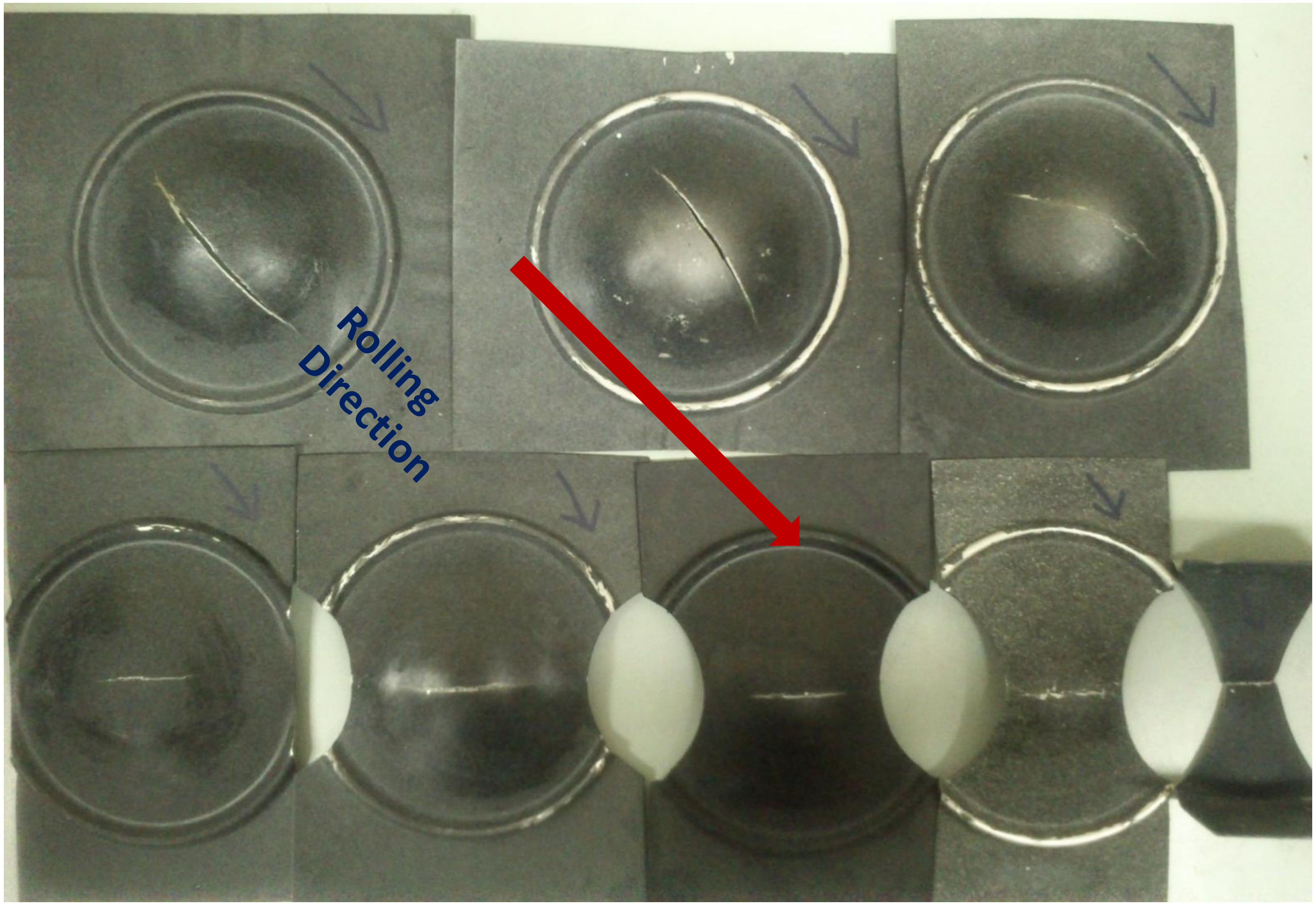

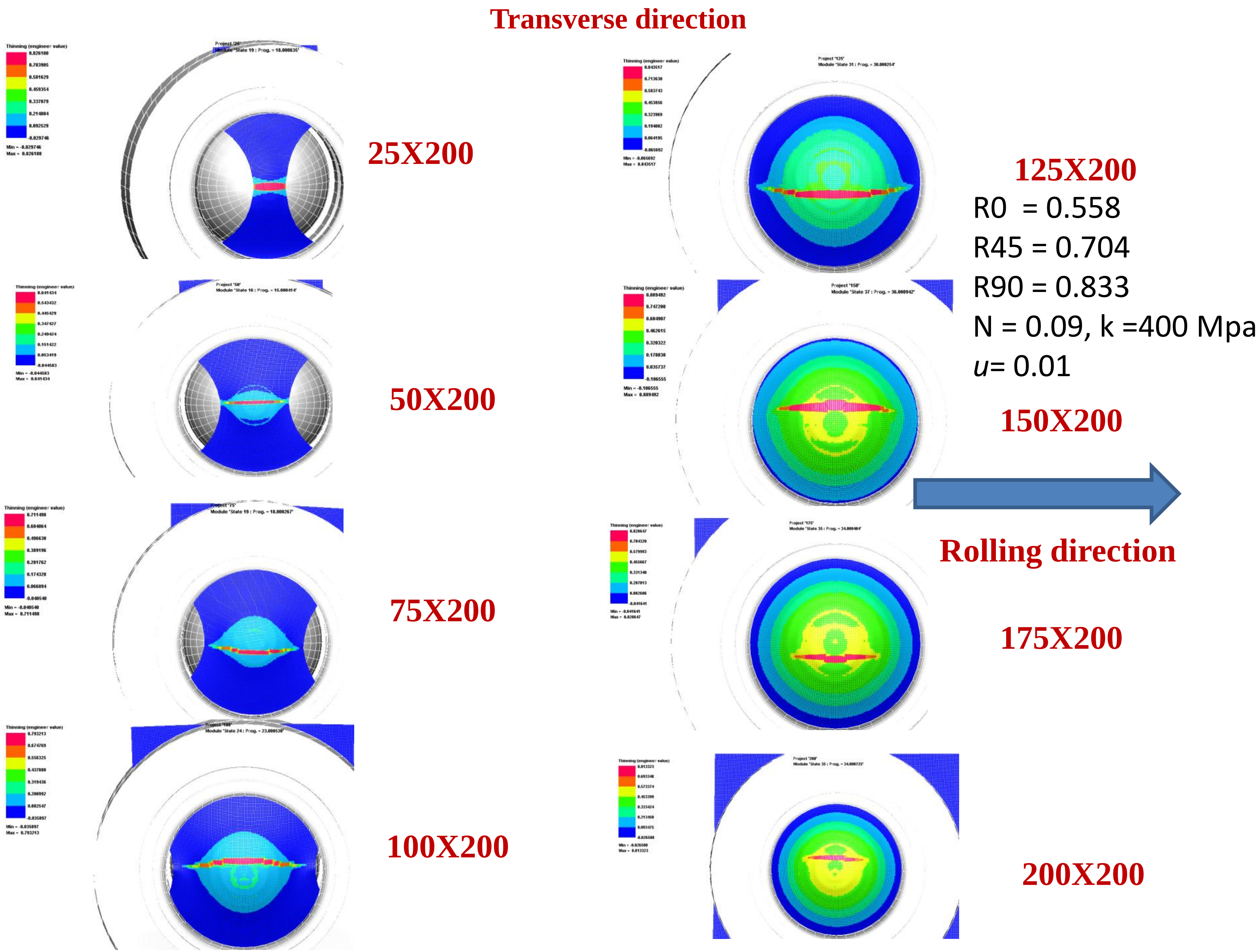
Transverse direction
25X200
50X200
75X200
100X200
125X200
R0 = 0.558
R45 = 0.704
R90 = 0.833
N = 0.09, k =400 Mpa
u= 0.01
150X200
Rolling direction
175X200
200X200

Inclined direction

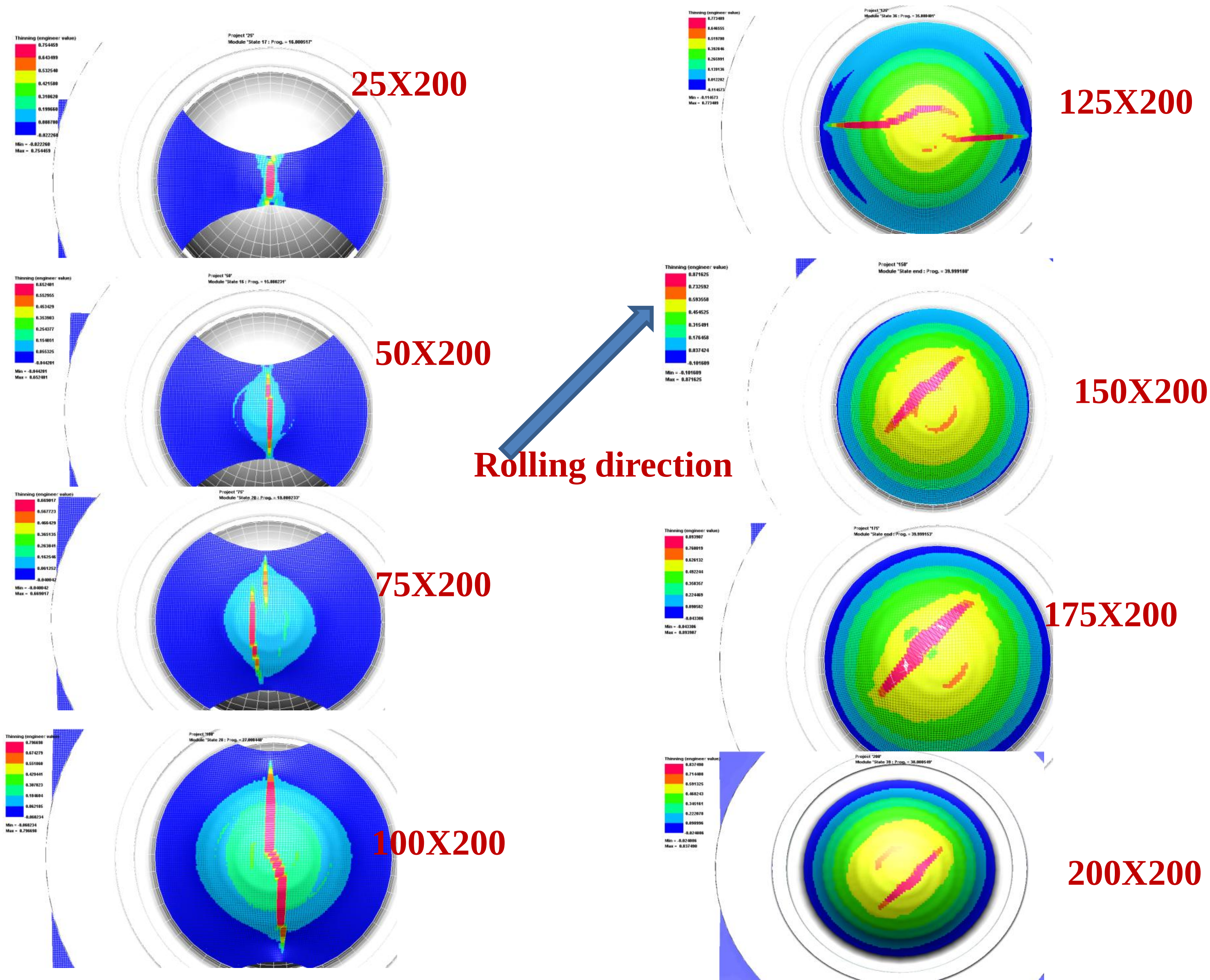

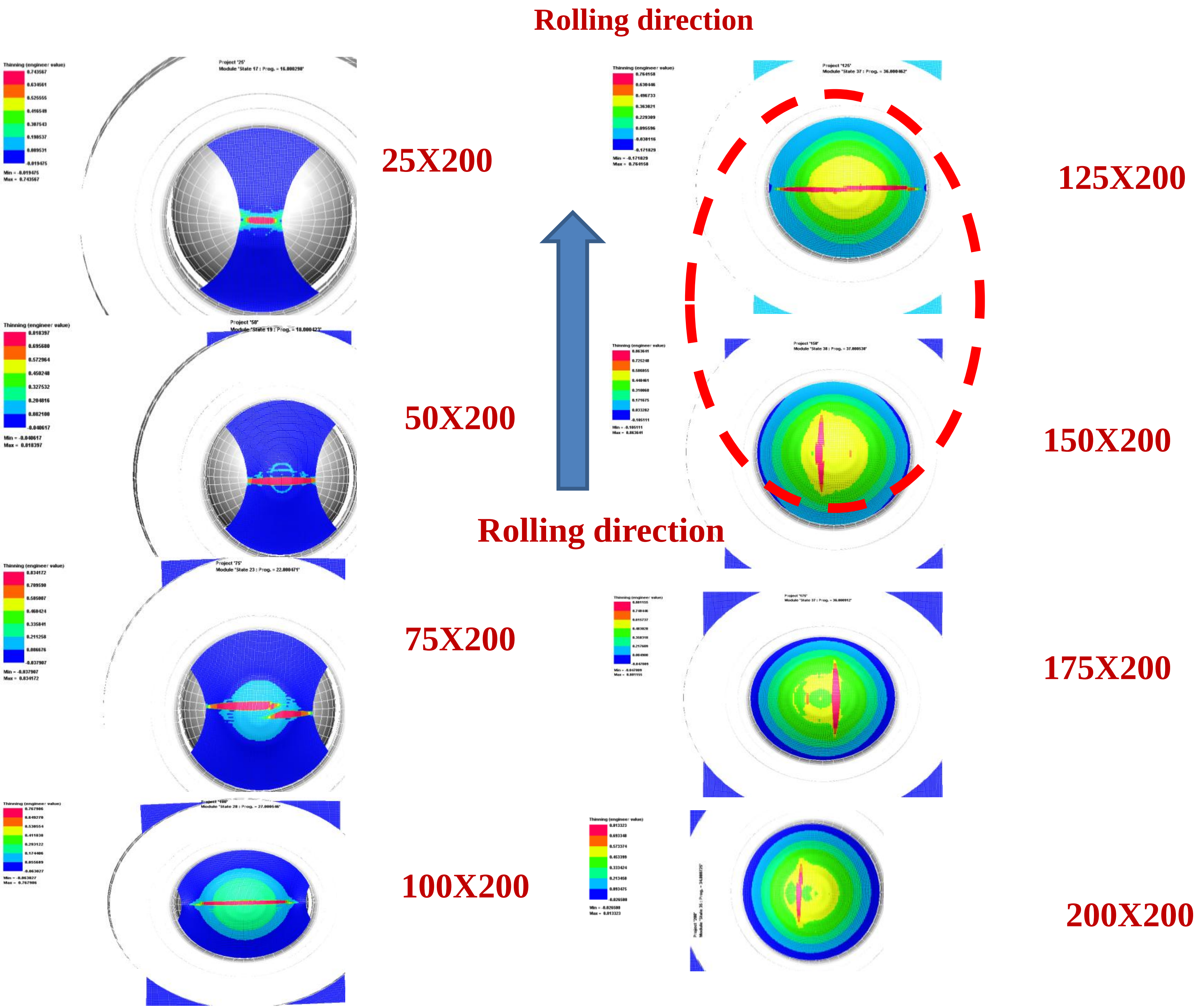
Rolling direction
25X200
50X200
75X200
100X200
125X200
150X200
175X200
200X200
Rolling direction

Summary

•The final fracture is a sum total effect of sample geometry (w.r.t. loading) and material anisotropy.

•The changeover from fracture along rolling direction to major stress direction can be captured by macro anisotropic analysis.

Case Study 2

Al sheet formability (DC vs CC)

Motivation

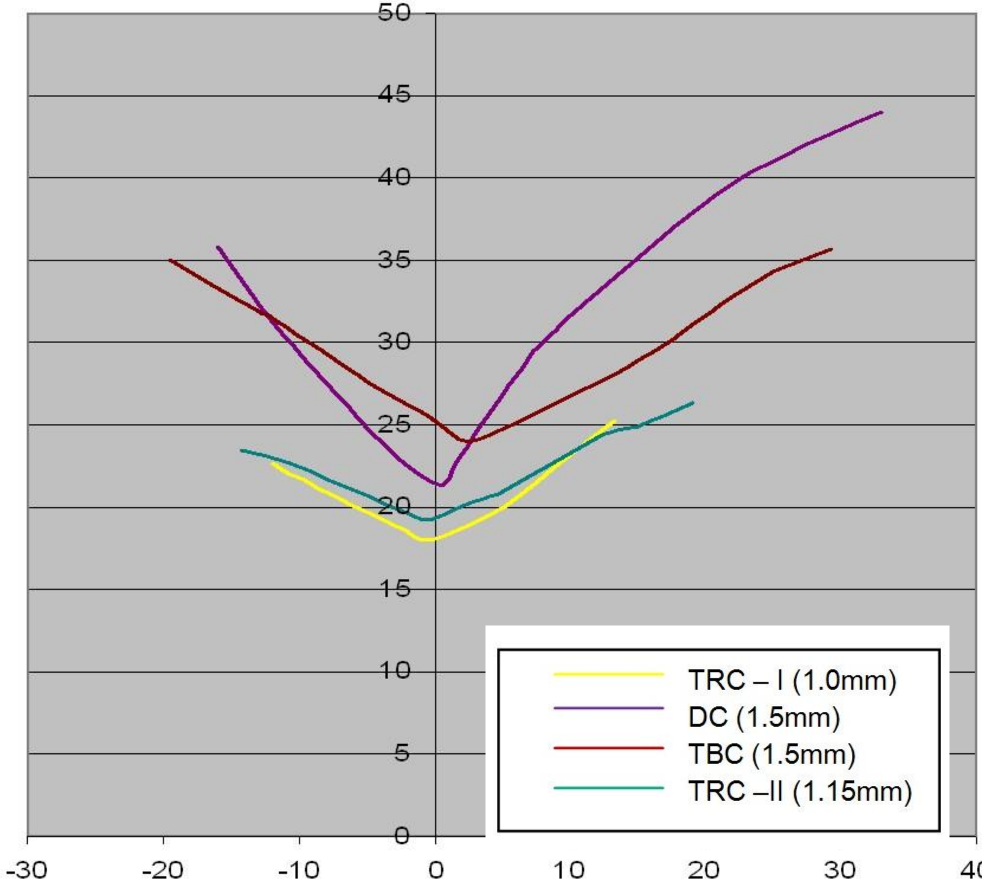

Large formability variation of same 5754 Al alloy processed through different processes

Automotive lightweighting

- Advantages
  - Fuel consumption and emissions
    - 10% weight reduction => 7% increase in fuel ecomony
  - Performance
    - Less inertia => better acceleration
  - Passive safety
    - Lighter thrust, optimal weight distribution
  - Active safety
    - Increased braking stability and efficacy
  - Acoustics
    - Dynamic alleviation
- FIVE KEY Challenges
  - Cost reduction
  - Manufacturability
  - Design data and test methodologies
  - Joining
  - Recycling and repair.

Cost Analysis

- Continuous casting vs direct chill cast sheets
  - 25% energy savings in CC
  - 14% economic saving in CC
- Manufacturability
  - Formability of CC in lower than DC (FLD)

Alloy composition and processing

5754 Alloy	Mg wt%	Mn wt%	Cr wt%	Fe wt%	Si wt%
DC	3.0	0.25	0.01	0.18	<0.10
TBC	3.1	0.25	<0.01	0.24	<0.10
TRC-I	2.8	0.01	<0.01	0.25	0.10
TRC-II	2.9	0.01	<0.01	0.24	0.08

Di

Co

Co

Typical microstructure of various 5754 alloys

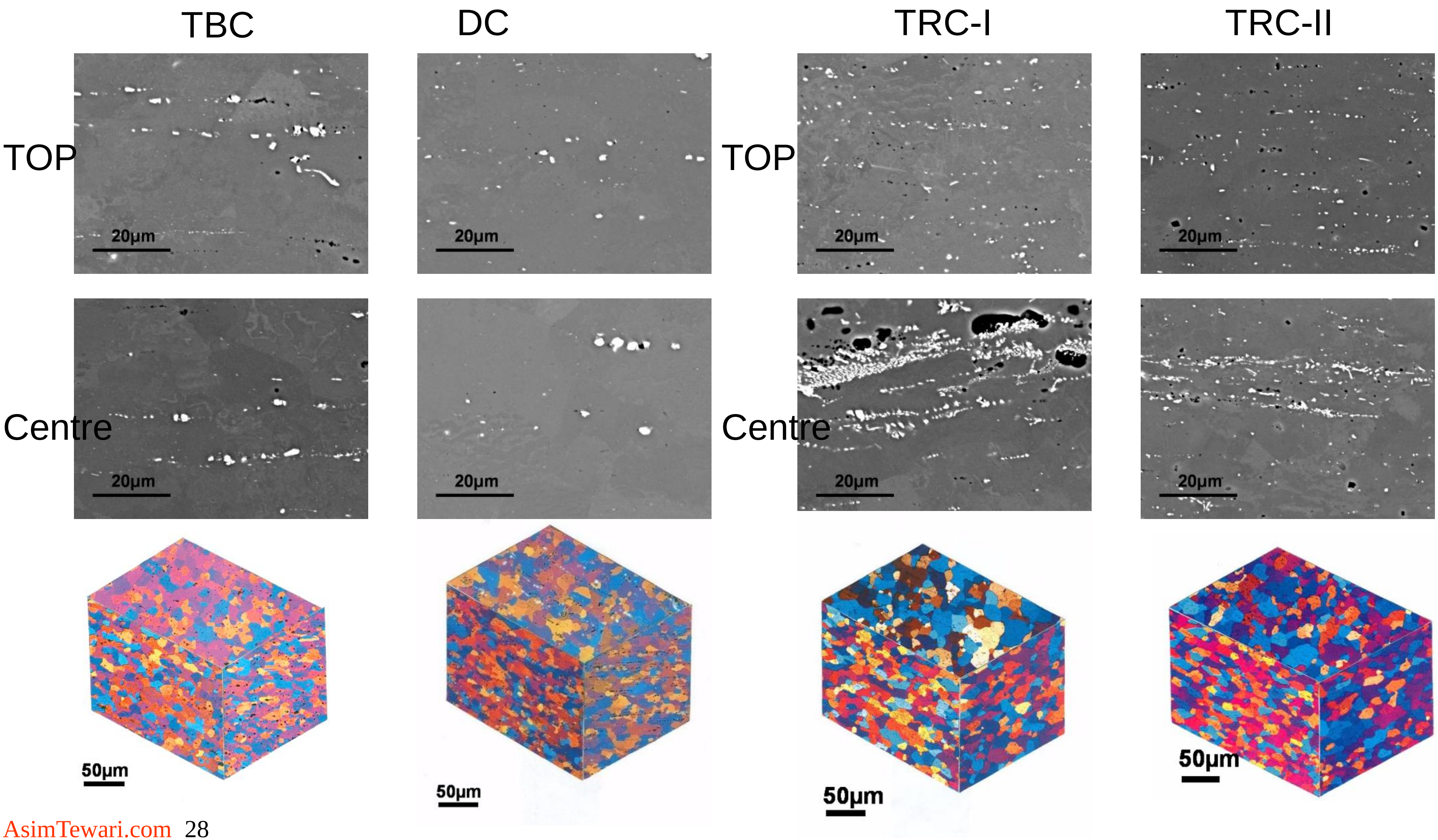

Center-line Segregation

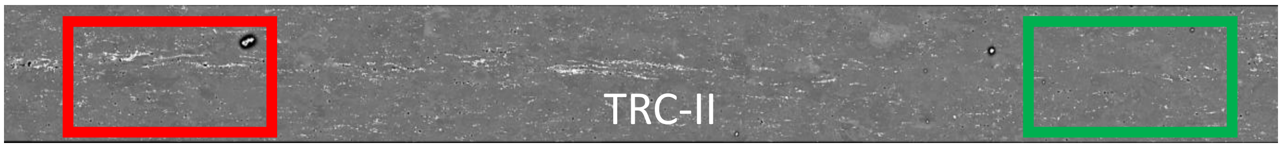

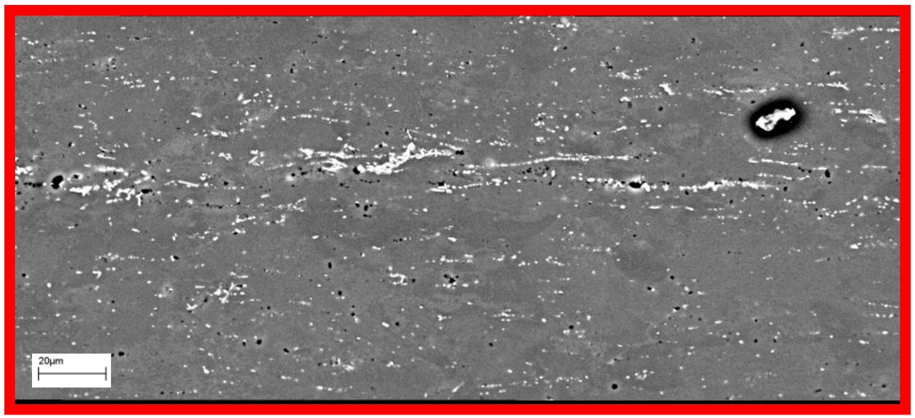

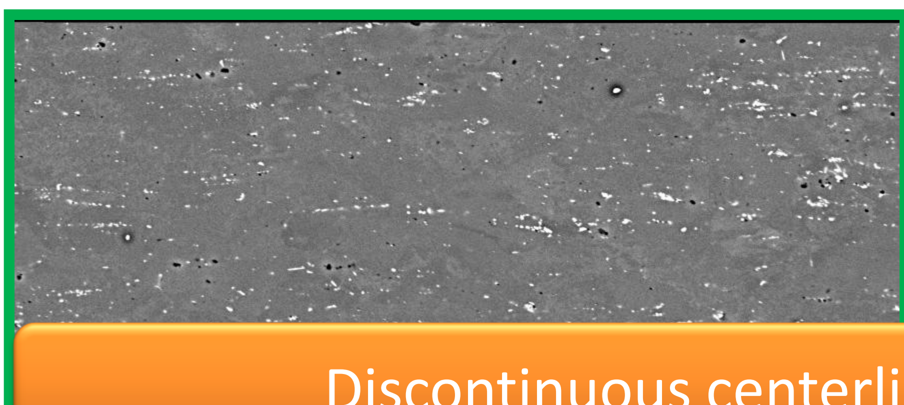

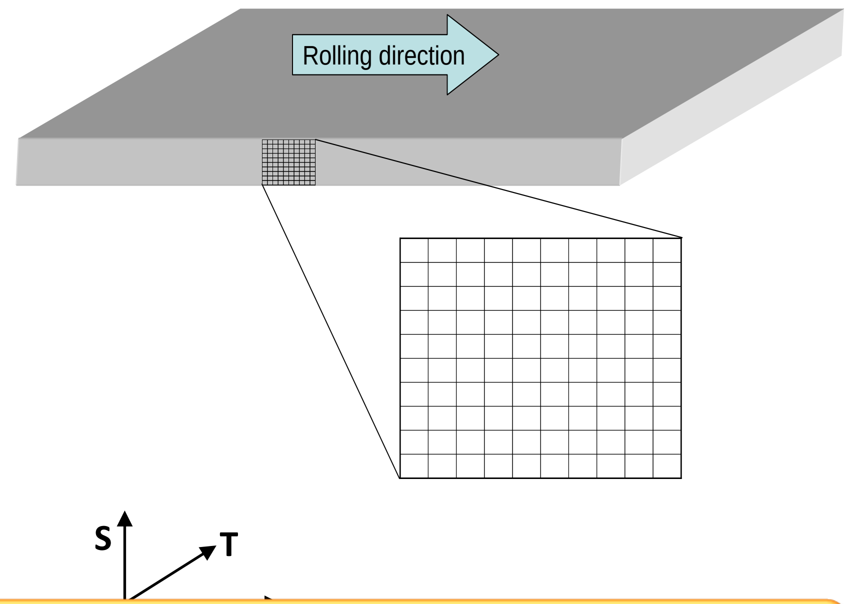

Discontinuous centerline segregation in TRC-II

Asi

Second phase particles

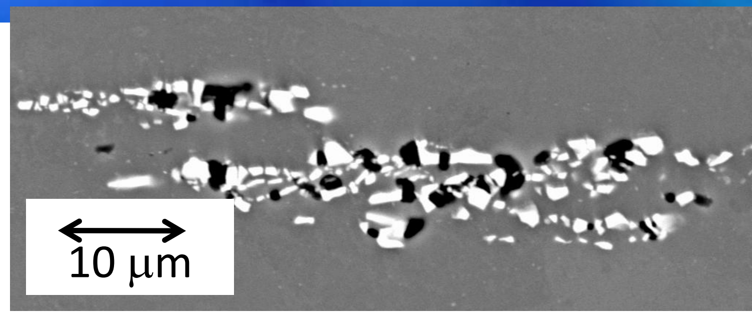

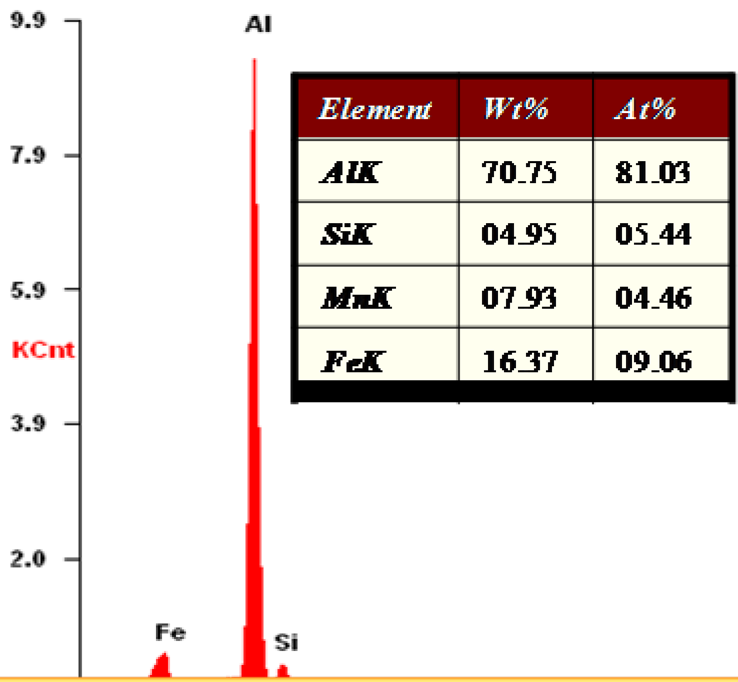

Element	Wt%	At%
AlK	70.75	81.03
SiK	04.95	05.44
MnK	07.93	04.46
FeK	16.37	09.06

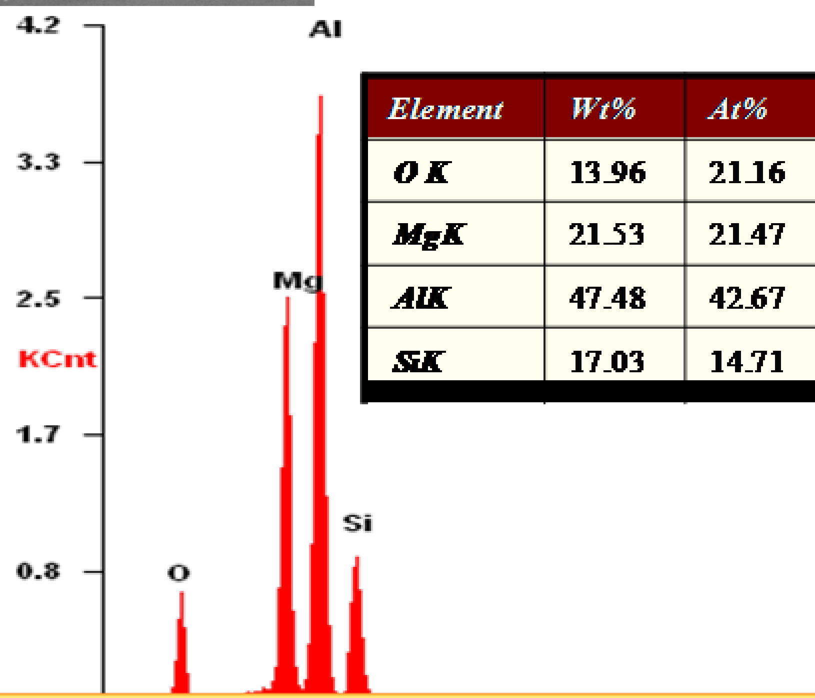

Element	Wt%	At%
O K	13.96	21.16
MgK	21.53	21.47
AlK	47.48	42.67
SiK	17.03	14.71

Two type of second phase particles are present

Through thickness microstructure variation

	Intermetallics		Oxides	
	Volume fraction	Size (μm)	Volume fraction	Size (μm)
DC	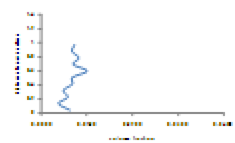	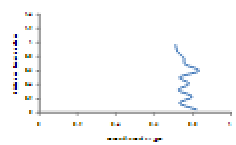	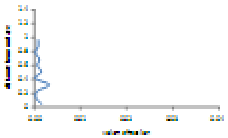	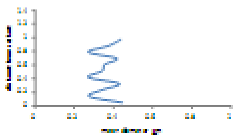
TBC	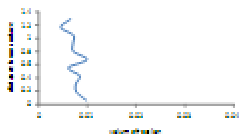	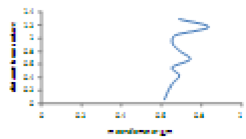	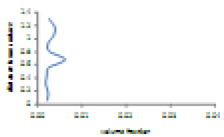	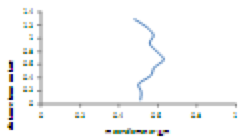
TRC - I	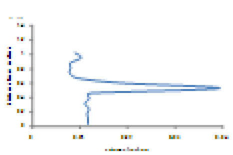	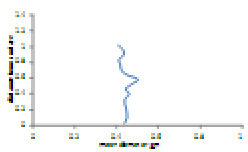	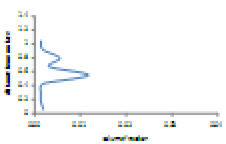	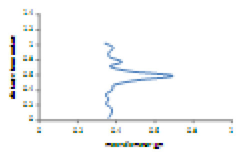
TRC - II	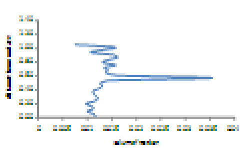	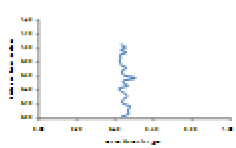	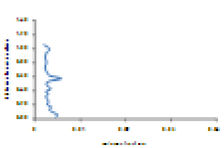	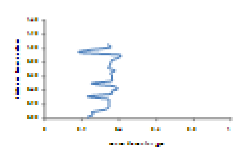

Mechanical properties along the rolling direction

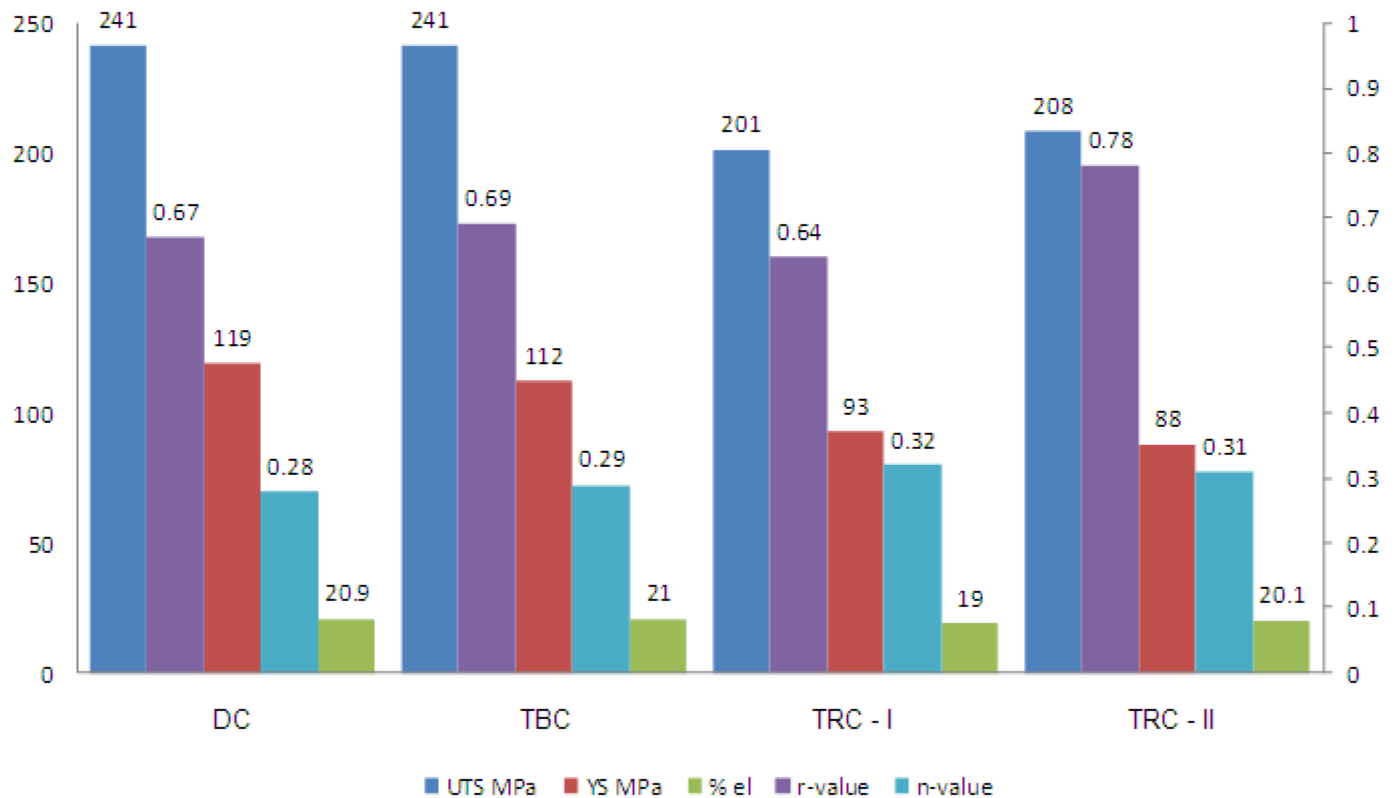

TRC has lower YS and UTS than TBC or DC

Asi

Fractographic investigation (TRC-I)

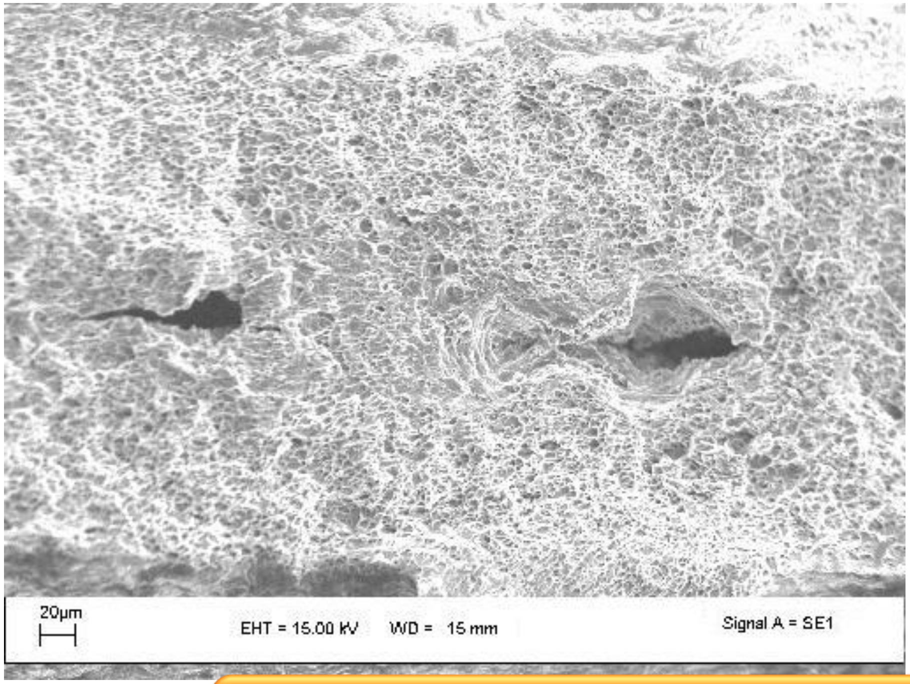

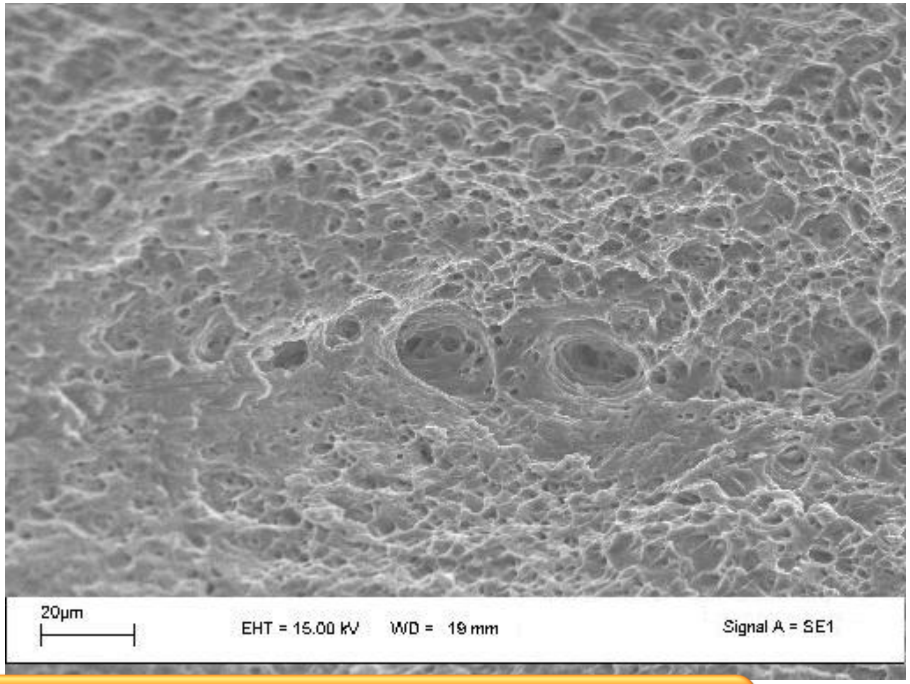

Microvoid formation at particle clusters

Microstructure based FEA

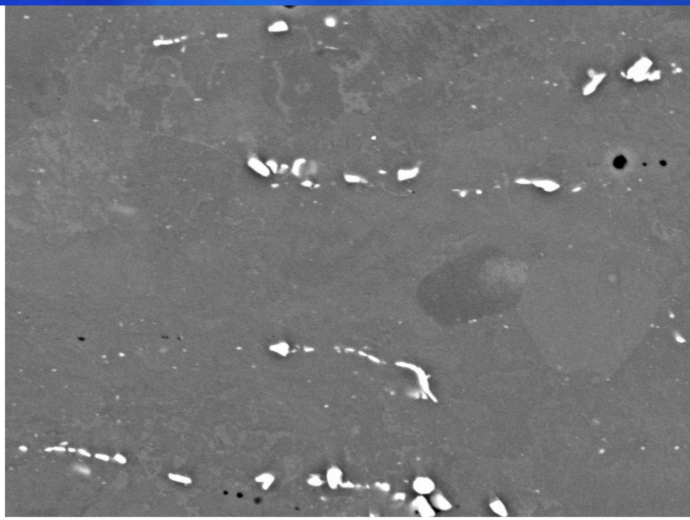

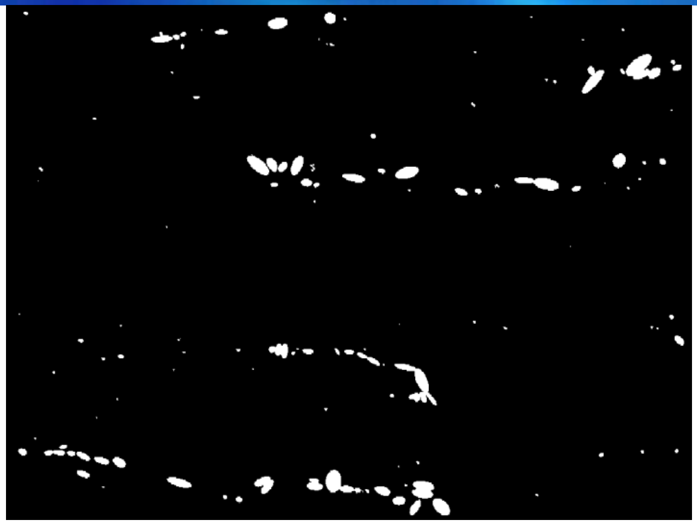

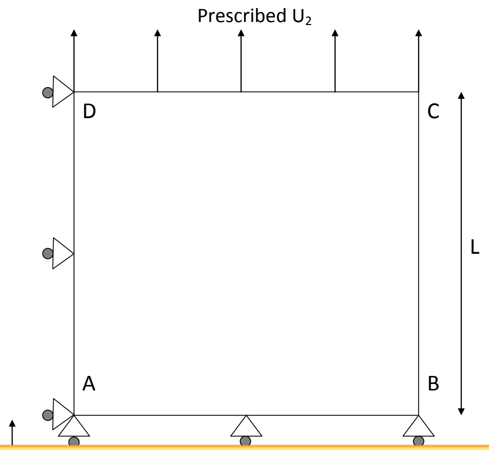

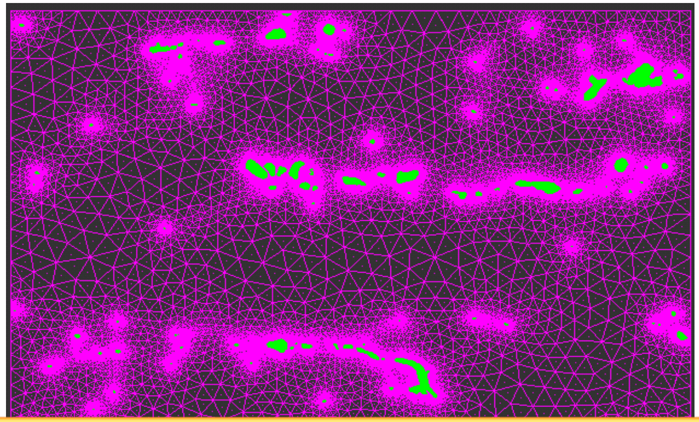

Modeling particles as intersecting ellipses is a good approximation

Asi

FE predictions of uniaxial stress-strain behavior

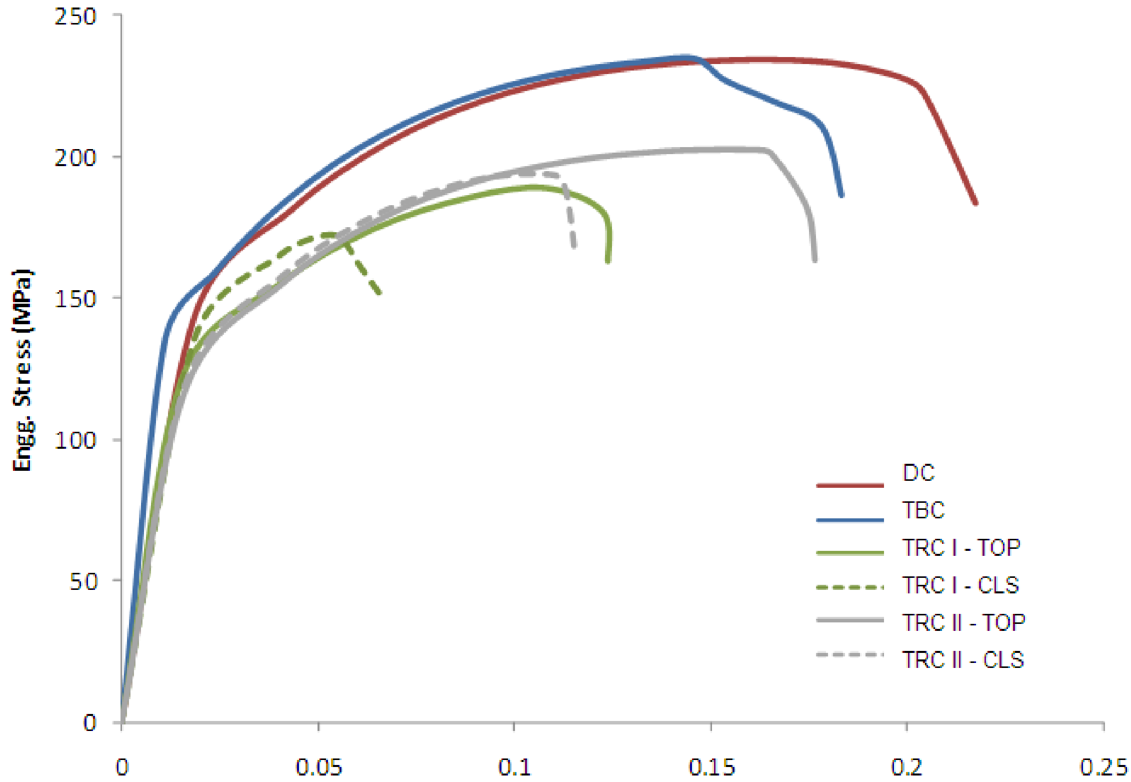

Novelis has higher localization strain than Assan
With in Assan, center region has lower localization strain than top

Correlation of localization strain and Extreme Property Index (EPI)

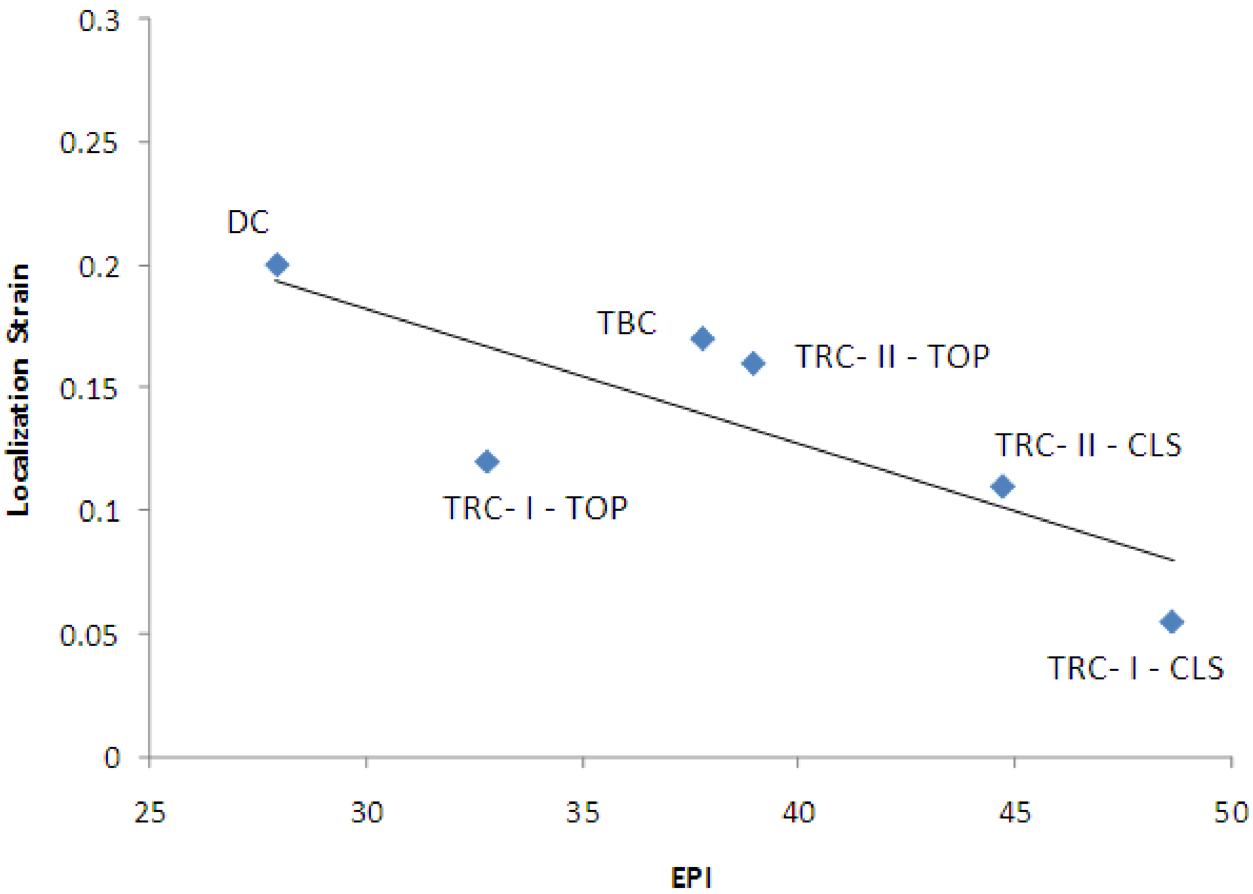

EPI is identified as a key microstructural attribute

Plastic deformation by slip

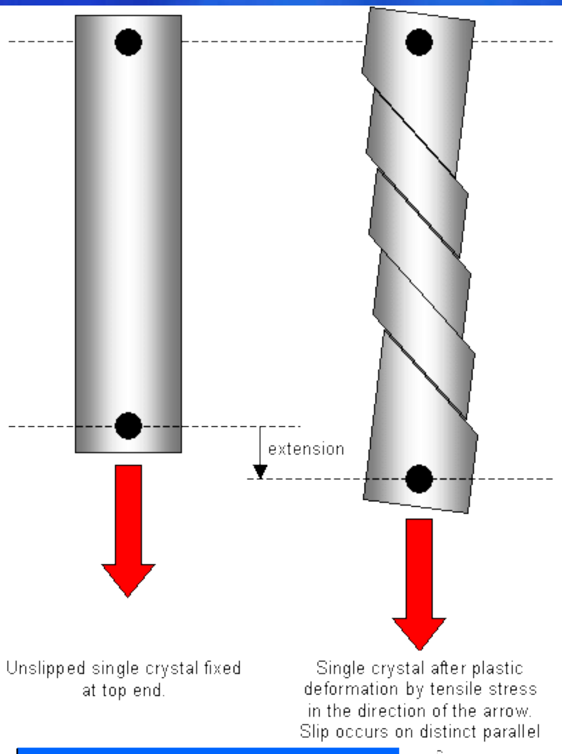

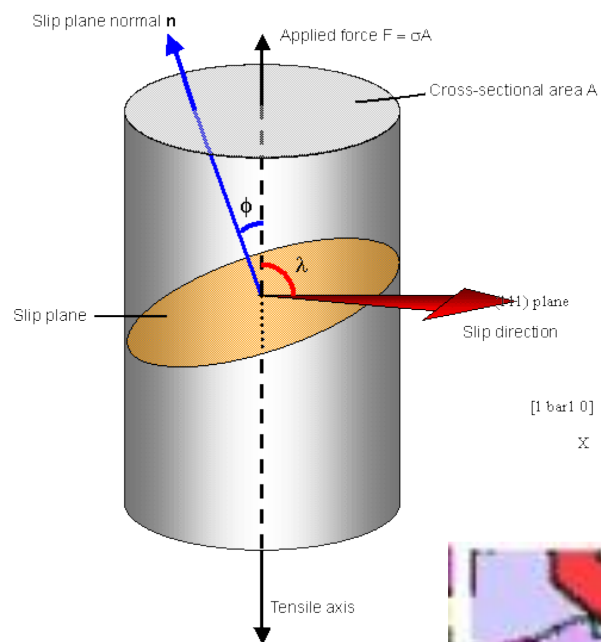

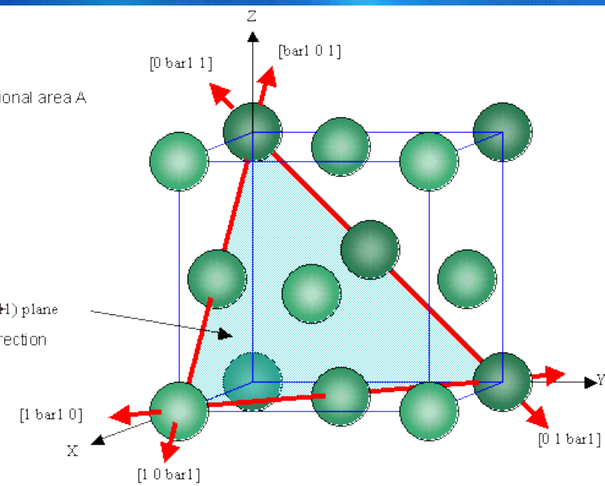

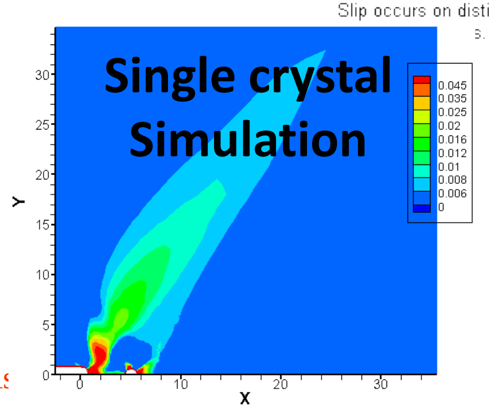

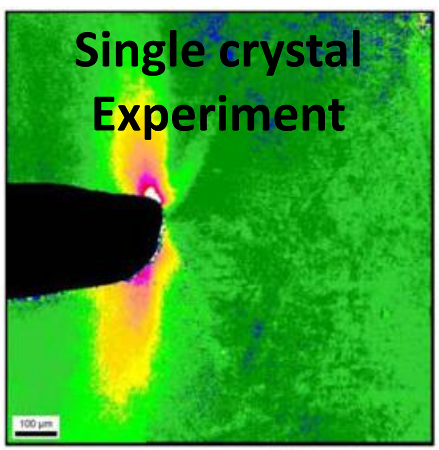

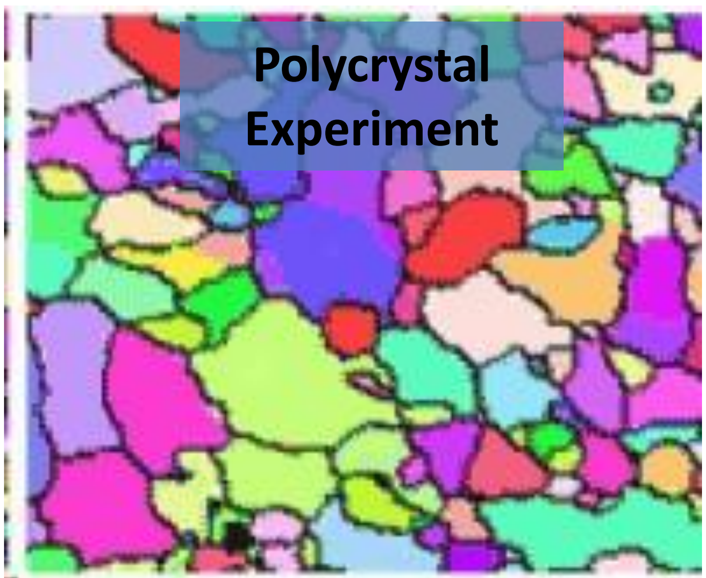

Inverse pole figure maps

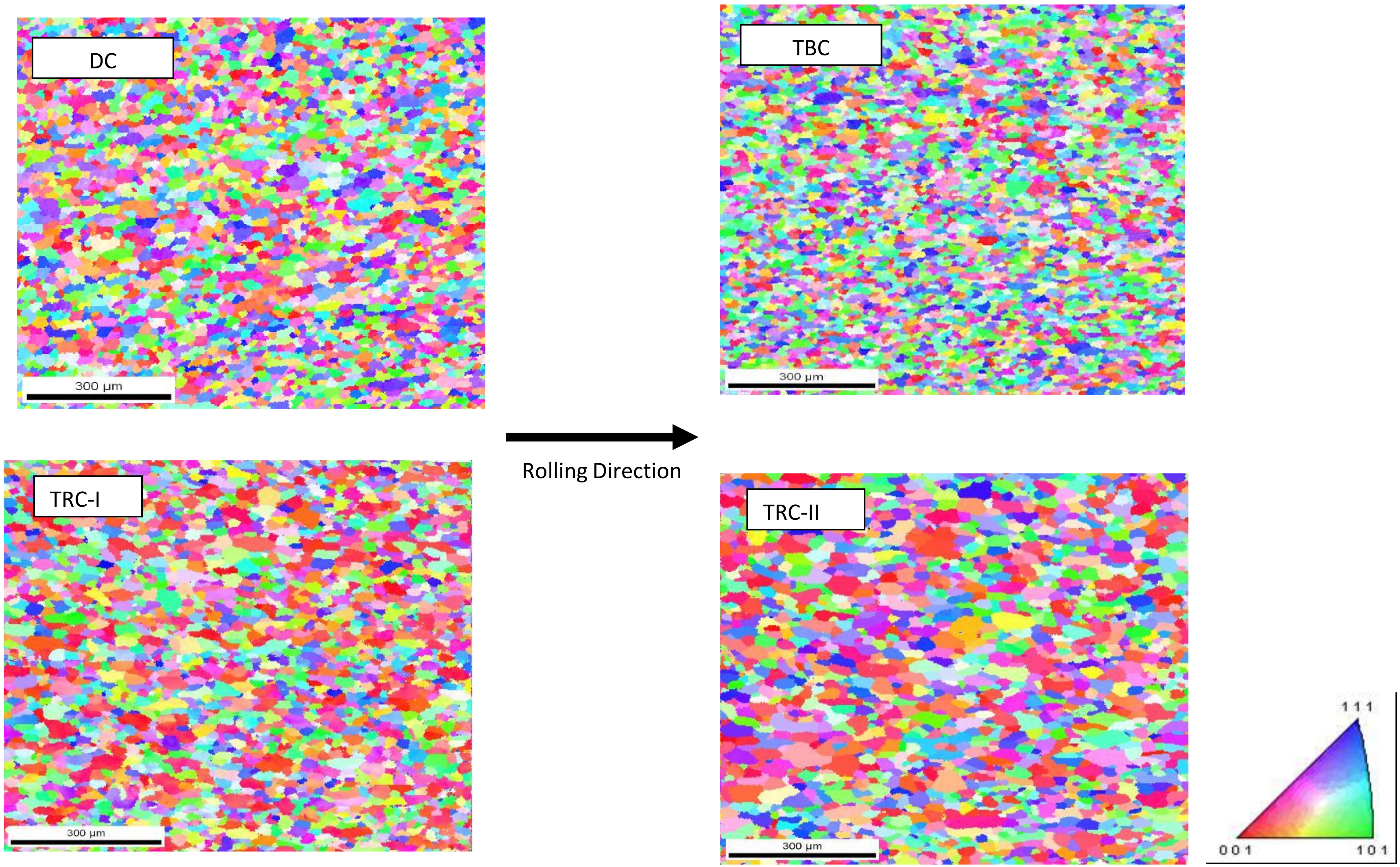

Fraction of various texture components

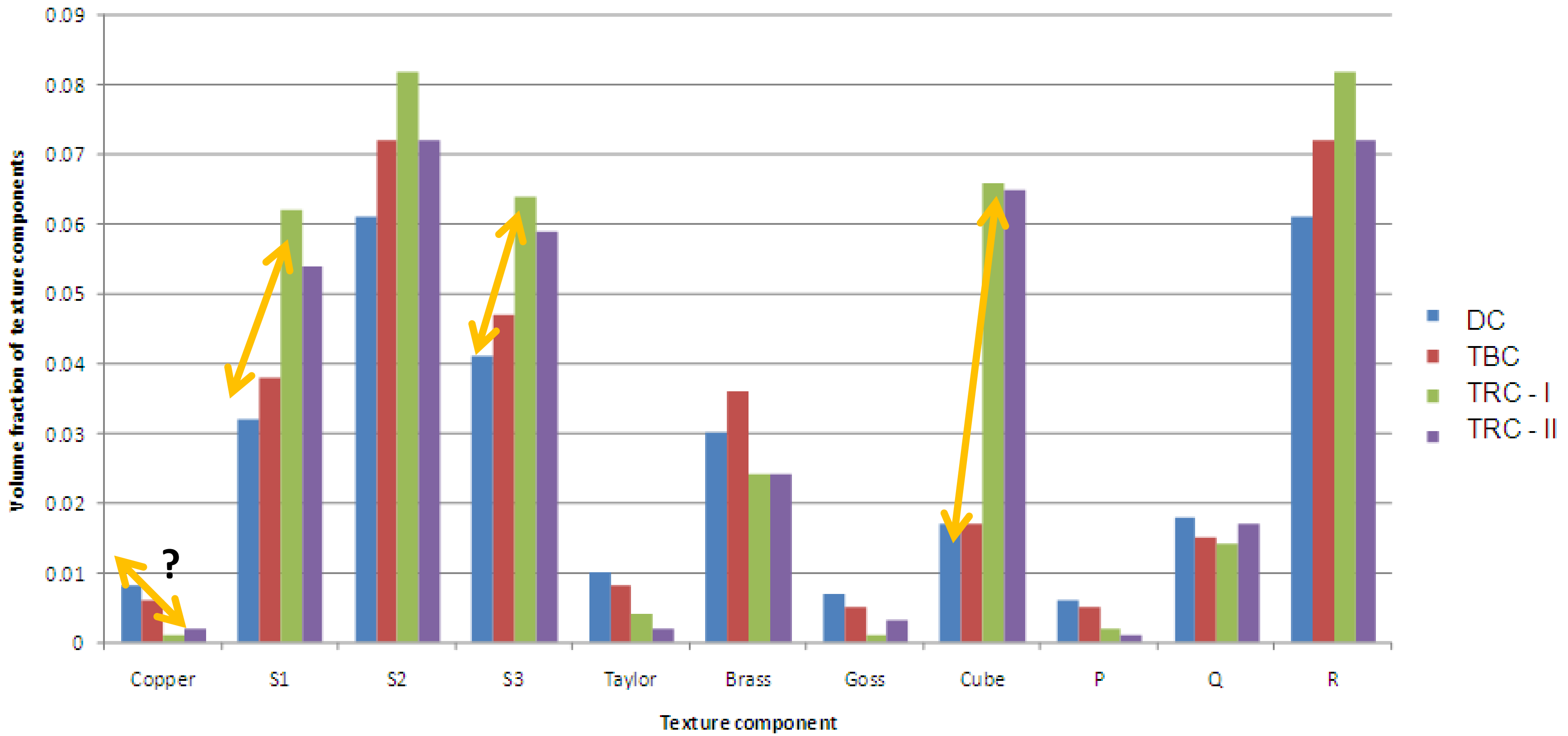

TBC has more rolling texture while TRC has more re-crystalization texture

Summary

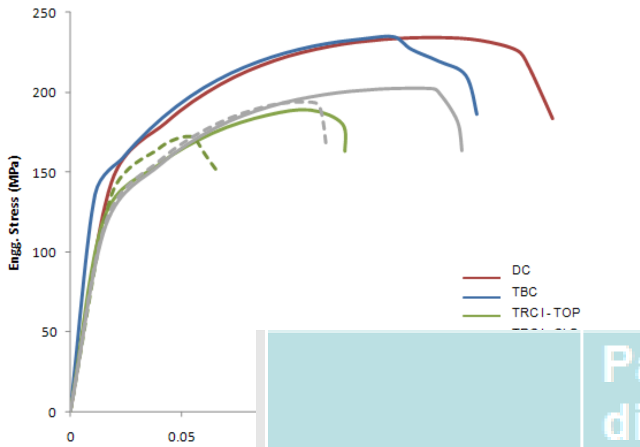

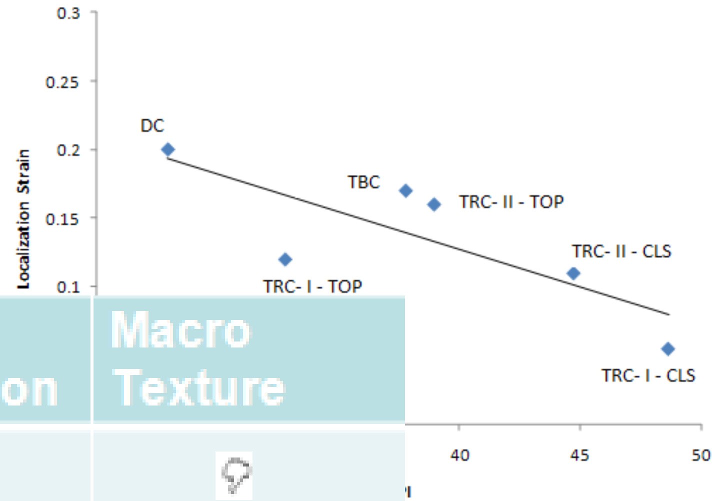

	Particle distribution	Macro Texture
DC	👍	👎
TB CC	👍 👎	👎
TR CC –I	👎	👍
TR CC– II	👍 👎	👍

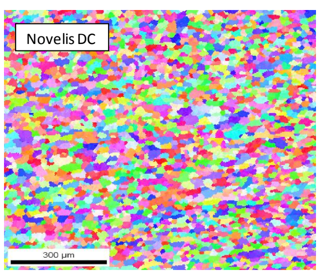

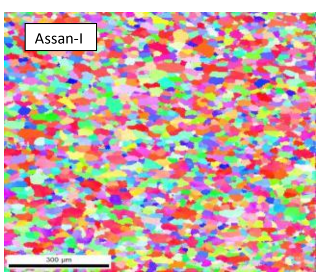

Rolling Direction

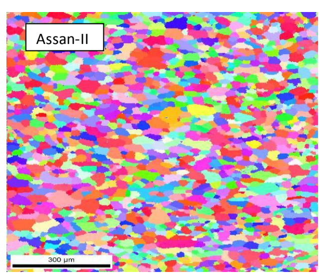

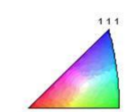

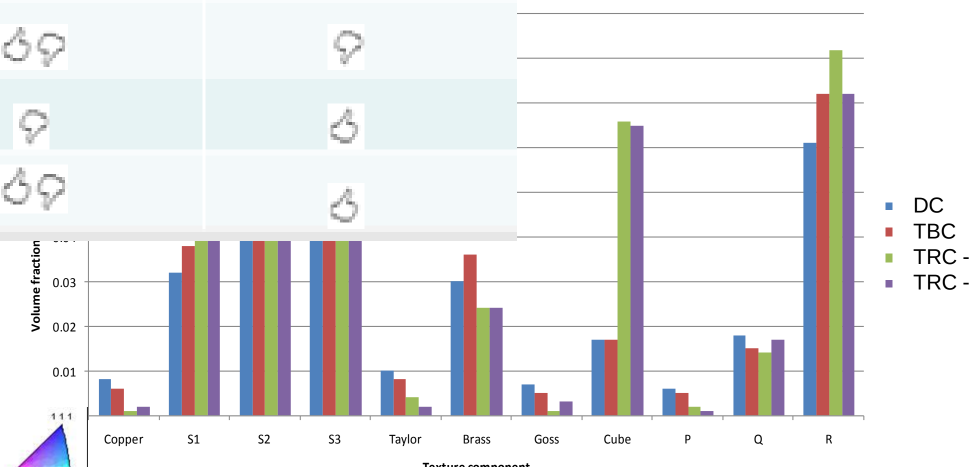

Case Study 3

Large scale formability simulations

Microstructural features in 5754 Al

Alloy	Mg	Mn	Cr	Fe	Si	Cu	Al
DC	3.0	0.25	0.01	0.18	<0.1	0.01	Bal.
CC	3.1	0.25	<0.01	0.24	<0.1	0.02	Bal.

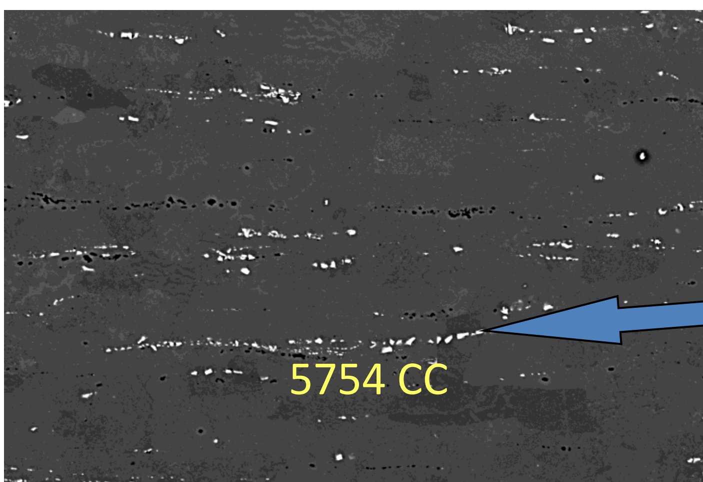

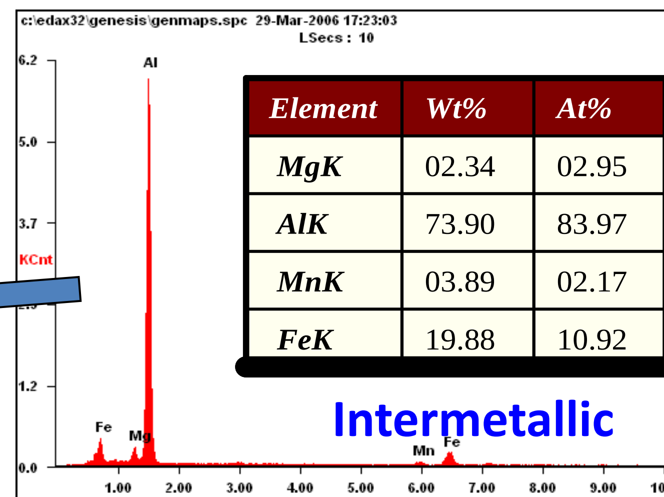

Element	Wt%	At%
MgK	02.34	02.95
AlK	73.90	83.97
MnK	03.89	02.17
FeK	19.88	10.92

Effect of Spatial arrangement of second phase

Clustered

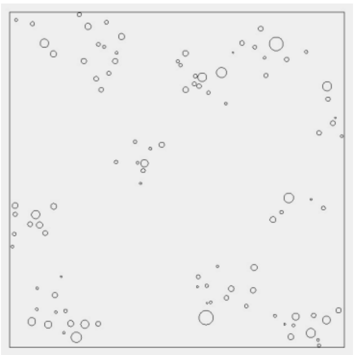

Random

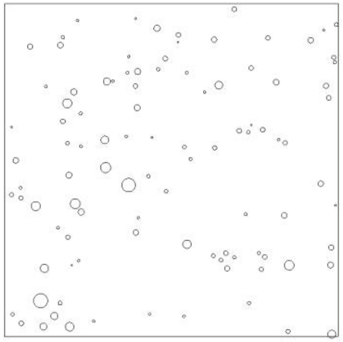

Ordered

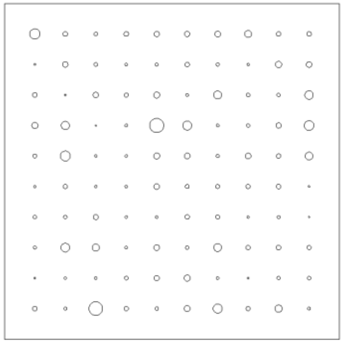

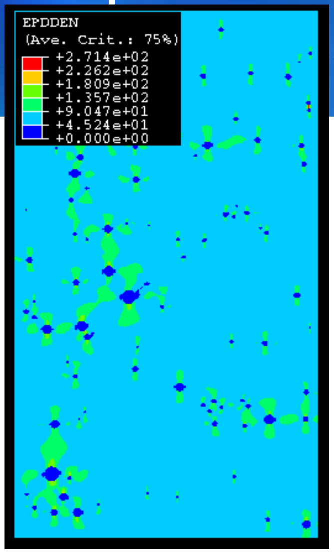

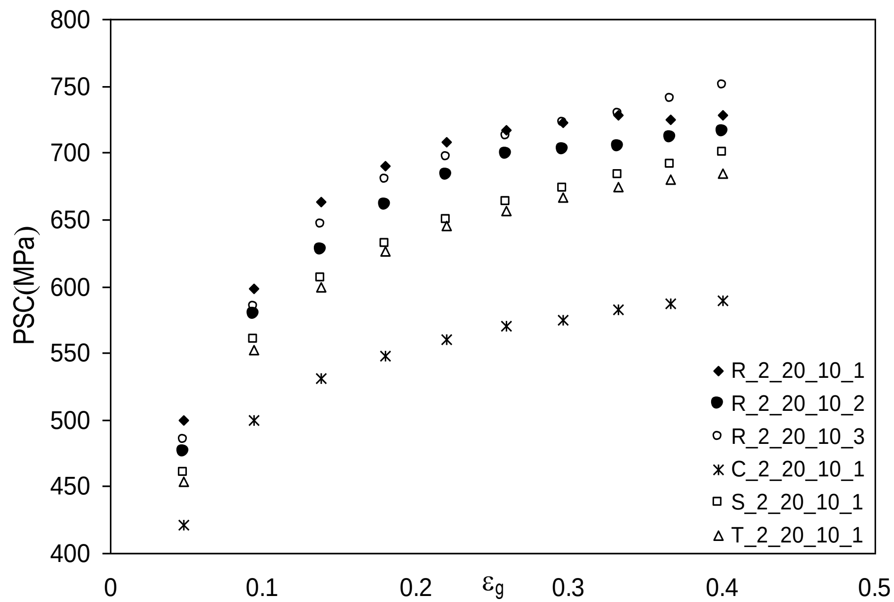

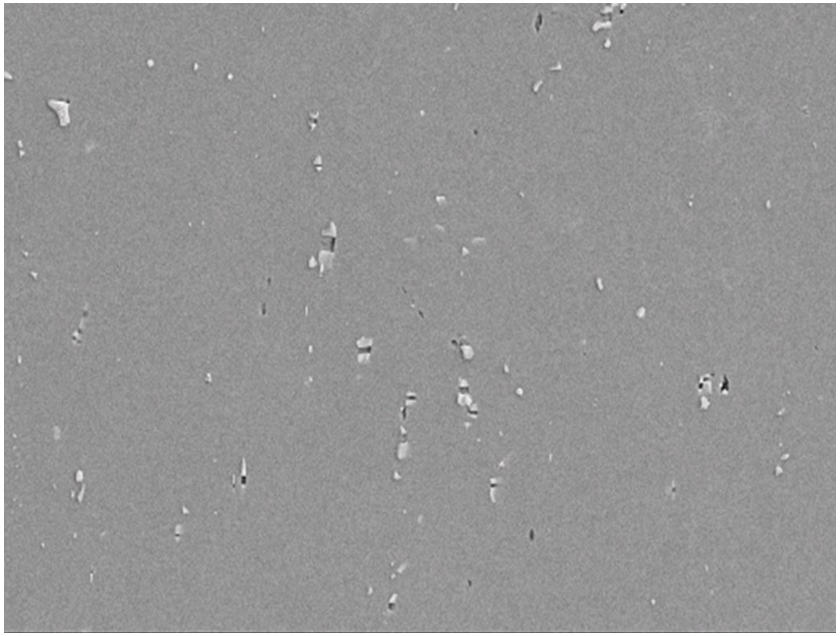

Virtual tensile test

Real Microstructure

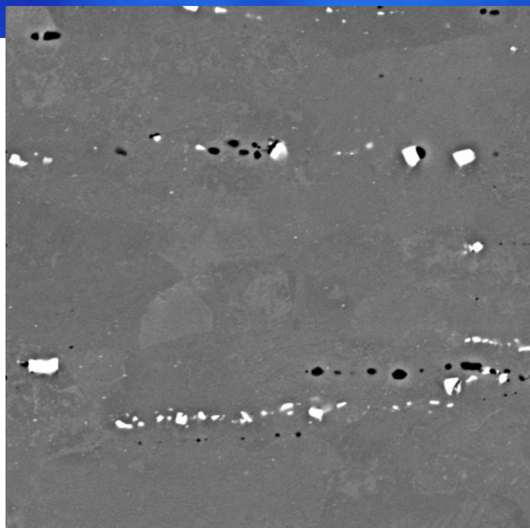

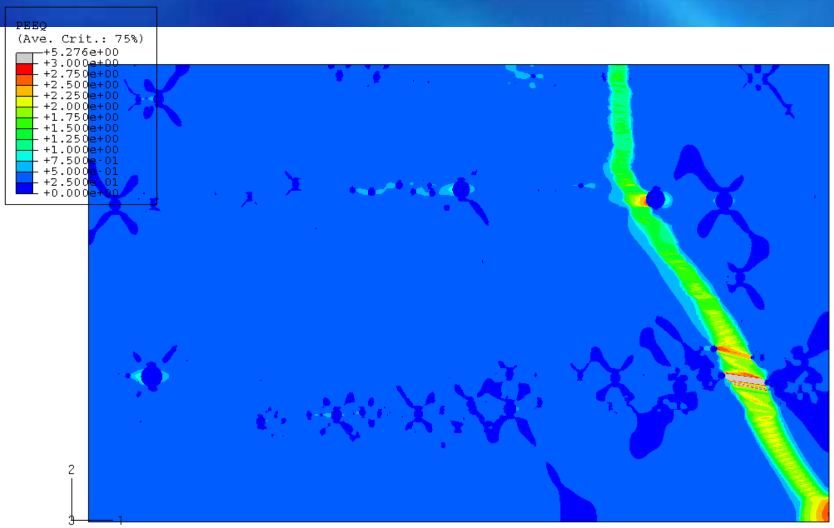

FE Representation

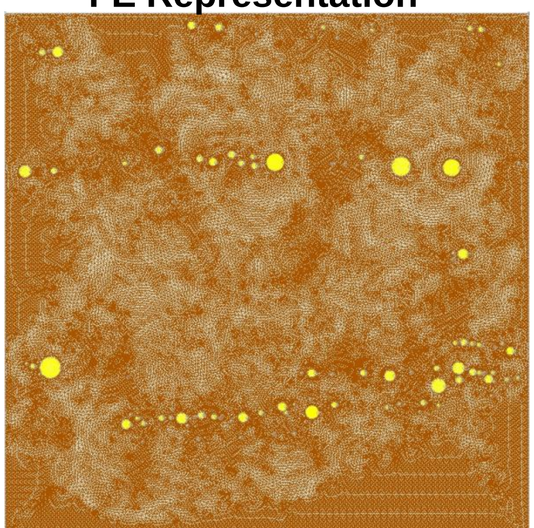

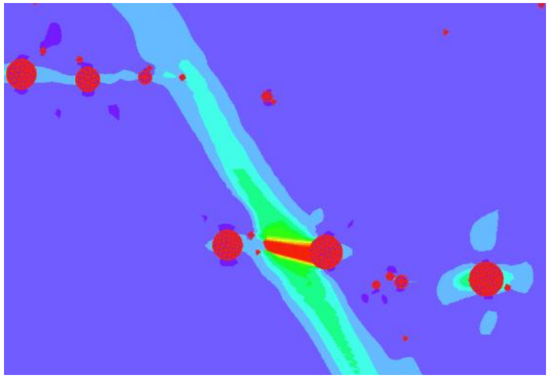

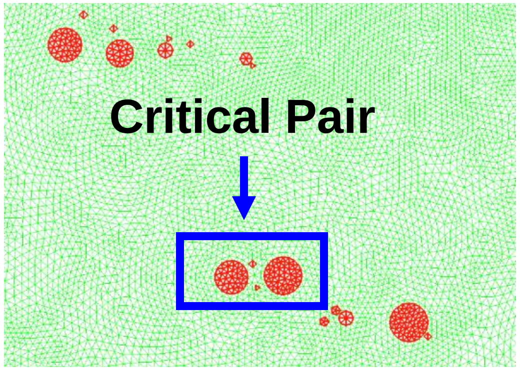

Comparison of DC vs CC alloy

Alloy	V_V	S_V (μm)$^{-1}$	λ(μm)	L_3 μm
DC	0.0095±0.0005	0.038±0.002	104.6	1.01
CC	0.0095±0.0010	0.045±0.005	87.5	0.84

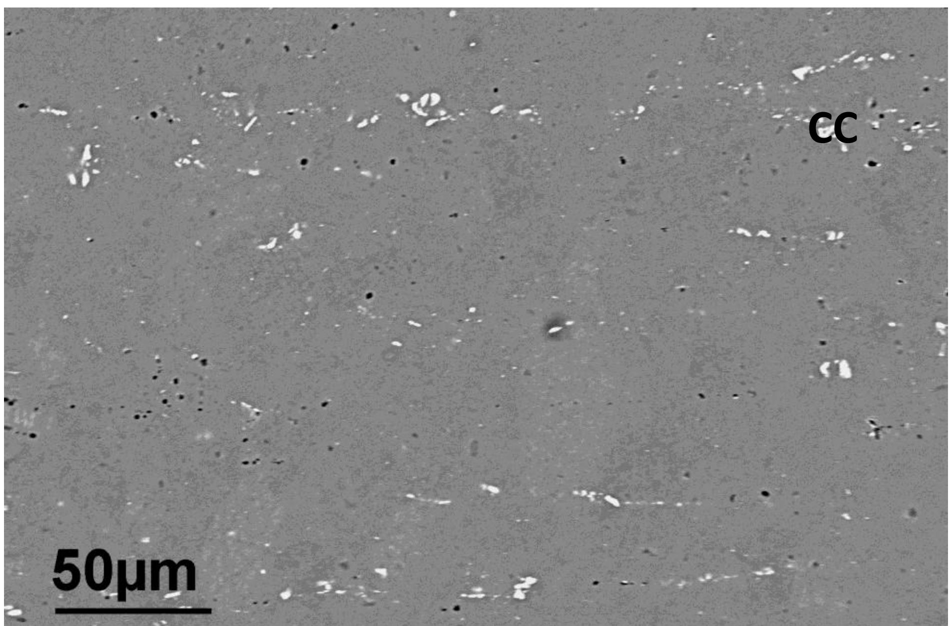

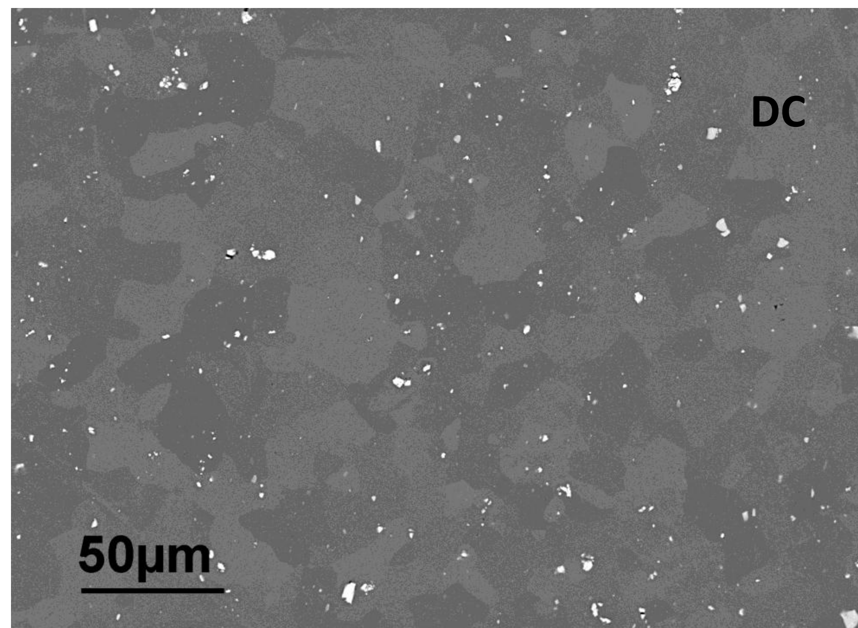

Vectorization approximation

- More emphases on spatial arrangement
- Partial shape parameterization
  - PCA
  - Distance transformation maps
  - SPHARM*

Orthonormal spherical harmonics of the solutions to Laplace's equation represented in spherical coordinates

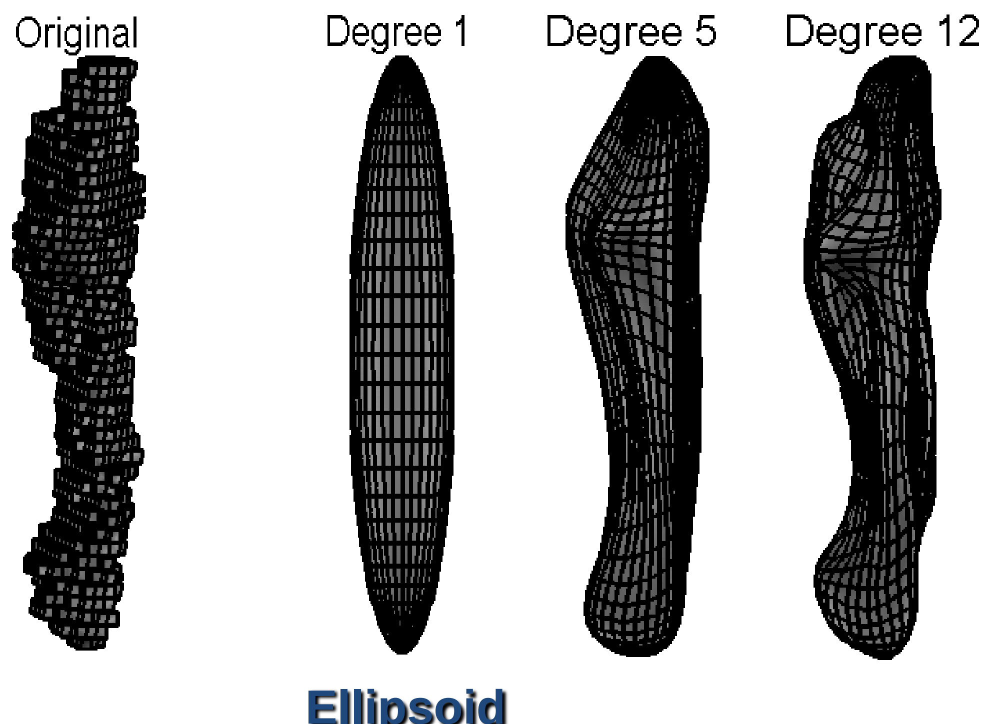

*L. Shen, J. Ford, F. Makedon, and A. Saykin, Intl Con Com Vis Patt Recog Img Proc, NC, 2003.

Ellipsoid shape approximation

– Sphere, prolate, oblate, scalene, egg

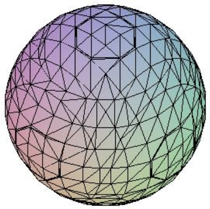

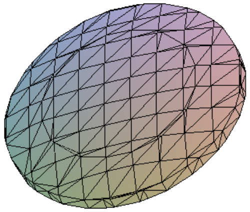

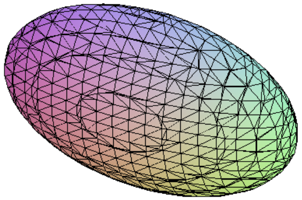

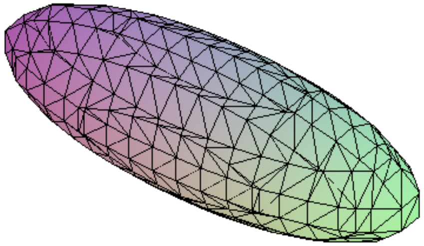

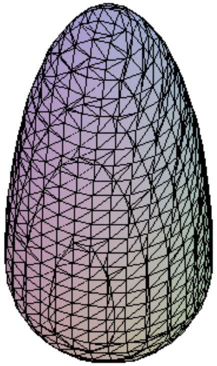

Ellipsoid shape approximation

Shape	Number of variables	Variables
Generalized ellipsoid	**9**	**Centriod (*h*,*k*,*l*)** **Radii a, b, and c** **Euler angles ϕ_1, Φ, ϕ_2**
Generalized spheroid	**7**	**Centriod (h,k,l)** **Radii a and b** **Angles θ and ϕ**
Axisymmetric Spheroid	**6**	**Centriod (h,k,l)** **Radii a and b** **Angles θ**
Sphere	**4**	**Centriod (h,k,l)** **Radii a**

2D vector image

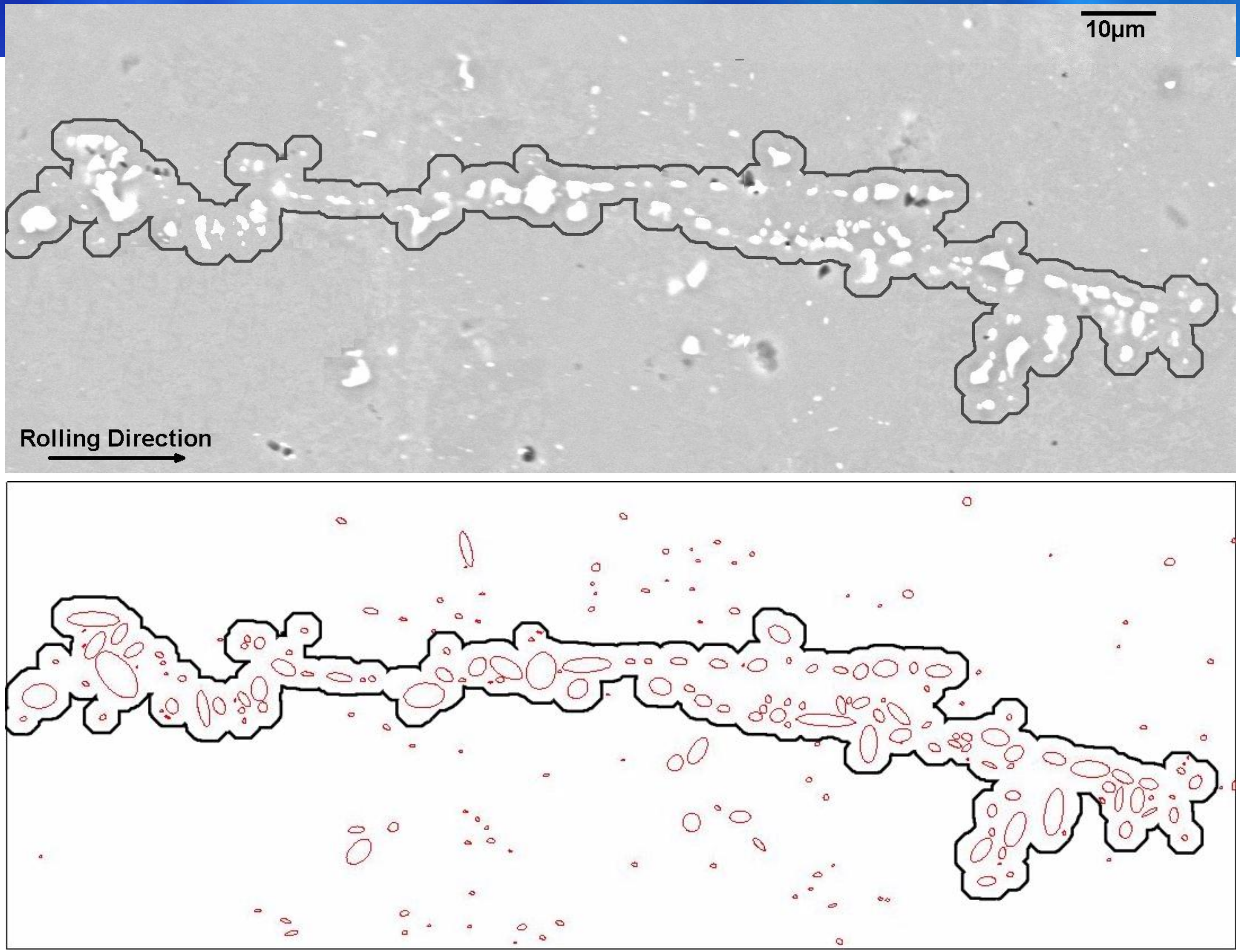

2D vector image

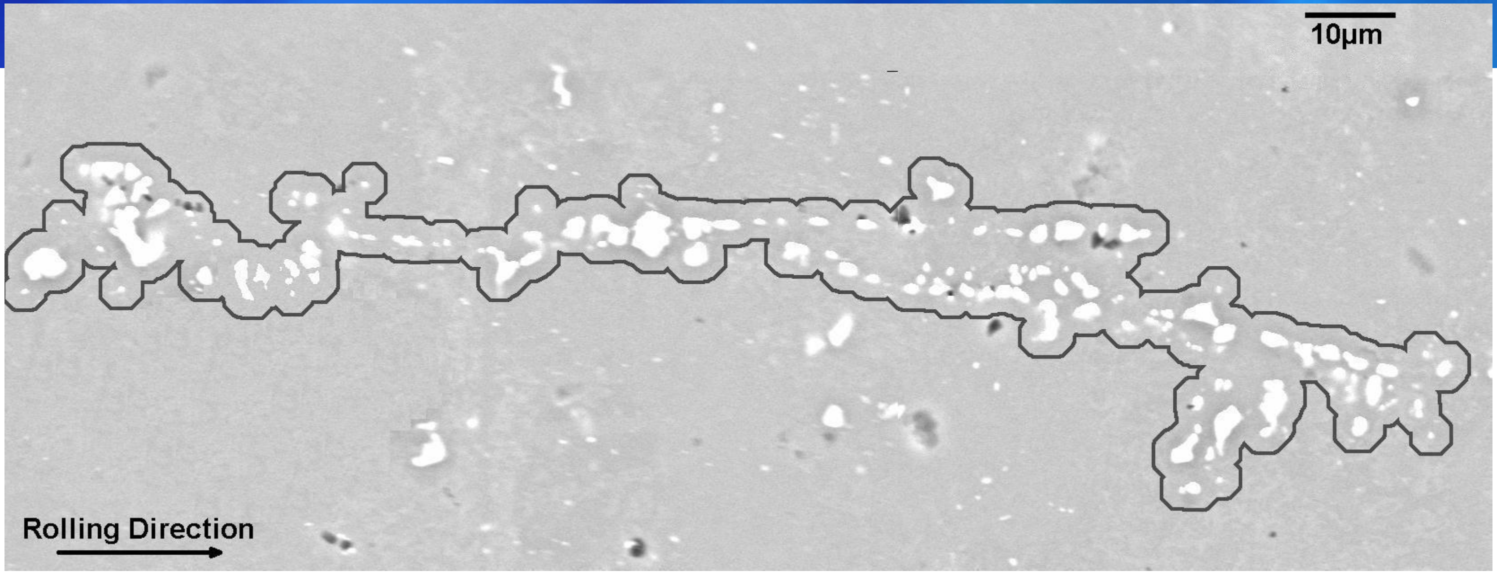

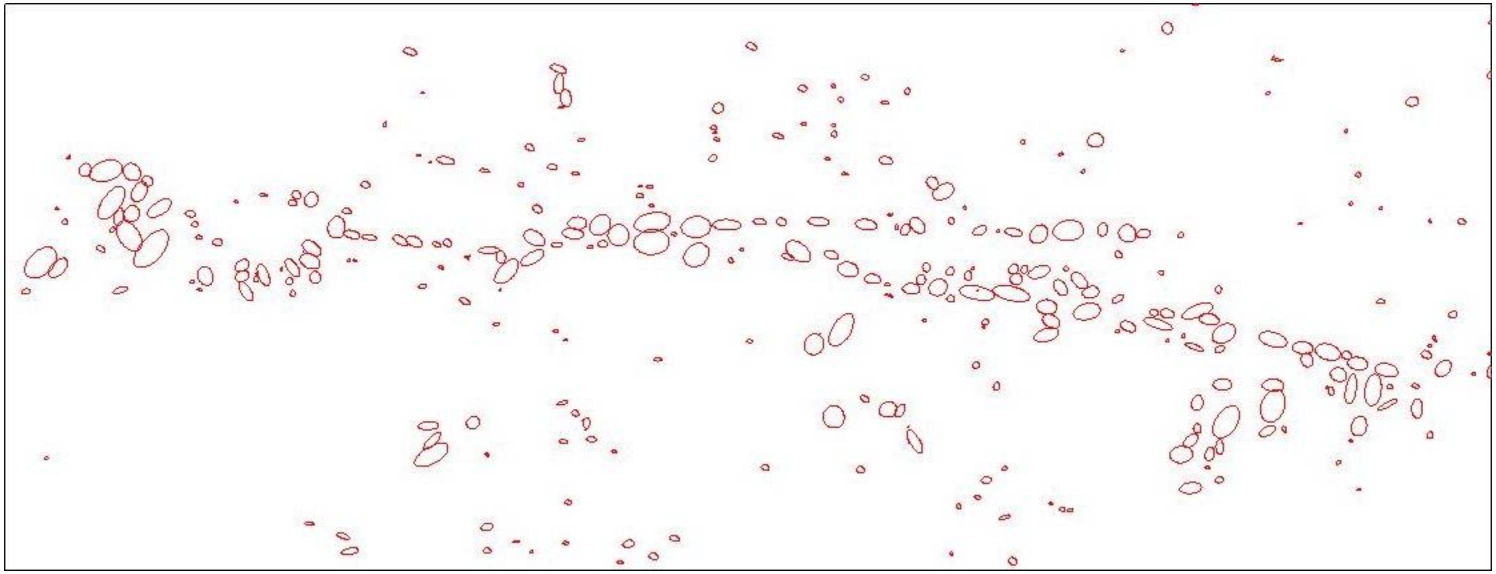

2D vector image

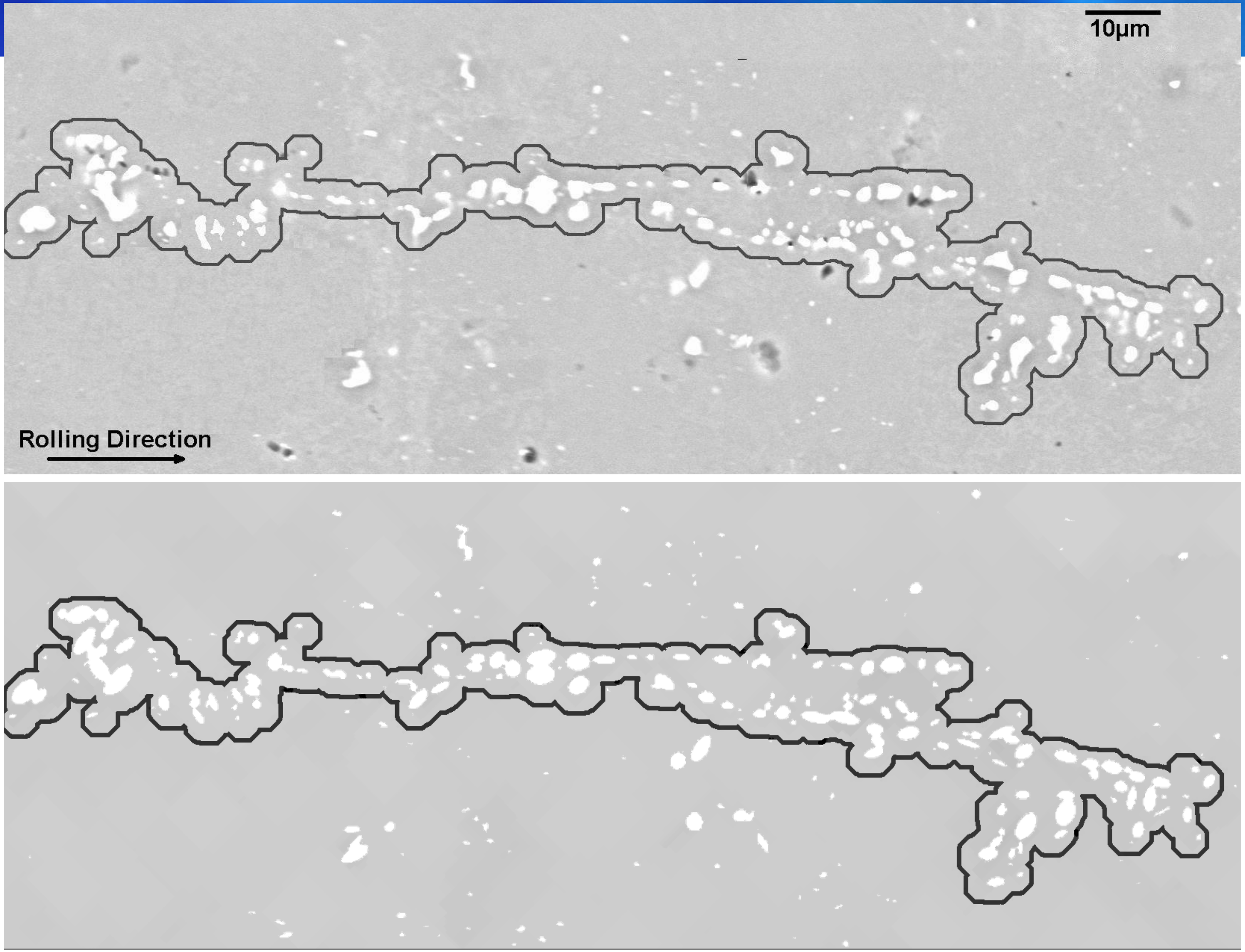

Intrinsic Volumes

- Minkowski Functions

$$W_k(Y) = \frac{b_d}{b_{d-k}} \int_{L_k} v_{d-k}(P_s \perp Y) U_k(dS)$$

d+1 intrinsic volumes in d dimensional space

In R^3

W_0, W_1, W_2, W_3

Hadwiger theorem

All additive, motion-invariant, and continuous functions of convex sets are linear combinations of these four characteristics.

For R^d this can be written as

$$h(Y) = \sum_{k=0}^{d} a_k W_k(Y)$$

Extension to convex rings

Convex Ring A

$$A = \bigcup_{i=1}^{n} Y_i \text{ for } Y_i \in C(K)$$

$$W_K(A) = \frac{b_d}{b_{d-k}} \int_{L_k} \int_S \chi(A \cap Ss) \nu_{d-k}(ds) U_k(ds)$$

Location and orientation transformation

- Eulerian rotation and translation

$$\mathbf{E} = \mathbf{Z_2} * \mathbf{X_1} * \mathbf{Z_1} * \mathbf{T} * \mathbf{X}$$

$$\mathbf{E} = \begin{bmatrix} e1 \\ e2 \\ e3 \\ 1 \end{bmatrix} \qquad \mathbf{X} = \begin{bmatrix} x \\ y \\ z \\ 1 \end{bmatrix}$$

$$\mathbf{Z}_2 = \begin{bmatrix} \cos\phi_2 & \sin\phi_2 & 0 & 0 \\ -\sin\phi_2 & \cos\phi_2 & 0 & 0 \\ 0 & 0 & 1 & 0 \\ 0 & 0 & 0 & 1 \end{bmatrix} \qquad \mathbf{X}_1 = \begin{bmatrix} 1 & 0 & 0 & 0 \\ 0 & \cos\phi & \sin\phi & 0 \\ 0 & -\sin\phi & \cos\phi & 0 \\ 0 & 0 & 0 & 1 \end{bmatrix}$$

$$\mathbf{Z}_1 = \begin{bmatrix} \cos\phi_1 & \sin\phi_1 & 0 & 0 \\ -\sin\phi_1 & \cos\phi_1 & 0 & 0 \\ 0 & 0 & 1 & 0 \\ 0 & 0 & 0 & 1 \end{bmatrix} \qquad \mathbf{T} = \begin{bmatrix} 1 & 0 & 0 & -h \\ 0 & 1 & 0 & -k \\ 0 & 0 & 1 & -l \\ 0 & 0 & 0 & 1 \end{bmatrix}$$

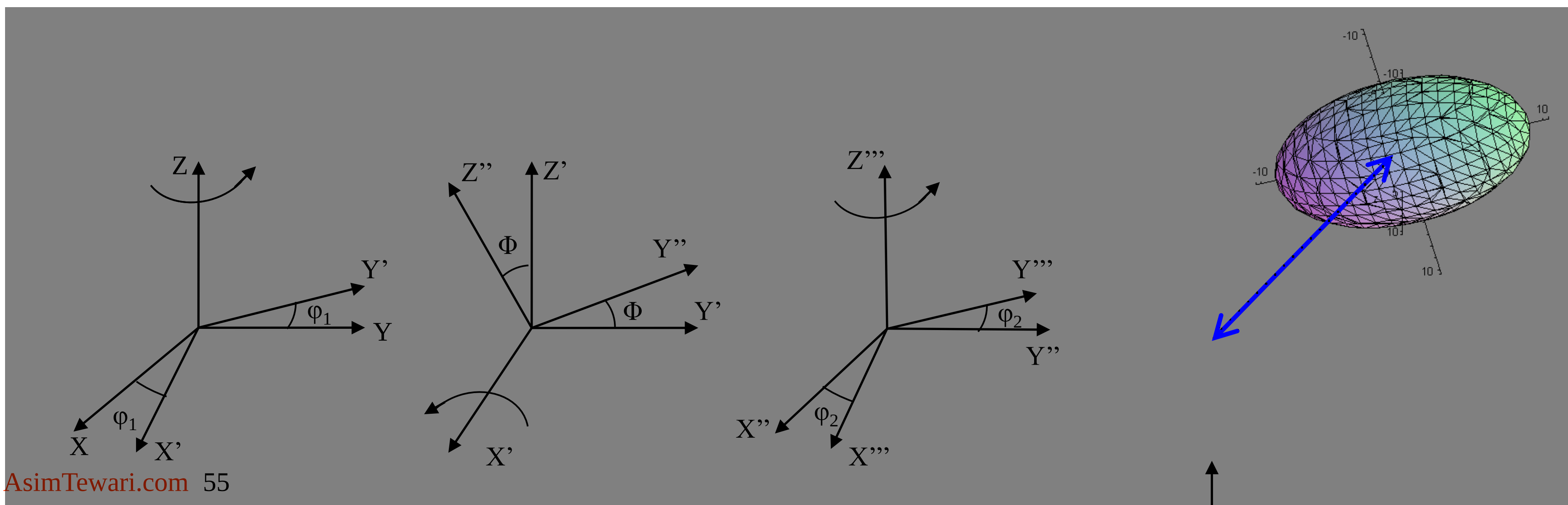

True 3D microstructural reconstruction

Serial sectioning
- Micro hardness indents
- Section alignment (Affine transform)
- 3D rendering

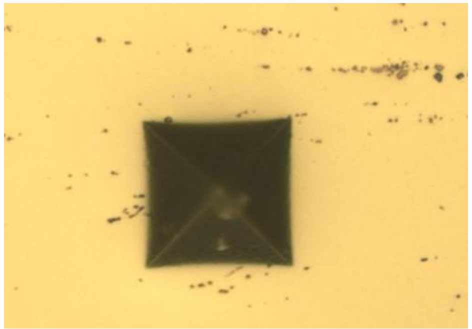

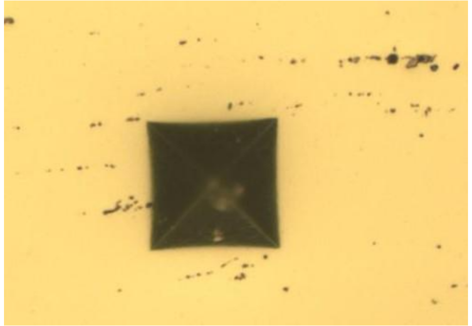

3D voxel data

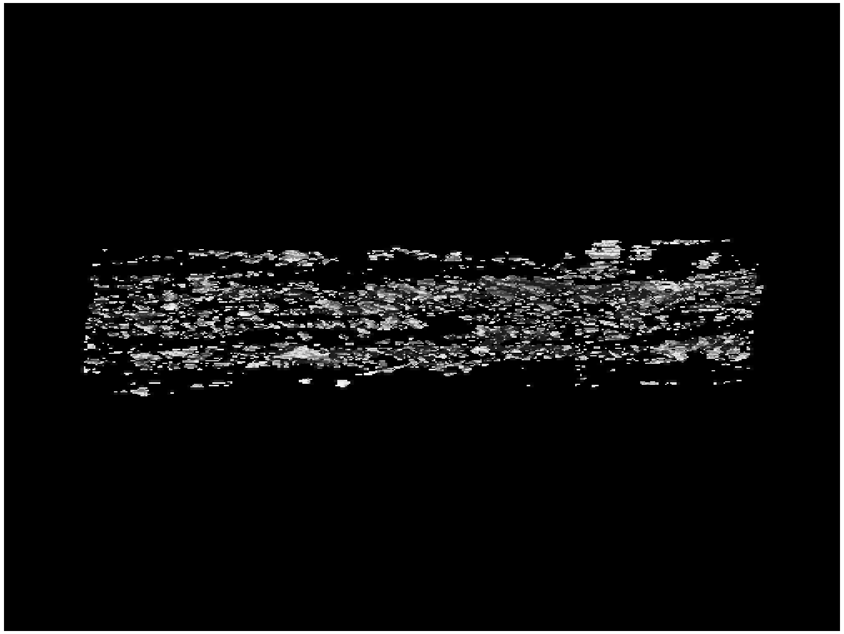

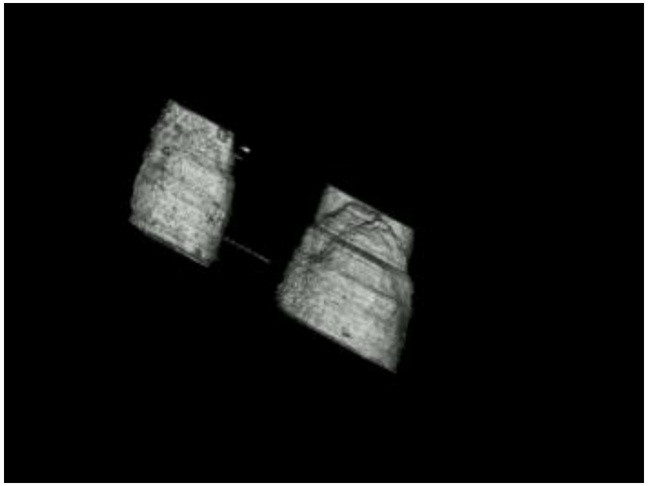

3D Vectorized Image

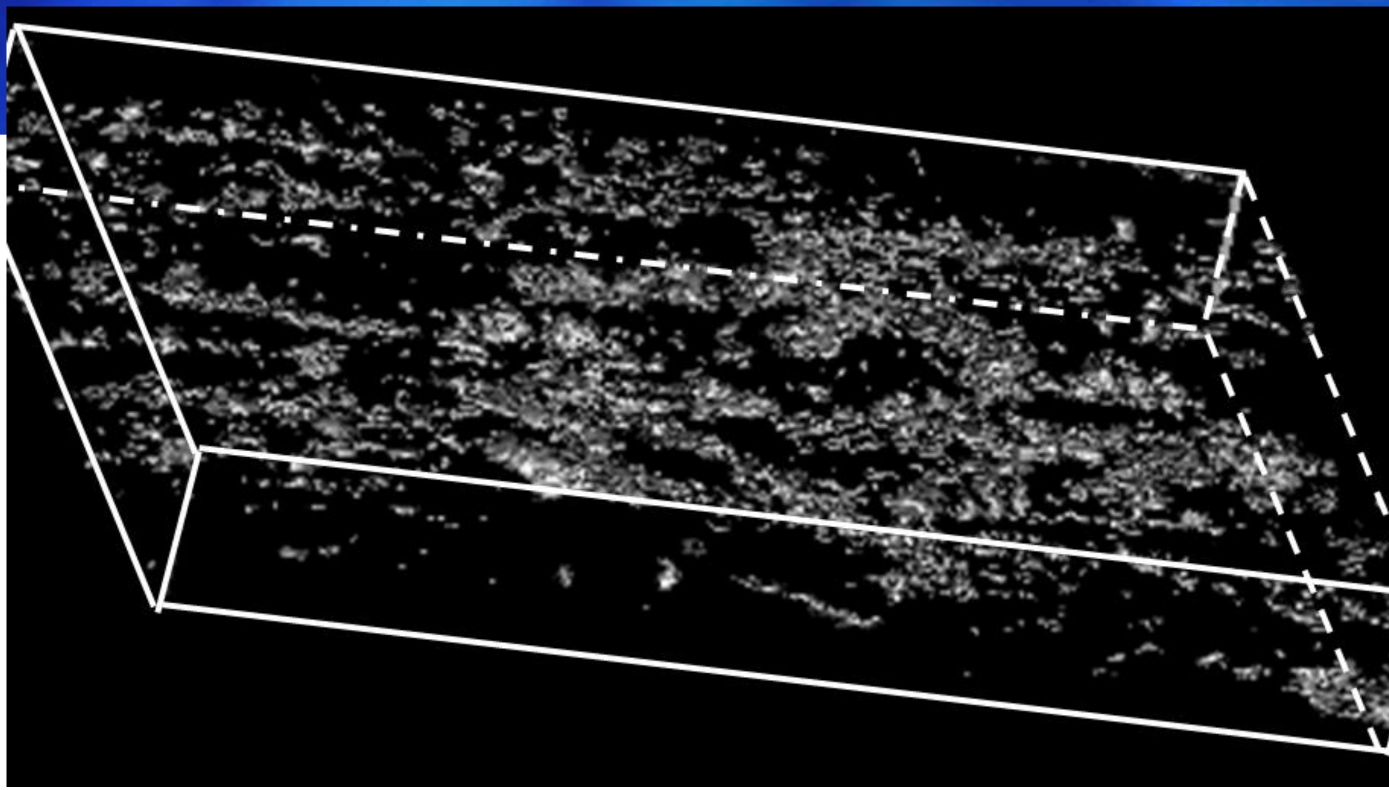

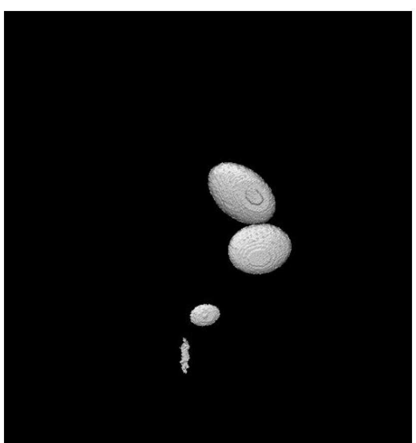

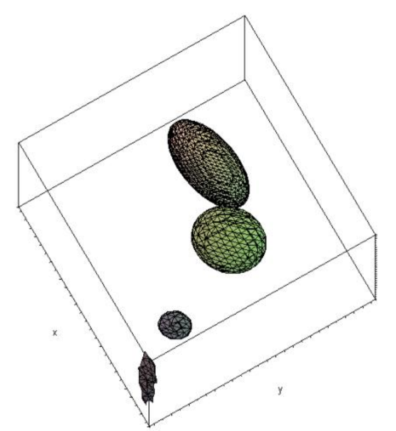

3D Graded FE mesh

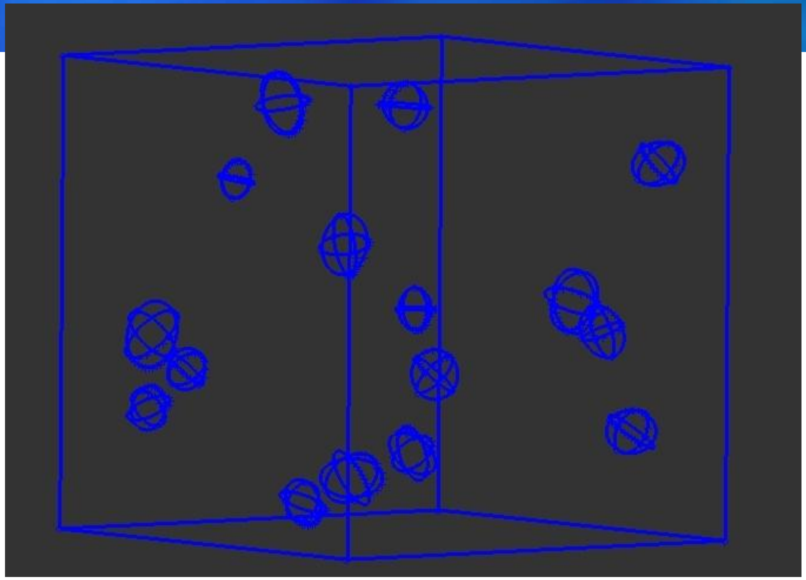

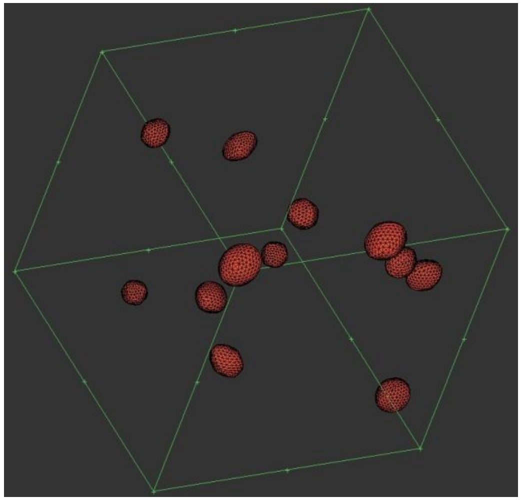

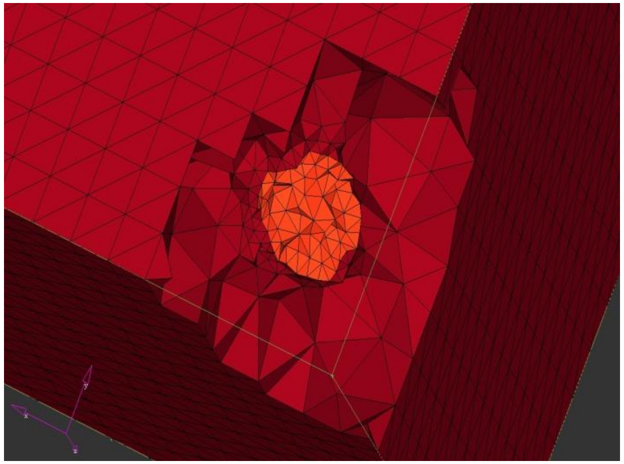

Typical microstructure

- Particle size ~ 1 μm
  - λ ~100 μm

Simulation size: (200 μm)^3

Re particle

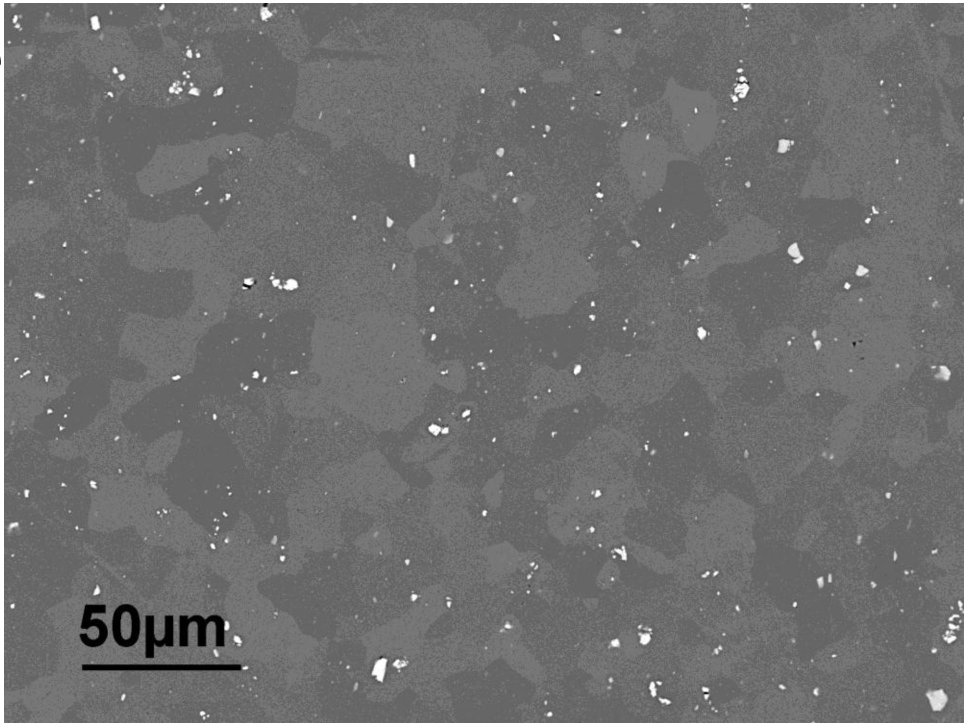

FEM Model size

Technique	Assumptions	Size	Data recovery
Brute force	None	~5x10^8	Perfect
Autocorrelation	Hilbert space Stationarity	~5x10^8 *	Good
Eigenvalue space	Hilbert space	~10^6	Not possible
Vectorized geometric primitives	Shape	~6x10^4	Good/Fair

Digital: not discrete but continuous

Summary

- Spatial arrangement of second phase play an important role in plastic localization
- Intersecting ellipsoids form Convex rings (extension of convex sets)
- Reduction of storage by ~4 orders
- Automated graded mesh generation

Future Directions

- Incorporation of other geometric primitives
- Parameterization of grains by four dimensional Poisson polyhedrons (and ordered texture triplets)
- Preserves three intrinsic volumes in 3D

Future is Digital but not discrete

- Modeling with meshless and finite point methods

Case Study 4

Nano structure modification using pre-form annealing

Experimental FLD (AA 6061)

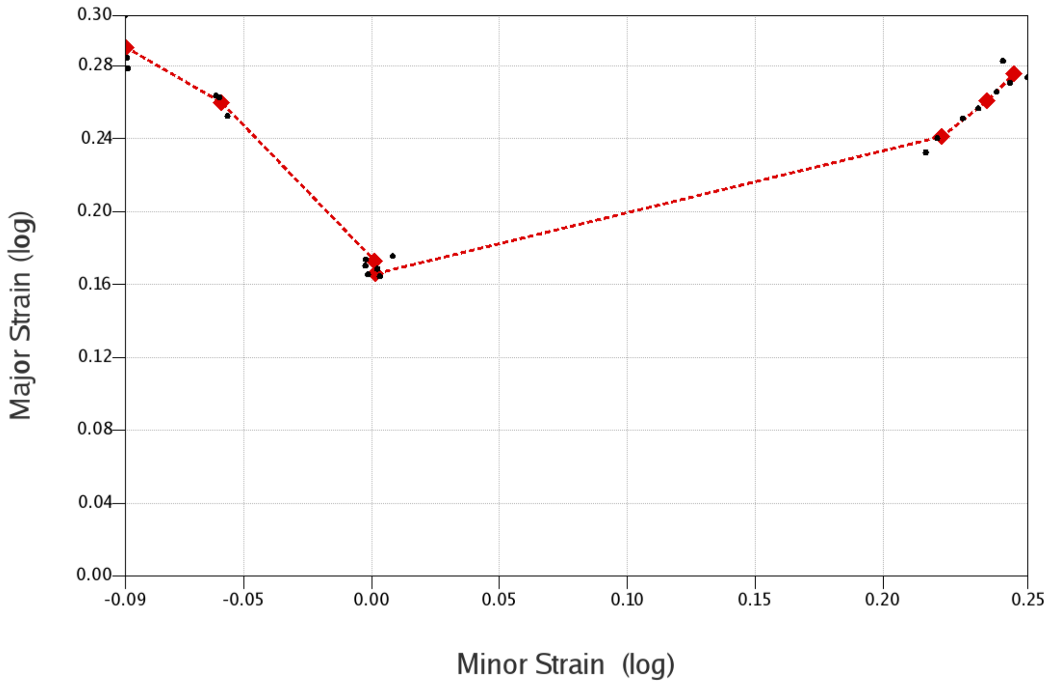

PFA Technology for Al 5000 series

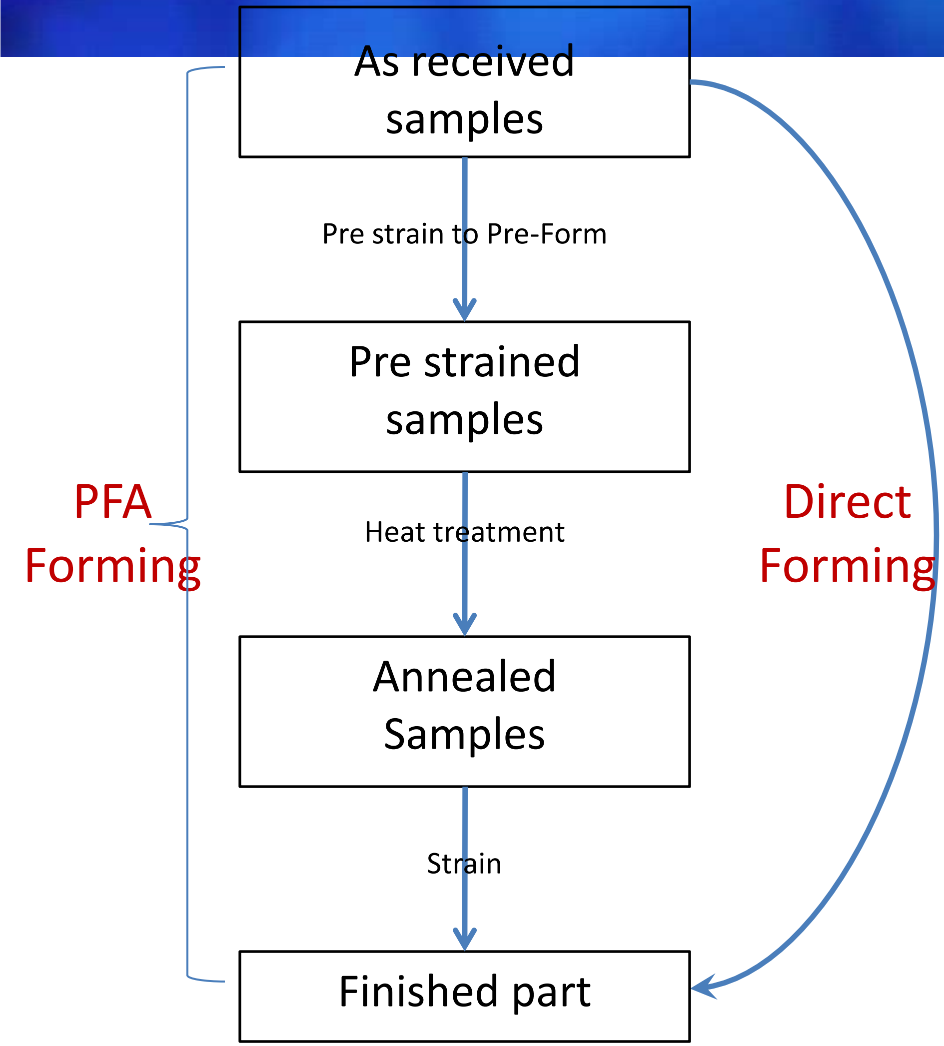

Heat Treatment:

- Direct Forming (1 and 4)
- PFA (Pre-Form Annealing) Forming (1, 2, 3 and 4)

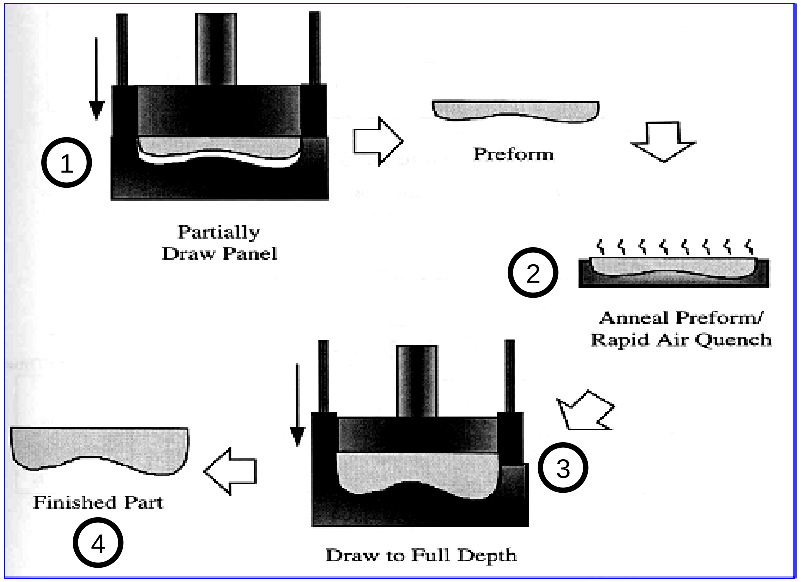

Pre-Form Annealing of Door Inner of SUV

Theresa Lee et. al. SAE Int , 2006

Patented technology for Al 5000 alloys in the process of DD at GM R&D

Scientific challenges

- Multiple-precipitate variants
- Multiple precipitation pathways
- Various states of coherency
- Role of dislocation landscape on thermodynamics and kinetics of precipices
- Simultaneous recovery and precipitate overaging
- Early recrystallization

Recovery

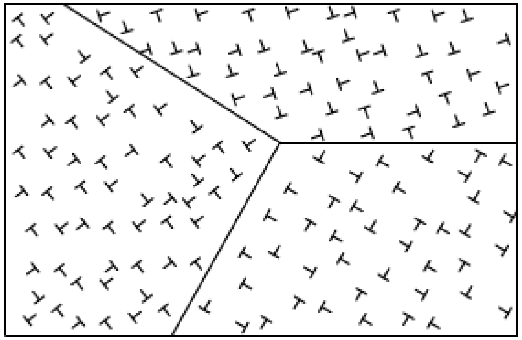

After straining

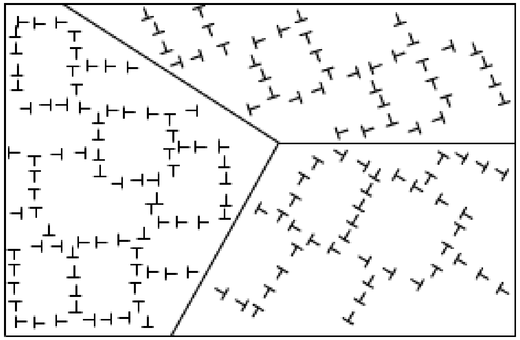

Annealing

After straining

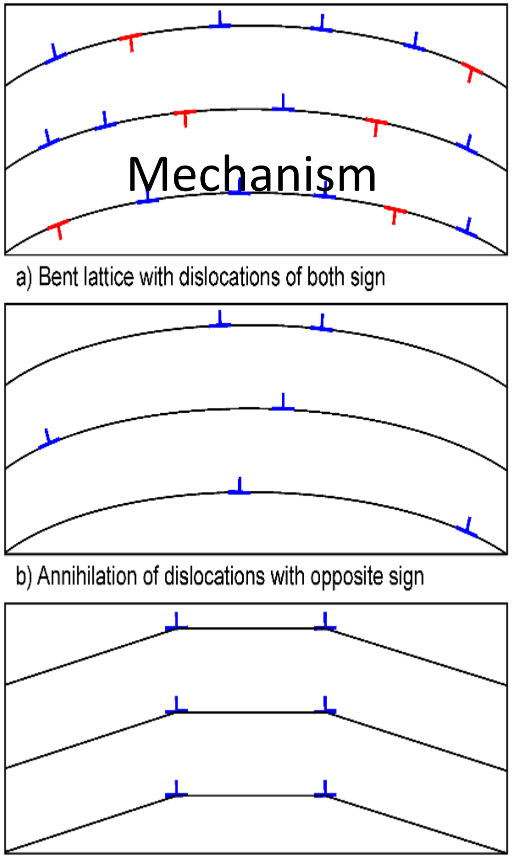

a) Bent lattice with dislocations of both sign

b) Annihilation of dislocations with opposite sign

c) Polygonization of the lattice

Process to reduce the total number of dislocations by:

- Annihilation
- Re-arrangement into lower energy configuration/s

Precipitation hardening

3 step heat treatment:

- Solution heat treatment, to dissolve the alloying elements
- Quenching, to form SSSS
- Aging, the controlled decomposition of the supersaturated solid solution (SSSS) to form a fine dispersion of precipitates

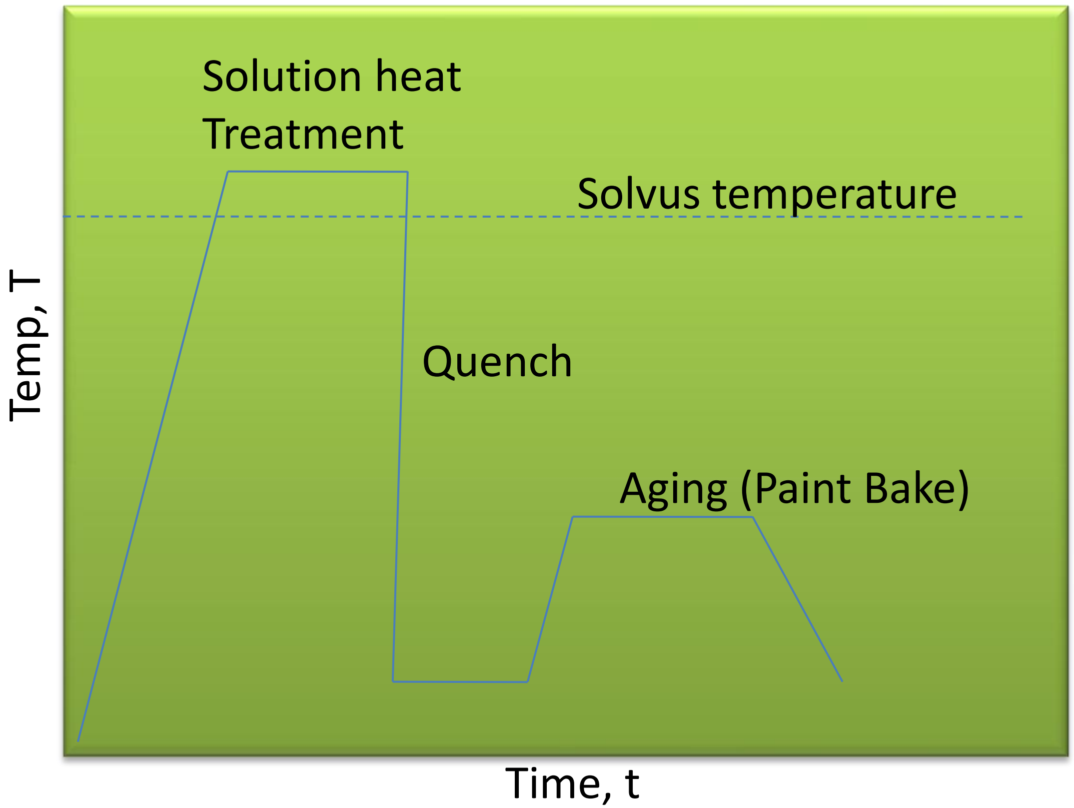

Microstructure Development: Aging

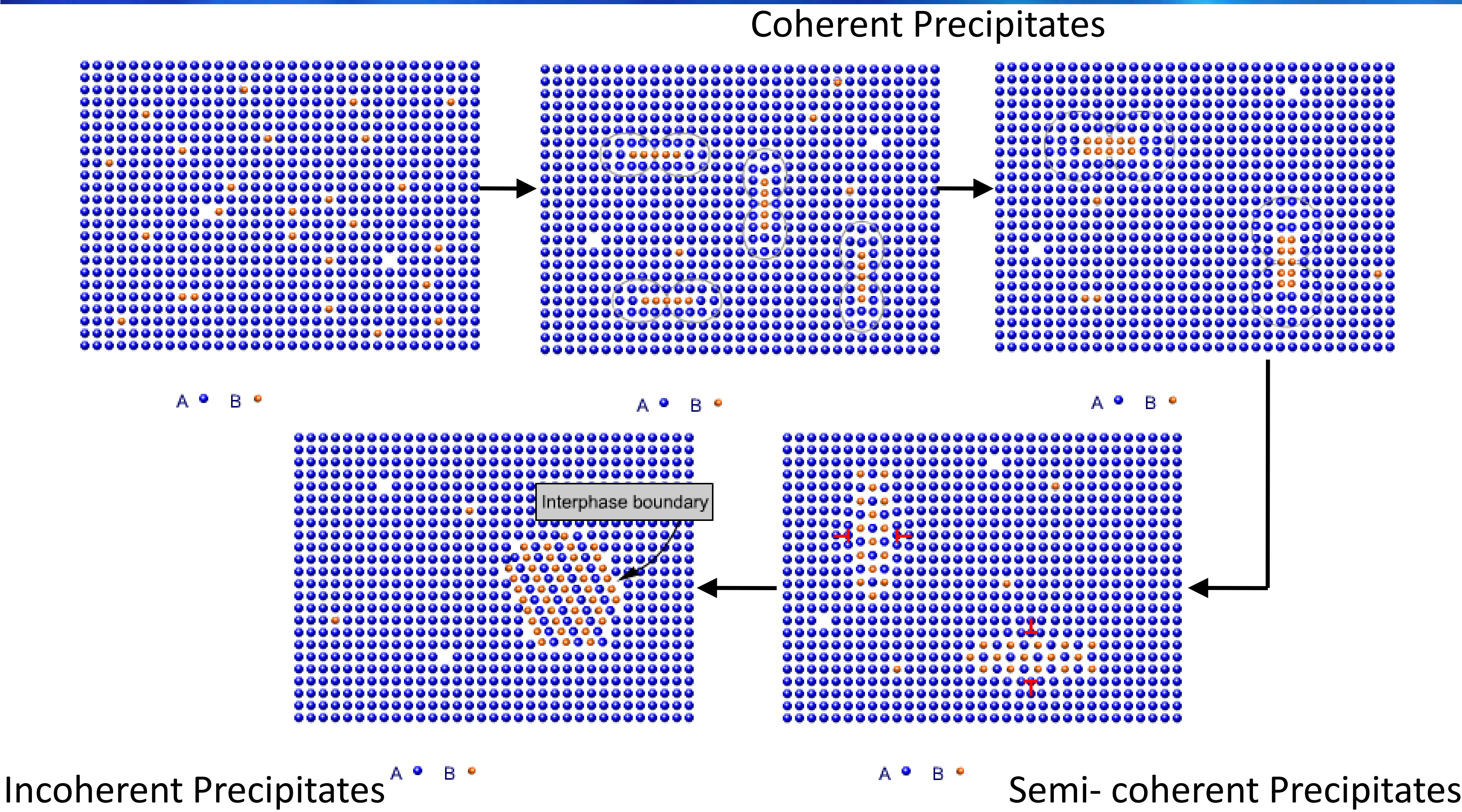

Strengthening Process

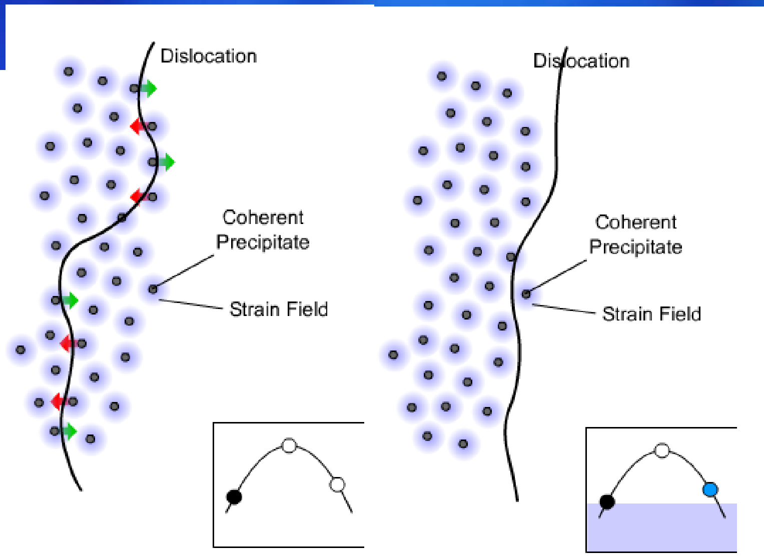

1. Fine Zone Spacing

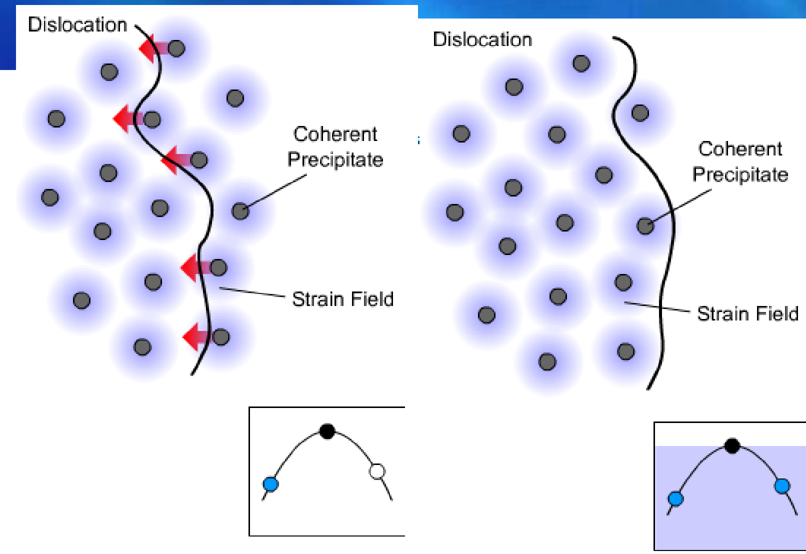

2. Medium Zone Spacing

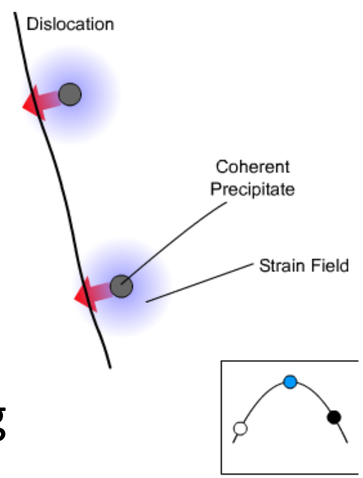

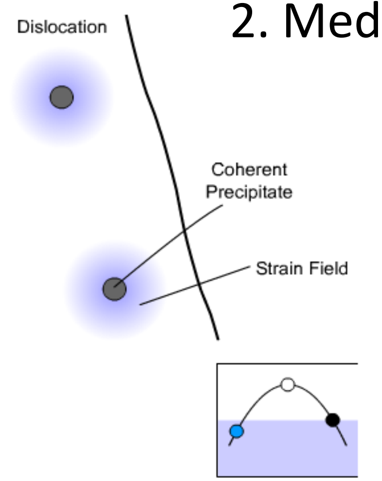

3. Coarse Zone Spacing

Strengthening Process

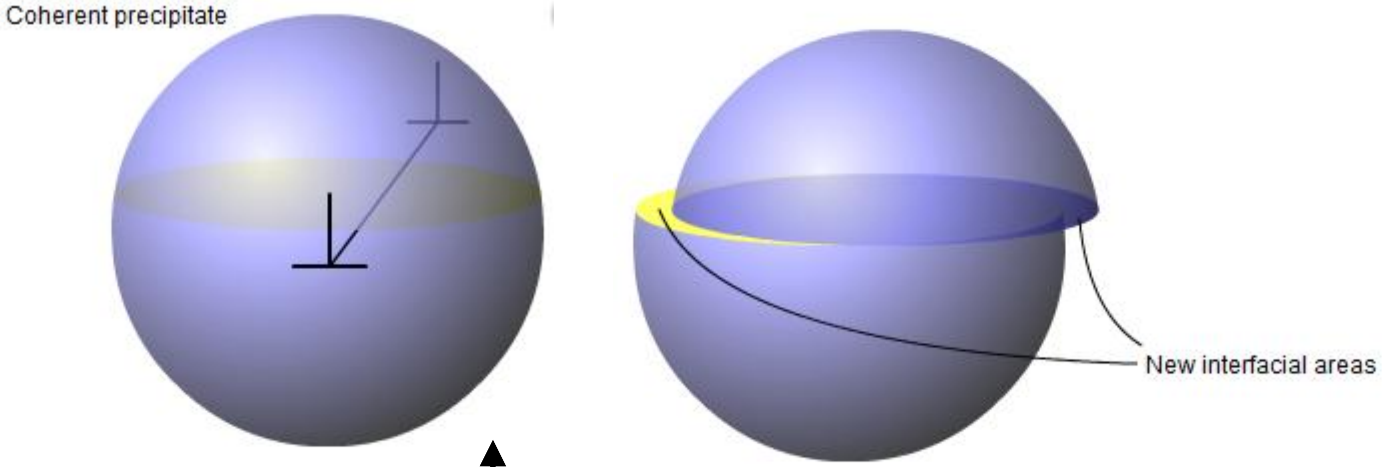

Chemical hardening

Dispersion Hardening

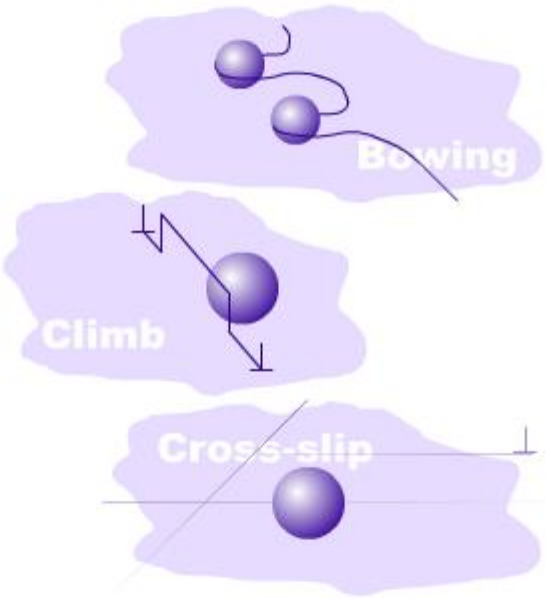

Yield strength

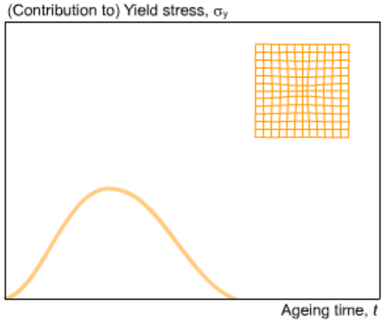

Coherency strain hardening

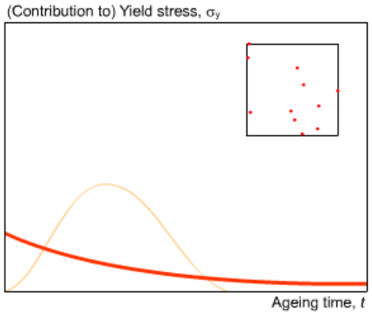

Solute hardening

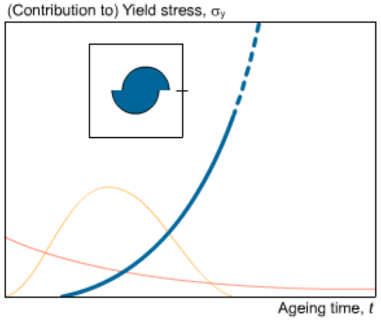

Chemical hardening

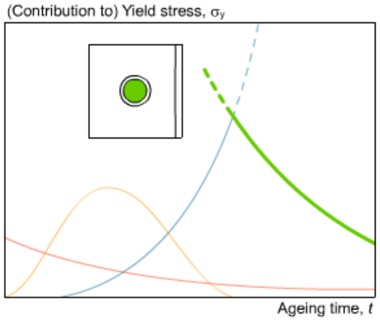

Dispersion hardening

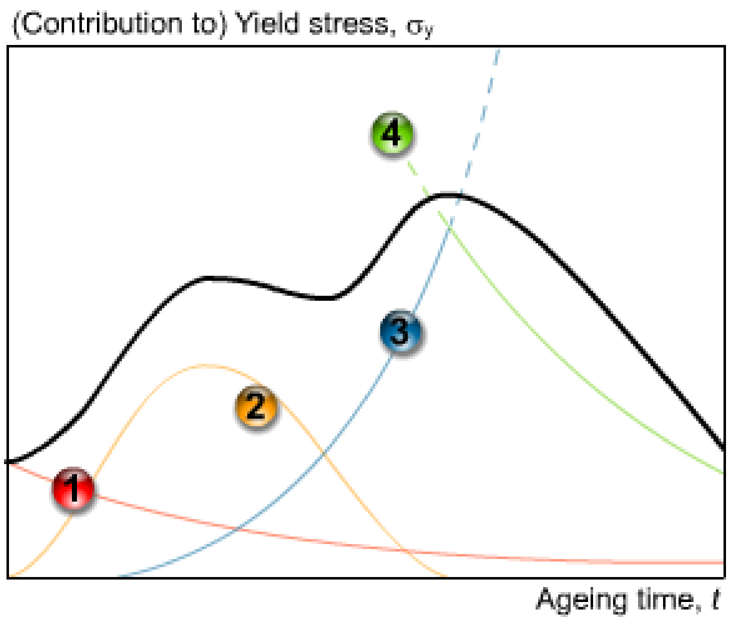

Cumulative yield strength curve

Texture Evolution: Al 6xxx and 5xxx

- Depends on the time/ temperature history
- Main difference is due to the precipitation of Mg_2Si in 6xxx alloys
- Mg_2Si impedes the progress of recrystallization by inhibiting Particle Simulated Nucleation (PSN)
- Leads to pronounced cube texture

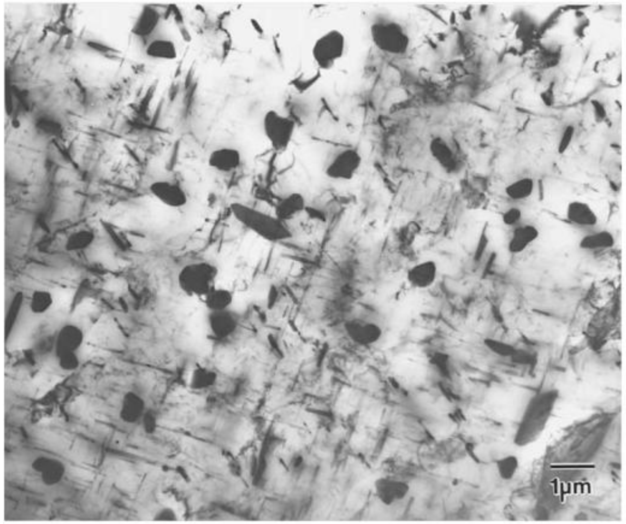

Ref [2]: Olaf Engler at. al.

Below 300 C, recrystallization patterns are unobserved,
In order to achieve that, higher temperatures are required

Effects of Si

- Si level does not have a significant influence on the aging kinetics but primarily affects the initial strength level
- Exception of the very highest Si level, the strength increases linearly with Si content
- Only a small offset in strength, which increases with increasing Si content

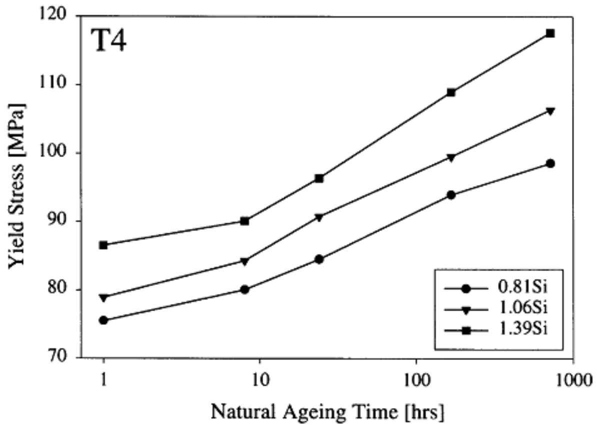

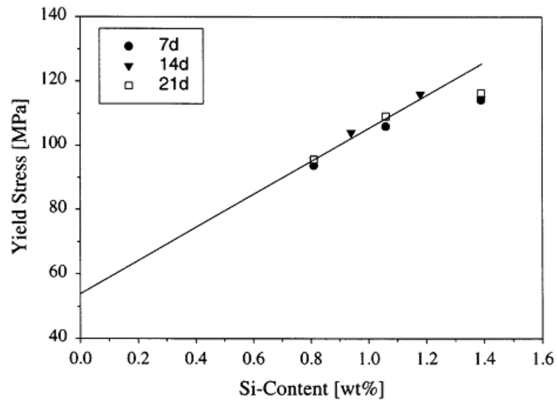

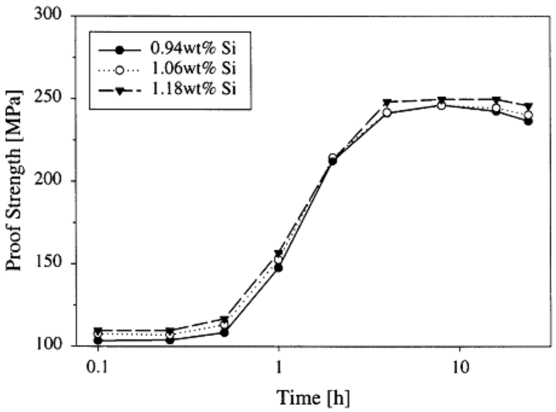

Al-Si-Mg Phase diagram

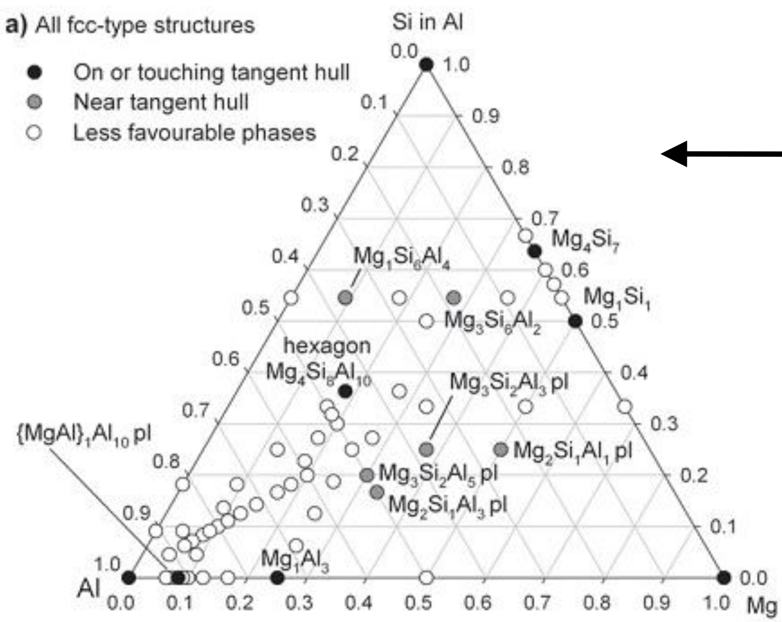

Most stable structures

Metastable structure in early stages of precipitation

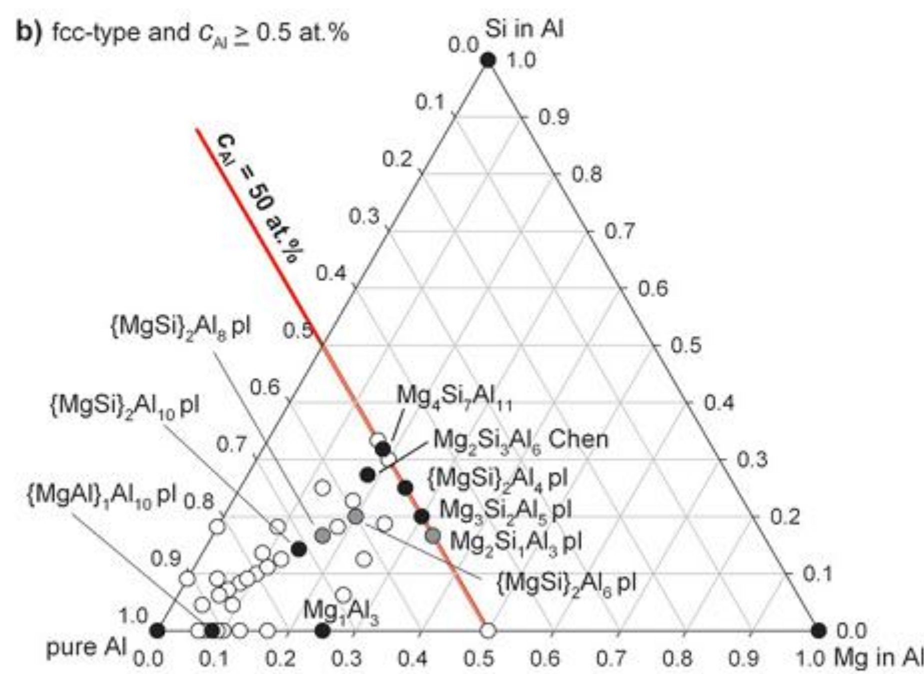

Van Huis at. al. Acta Mater pp. 2183-2199, 2007

Metastable states

Phase	Composition	Structure	Exp. Lattice parameters
GP zone	$Mg_1\ Si_1$	Monoclinic P2/m	a= 4.05 A b= 4.05 A c= 4.05 A β= 90.0
Pre β″	(Mg + Al) 5Si6 before 0.5b shift	Monoclinic C2/m	a= 14.78 A b= 4.05 A c= 6.74 A β= 106.8
Pre β″	Mg4Si7 before 0.5b shift	Monoclinic C2/m	a= 14.6 A b= 4.05 A c= 6.40 A β= 105.3
β″	Mg5Si6 after 0.5b shift	Monoclinic C2/m	a= 15.16 A b= 4.05 A c= 6.74 A β= 105.3
β″	(Mg + Al) 5Si6 after 0.5b shift	Monoclinic C2/m	a= 14.78 A b= 4.05 A c= 6.74 A β= 106.8
U1	Mg1Si2 Al2	Trigonal P3m1	a= 4.05 A c= 6.74 A
U2	Mg4 Si4 Al4	Orthorhombic Pnma	a= 6.75 A b= 4.05 A c= 7.94 A
U3	Mg_4Si_8	Imma	a= 6.40 A b= 4.05 A c= 7.46 A
B′	Al3Mg9Si7	Hexagonal P6	a= 10.4 A c= 4.01 A
β'	Mg9Si5	Hexagonal $P6_3/m$	a= 7.15 A c= 12.15 A
β	Mg6 Si3 $Mg\ _2Si$	Anti-flourite Fm3m	a= 6.39 A

SSSS → clusters → initial-β''

→ *pre-β''* → β'' (Mg_5Si_6) ↑↓ U2, U1 → β' (Mg_9Si_5) → β (*stable*).

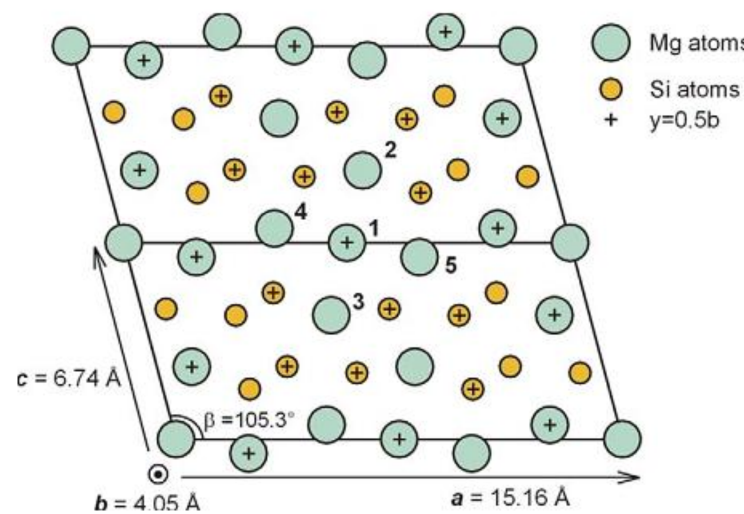

Van Huis at. al. Acta Mater pp. 2945-2955, 2006

Precipitation Phases

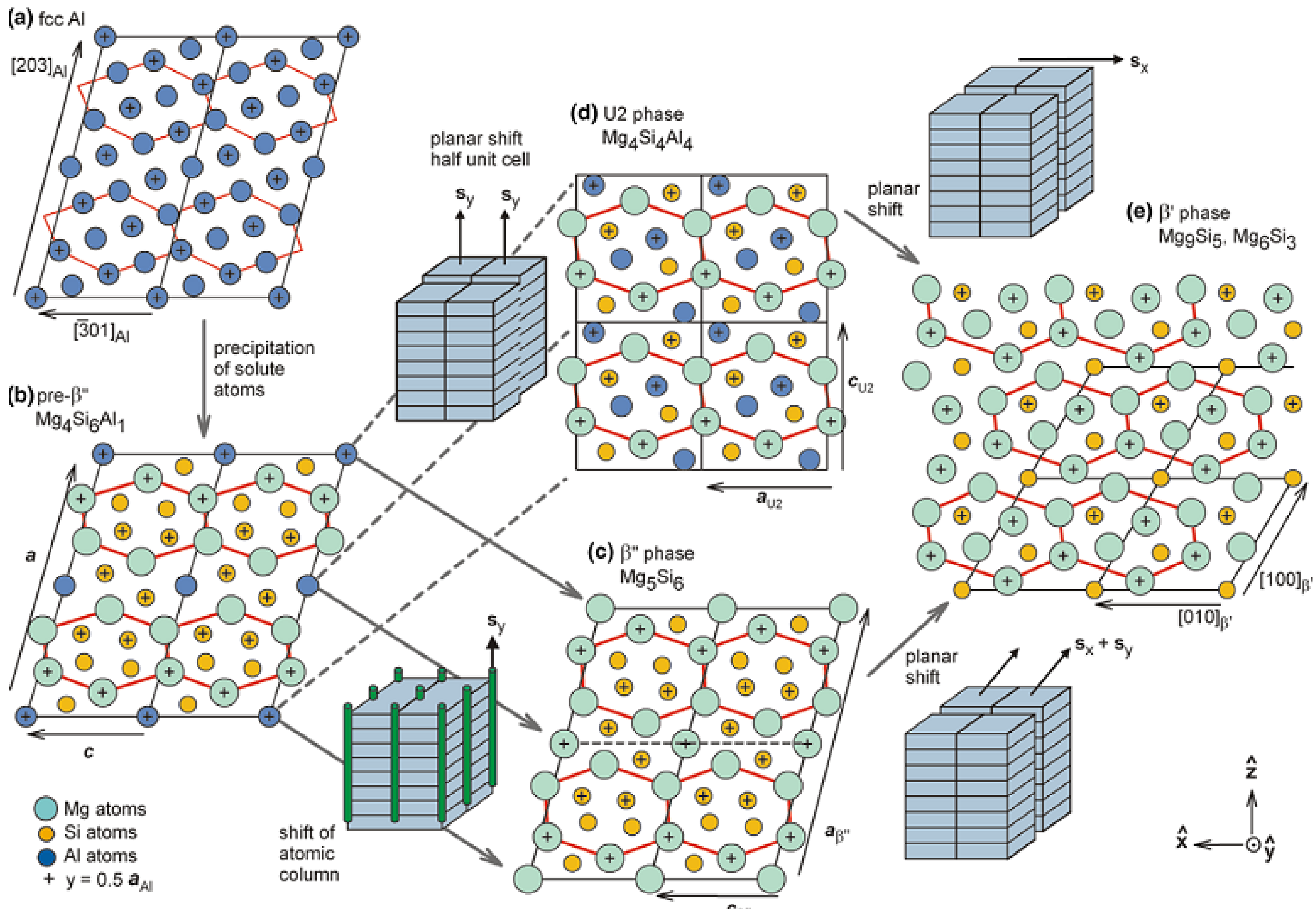

Van Huis at. al. Acta Mater pp. 2945-2955, 2006

Phase transformation

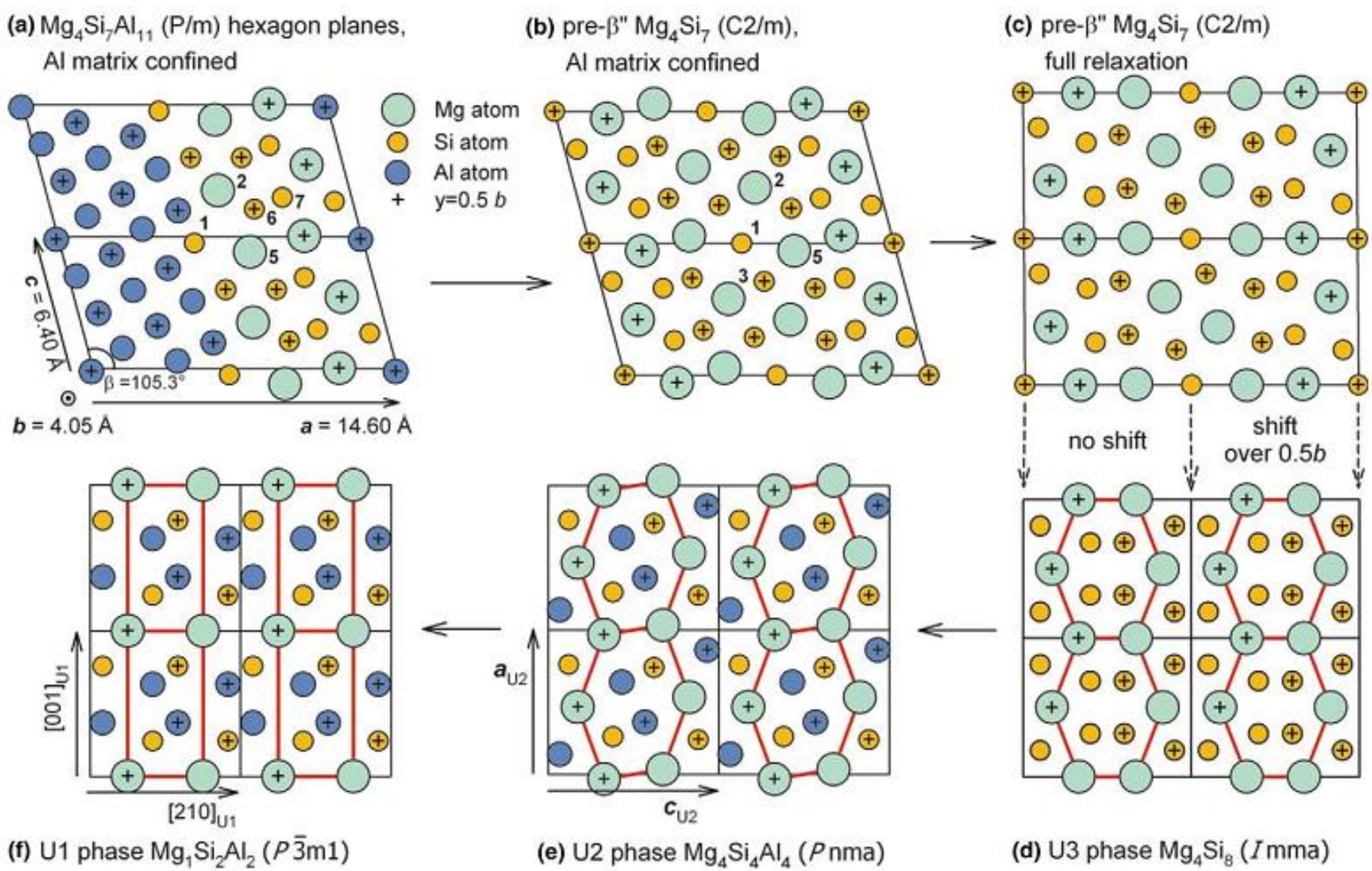

Van Huis et. al. Acta Mater pp. 2945-2955, 2006

TEM experiments

Sample	Pre-Strain	Annealing time	Annealing temp.	Annealing source
Sample 1	15%	0	NA	NA
Sample 2	15%	10 s	250^{o}C	SALT BATH
Sample 3	15%	60 s	250^{o}C	SALT BATH
Sample 4	15%	5 min	250^{o}C	SALT BATH
Sample 5	15%	60 min	250^{o}C	SALT BATH
Sample 6	15%	5 min	250^{o}C	FURNACE
Sample 7	15%	60 min	250^{o}C	FURNACE
Sample 8	0%	0	NA	NA

15% prestrain with no annealing

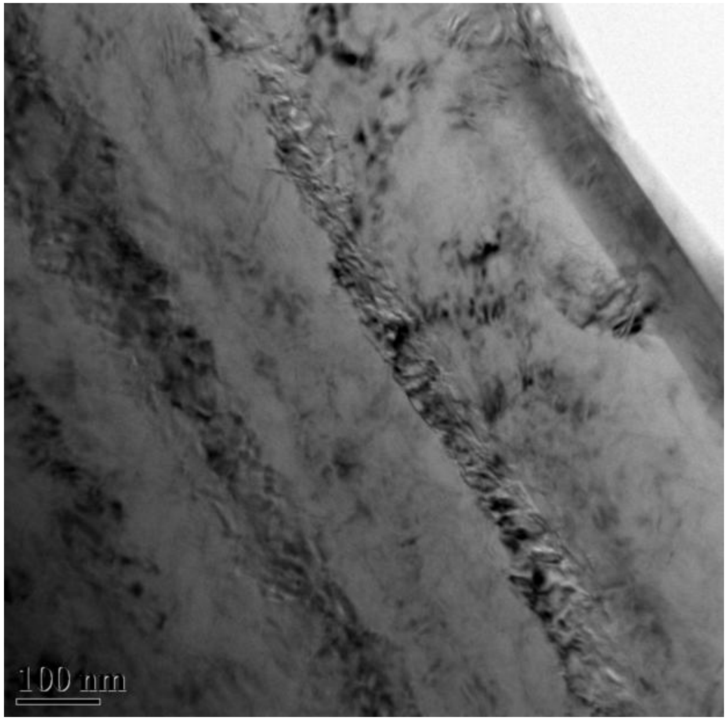

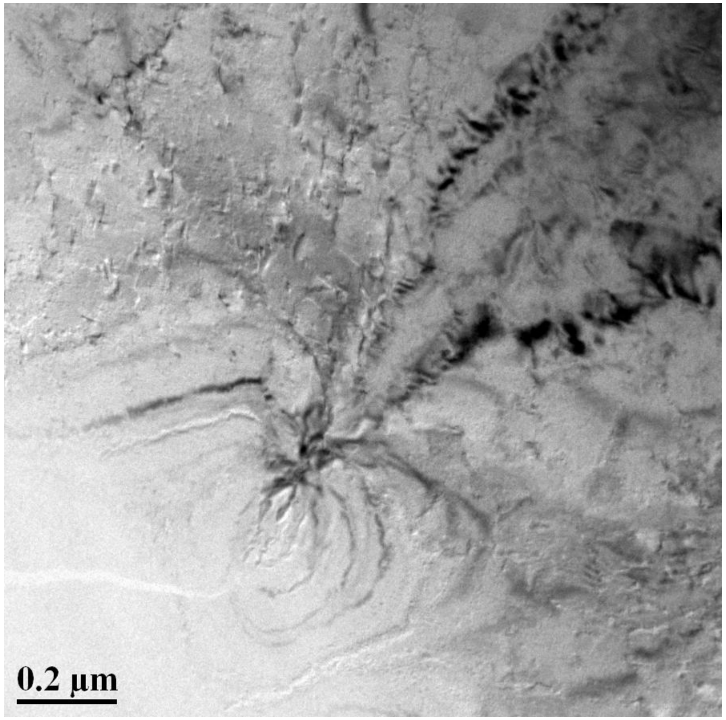

15% prestrain with annealing (sub-grain structure)

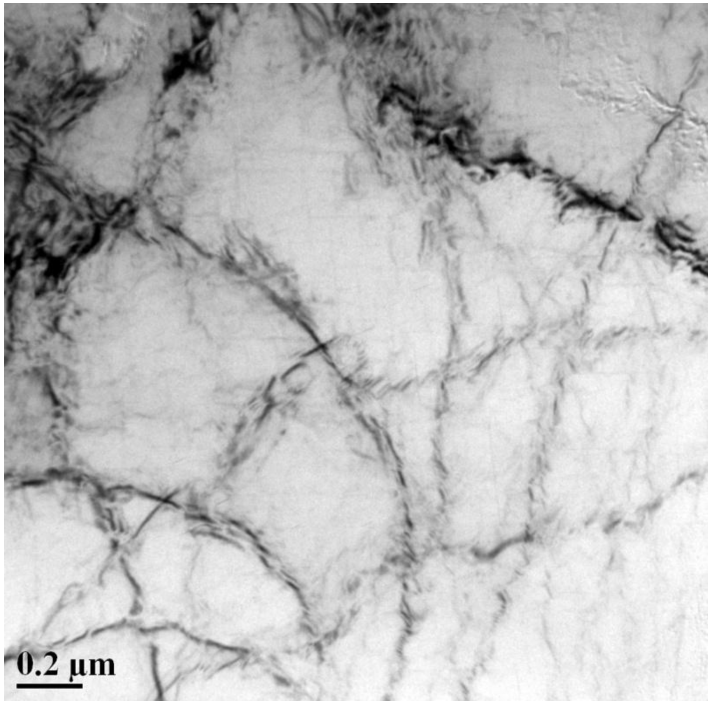

Sub-structure

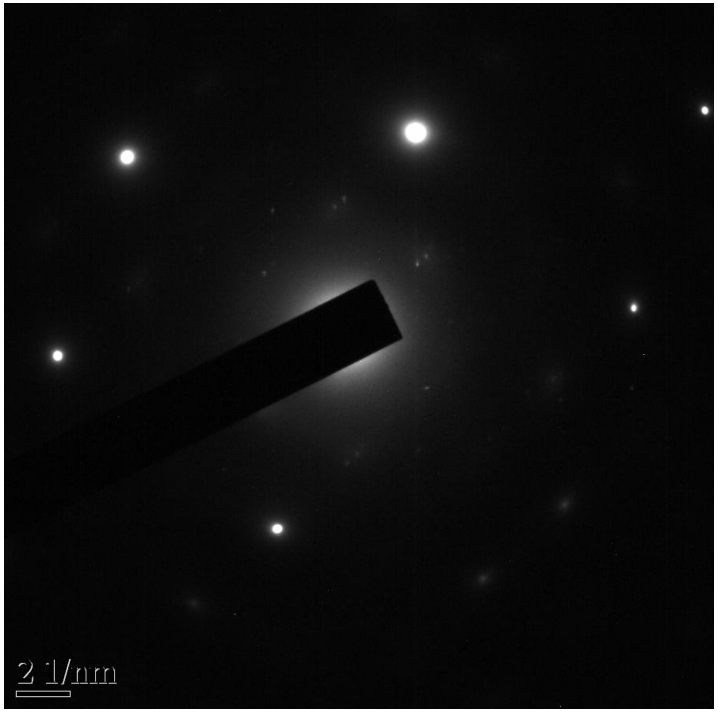

Diffraction pattern of left micrograph

15% prestrain with annealing (β'' and β' observed)

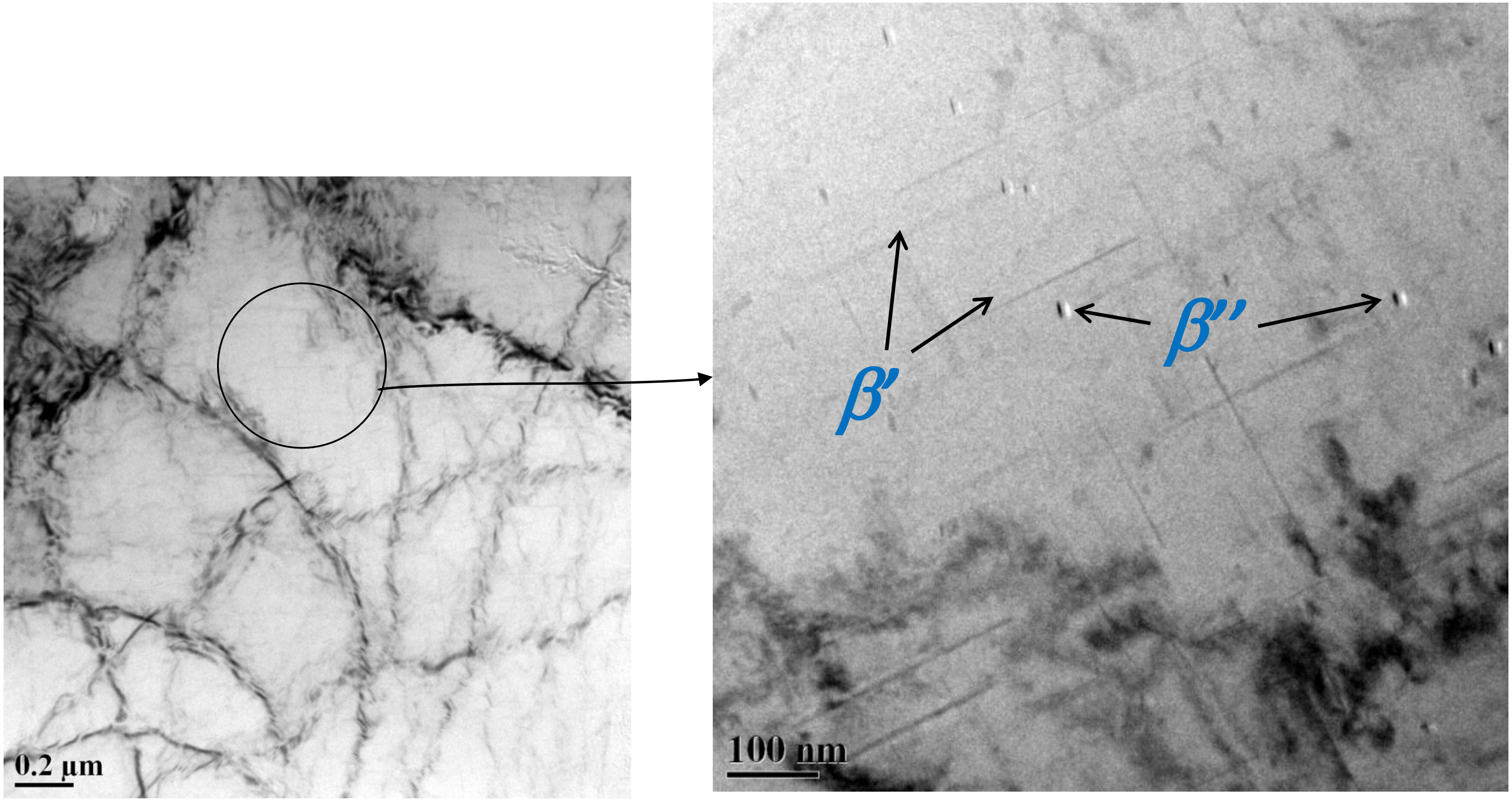

15% prestrain with annealing (β')

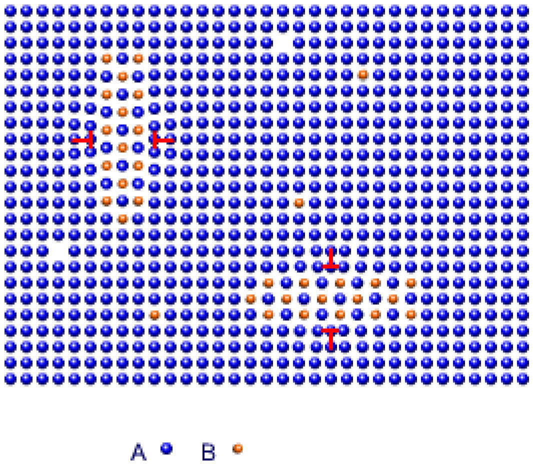

Semi- coherent Precipitates

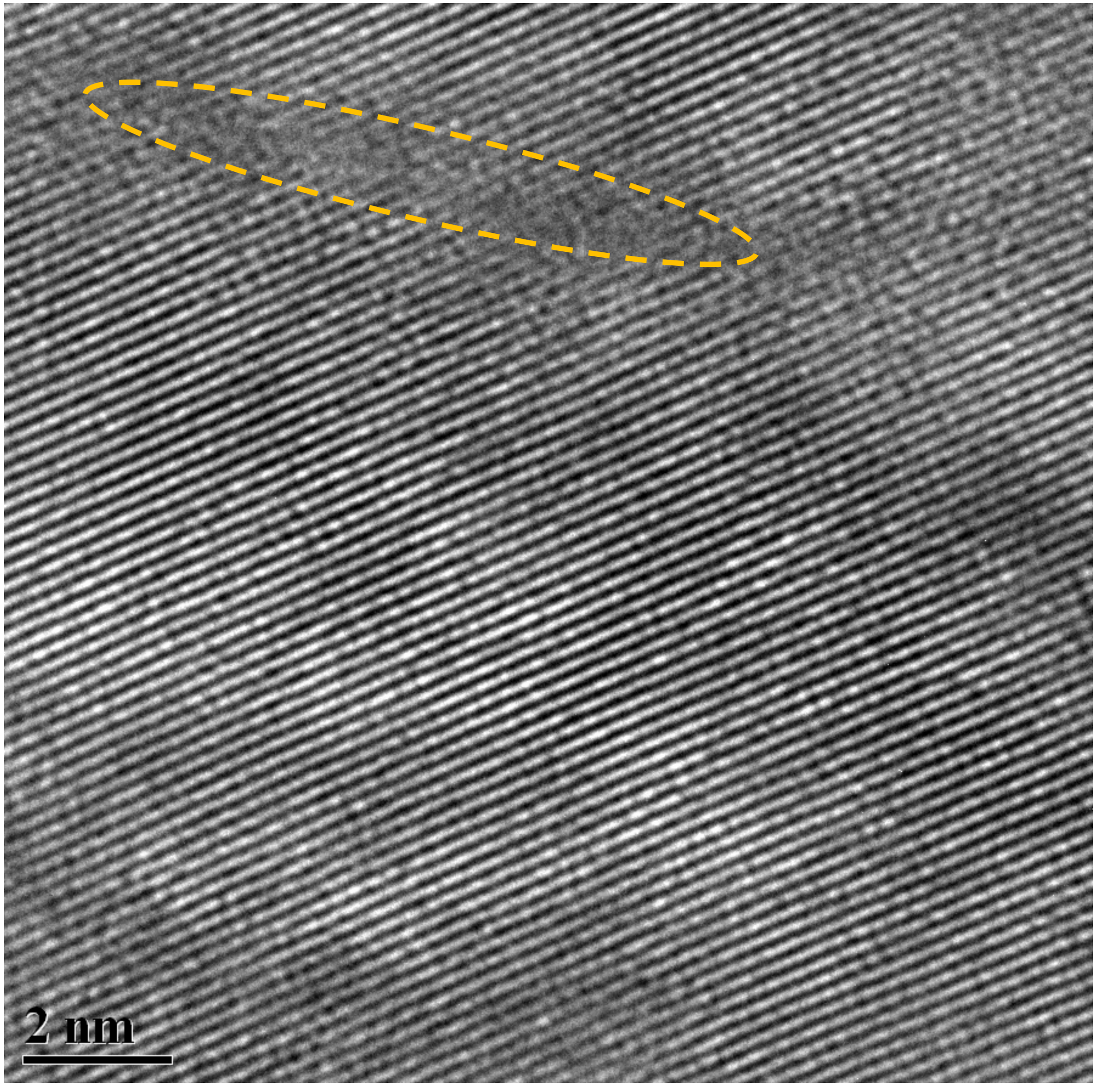

Summary

- Large localized shear zones in pre-straining
- Evidence of recovery (sub-grain structure) on annealing
- Presence of both plate-like β' and needle-like β'' on annealing
- Stoichiometry of β' and β'' (start and end Temp)?